

Impact of Volumetric Properties on Protein Structure and Function

Dissertation

zur Erlangung des akademischen Grades eines
Doktors der Naturwissenschaften
(Dr. rer. nat.)

eingereicht an

**der Fakultät Chemie der
Technischen Universität Dortmund**

vorgelegt von

Saba Suladze

Aus Tbilisi, Georgien
Januar 2016, Dortmund

Impact of Volumetric Properties on Protein Structure and Function

Dissertation

For the achievement of the academic degree of the
Doctors in Natural Sciences
(Dr. rer. nat.)

Submitted to

The Department of Chemistry
TU Dortmund University

By

Saba Suladze

From Tbilisi, Georgia

January 2016, Dortmund

To my beloved parents, Sulkhan & Natalia

“There are two possible outcomes: if the result confirms the hypothesis, then you've made a measurement. If the result is contrary to the hypothesis, then you've made a discovery.”

1st Examiner

Prof. Dr. Roland Winter

Department of Chemistry

Physical Chemistry-I, Biophysical Chemistry

TU Dortmund University

Dortmund

2nd Examiner

Prof. Dr. Heinz Rehage

Department of Chemistry

Physical Chemistry II

TU Dortmund University

Dortmund

Declaration/Erklärung

The work described in this thesis was performed from September 2012 to September 2015 at the Department of Chemistry and Chemical Biology, TU Dortmund University under the guidance of Prof. Dr. Roland Winter. I hereby declare that the dissertation is the result of my own work, except where specifically indicated in the text.

Die vorliegende Arbeit wurde in der Zeit von September 2012 bis September 2015 an der Fakultät für Chemie und chemische Biologie der Technischen Universität Dortmund unter der Leitung von Prof. Dr. Roland Winter angefertigt. Hiermit erkläre ich an Eides statt, dass ich die vorgelegte Dissertation selbstständig angefertigt und dass alle Stellen, die ich wörtlich oder dem Sinne nach aus anderen Veröffentlichungen entnommen habe, kenntlich gemacht worden sind.

Dortmund 2016

Saba Suladze

Acknowledgements

First and foremost, I am sincerely and heartily grateful to my supervisor Prof. Dr. Roland Winter, who has been a superb mentor. I would like to thank him for his enormous support, insightful discussions, contagious enthusiasm and for giving me personal freedom to pursue various projects independently, which undoubtedly strongly enhanced my productivity over the time course of Ph.D. studies. I am very thankful for all his contributions of time, ideas and priceless advices, corrections of posters, presentations and paper drafts. Next, I would like to thank the members of my committee, for their time and interest.

I convey my special thanks to Prof. Dr. Claus Czeslik for numerous fruitful discussions. I would also like to thank all present and some past members of the Winter's group, especially Dr. Shobhna Kapoor, Dr. Mirko ErIkamp and Dr. Salome Pataraiia for all their support through all the turbulent times in my PhD. I also thank people who were not part of the Winter group but helped me out, including Dr. Shehab Ismail (with PDE δ purification) and Dr. Matthias M \ddot{u} ller (with stopped-flow instrumentation). I gratefully acknowledge the generous funding and resources from the Max-Planck-Gesellschaft and Technische Universit \ddot{a} t Dortmund. I have been highly honored for being a member of the outstanding IMPRS (International Max Planck Research School). A special thank is rendered to the IMPRS-team, including Christa Hornemann, whose attention and care helped me tremendously during my Ph.D. studies. I am grateful to Andrea Kreuzel and Bertina Schuppan for being helpful in solving all problematic formal and non-formal issues with patience. Last, but by no means least, I thank all staff members from the University of Dortmund and IMPRS, who helped in making my thesis possible.

My time in Dortmund was made enjoyable in large part due to the many friends that became part of my life (too many to list here, but you know who you are!). I am grateful for fun activities we have done together. Finally, I need to thank my family members, my mom, dad, sisters, grandma and uncle for all their unconditional love, spiritual support and encouragement that makes accomplishments like this so much sweeter. And most of all is for my love, Tamta, whose unwavering support and patience during all stages of this work is so much appreciated. Thank you!

Abstract

In the first part of this dissertation, the effects of pressure on the structure and function of membrane-associated phospholipases A2 (PLA2) protein are examined. PLA2s catalyze the hydrolysis reaction of *sn*-2 fatty acids of membrane phospholipids and are also involved in receptor signaling and transcriptional pathways. Here, we used pressure modulation of the PLA2 activity and of the membrane's physical-chemical properties to reveal new mechanistic information about the membrane association and subsequent enzymatic reaction of PLA2. Although the effect of high hydrostatic pressure (HHP) on aqueous soluble and integral membrane proteins has been investigated to some extent, its effect on enzymatic reactions operating at the water/lipid interface has not been explored, yet. This study focuses on the effect of HHP on the structure, membrane binding and enzymatic activity of membrane-associated bee venom PLA2, covering a pressure range up to 2 kbar. To this end, high-pressure Fourier-transform infrared and high-pressure stopped-flow fluorescence spectroscopies were applied. The results show that PLA2 binding to model biomembranes is not significantly affected by pressure and occurs in at least two kinetically distinct steps. Followed by fast initial membrane association, structural reorganization of α -helical segments of PLA2 takes place at the lipid water interface. FRET-based activity measurements reveal that pressure has a marked inhibitory effect on the lipid hydrolysis rate, which decreases by 75% upon compression up to 2 kbar. Lipid hydrolysis under extreme environmental conditions, such as those encountered in the deep sea where pressures up to the kbar-level are encountered, is hence markedly affected by HHP, rendering PLA2, next to being a primary osmosensor, a good candidate for a sensitive pressure sensor *in vivo*.

The second part of this dissertation addresses the question of how the binding of PDE δ to the farnesyl lipid anchor of signaling proteins affects its dynamic, thermodynamic and solvation properties. The protein PDE δ is an important solubilizing factor for several prenylated proteins including the Ras subfamily members. The binding occurs mainly through the farnesyl anchor of Ras proteins which is recognized by a hydrophobic pocket of PDE δ . In this study, we carried out a detailed study of the thermodynamic and solvational properties of PDE δ binding to farnesyl-cystein, which serves as a model for PDE δ association to prenylated proteins. Using various biophysical approaches in conjunction with theoretical considerations, we show here that binding of the largely hydrophobic ligand surprisingly has

enthalpy-driven signature and the entropy change is largely controlled by the fine balance between the hydrational and conformational terms. Moreover, binding of PDE δ to farnesyl-cystein is accompanied by an increase in thermal stability, the release of about 150 water molecules from the interacting species, a decrease in solvent accessible surface area, and a marked decrease of the volume fluctuations and hence dynamics of the protein. Altogether, our results shed more light on the molecular mechanism of PDE δ interaction with prenylated Ras proteins, which is also prerequisite for an optimization of the structure-based molecular design of drugs against Ras related diseases and for understanding the multitude of biological functions of PDE δ .

TABLE OF Contents

LIST OF FIGURES	vi
LIST OF TABLES	vii
LIST OF ABBREVIATIONS	ix
LIST OF FLUOROPHORES	xi
CHAPTER 1. INTRODUCTION TO PHOSPHOLIPASE A2 AND PDEδ	1
1.1 Function and Structure of Phospholipase A2	3
1.1.1 The Phospholipase A2 Superfamily	3
1.1.2 Structure of Bee Venom PLA2.....	5
1.1.3 Secretory PLA2 Interfacial Binding and Activity.....	7
1.1.4 Mechanism of the sPLA2 Reaction.....	11
1.2 Structural and Functional Aspects of PDEδ, A Cytosolic Carrier for Farnesylated Ras Proteins	13
1.2.1 GTP Binding Proteins.....	13
1.2.2 PDE δ as a Regulatory Molecular Chaperone.....	15
1.2.3 Structure of PDE δ	17
CHAPTER 2. EXPERIMENTAL PROCEDURES & BIOPHYSICAL METHODS	21
2.1 Materials	23
2.1.1 Phospholipids and Reagents.....	23
2.1.2 Pde δ Expression and Purification.....	24
2.2 Spectroscopic Methods	24
2.2.1 Fourier Transform Infrared (FTIR) Spectroscopy	24
2.2.2 Ambient and High-Pressure Stopped Flow	26
2.2.3 Fluorogenic Assays for Studying PLA2-membrane Interactions and Enzyme Kinetics.....	34
2.3 Atomic Force Microscopy (AFM)	38
2.4 Calorimetric and Volumetric Methods	39
2.4.1 Isothermal Titration Calorimetry (ITC).....	39
2.4.2 Differential Scanning Calorimetry (DSC) and Pressure Perturbation	

Calorimetry (PPC).....	41
2.4.3 Ultrasonic Resonator Technology (UTR).....	45
2.4.4 Densitometry	46
2.4.5 Calculation of the Adiabatic Compressibility, Isothermal Compressibility and Relative Volume Fluctuations.....	47
CHAPTER 3. PRESSURE MODULATION OF THE ENZYMATIC ACTIVITY	
OF PHOSPHOLIPASE A2.....	51
3.1 Background and Overview	53
3.1.1 Biomembranes and Lipid Protein Interactions.....	53
3.1.2 Pressure Effects on Membrane Organization.....	57
3.1.3 Pressure Effects on the Structure and Enzymatic Activity of Membrane-Associated Proteins.....	59
3.2 Introduction and Objectives.....	62
3.3 Results and Discussion.....	65
3.3.1 Effect of Pressure on the Conformation of BvPLA2 in Bulk Solution and upon Membrane Binding.....	65
3.3.2 Membrane Association of BvPLA2.....	70
3.3.3 Pressure Dependence of the Hydrolysis Reaction of BvPLA2.....	76
3.3.4 AFM Imaging of BvPLA2 Activity.....	82
3.4 Summary and Outlook.....	83
CHAPTER 4. DYNAMIC, THERMODYNAMIC AND SOLVATIONAL PROPERTIES OF PDEδ	
BINDING TO FARNESYLATED CYSTEIN.....	87
4.1 Background and Overview	89
4.1.1 Thermodynamics of Ligand-Protein Interactions.....	89
4.1.2 Binding Enthalpy, Entropy and Heat Capacity Changes.....	92
4.1.3 Experimental Approaches for Measuring Binding Thermodynamics.....	94
4.2 Introduction and Objectives.....	96
4.3 Results and Discussion.....	98
4.3.1 Thermodynamic Properties of Binding.....	98
4.3.2 Changes in Thermal Stability of PDE δ upon Binding and Links to Hydration, Packing and Fluctuation Properties	102

4.3.3 Determination of the Intrinsic Volume and Accessible Surface Area using X-ray Crystallographic Structural Data	108
4.3.4 Number of Released Water Molecules upon PDE δ Binding to Farnesylated Cystein.....	108
4.3.5 Dissection of Hydration and Configurational Contributions to the Binding Entropy	111
4.3.6 Changes in Protein Dynamics upon Complex Formation.....	112
4.4 Summary and Outlook.....	113
CHAPTER 5. Summary and Future perspectives.....	115
Zusammenfassung und Ausblick	123
CHAPTER 6. Appendices (An Example of Using the HPSF Method to Characterize Enzymatic Reactions).....	131
6.1 Basics of Ambient and High Pressure Enzymology.....	133
6.2 The Influence of High Pressure on the Kinetics of α-chymotrypsin.....	137
CHAPTER 7. Bibliography	143
CHAPTER 8. Publications and Presentations.....	161
CHAPTER 9. Curriculum Vitae	163

List of Figures

Chapter 1

Figure 1.1	<i>Reaction catalyzed by PLA2</i>	3
Figure 1.2	<i>Ribbon drawing of bee venom phospholipase A2</i>	5
Figure 1.3	<i>Interfacial binding and mechanism of PLA2 action</i>	7
Figure 1.4	<i>Schematic representation of the binding and catalysis by PLA2</i>	10
Figure 1.5	<i>Water-assisted catalytic mechanism of sPLA2</i>	12
Figure 1.6	<i>The proto-oncogene, Ras, acts as a molecular switch</i>	13
Figure 1.7	<i>Regulation of GTPase Trafficking by PDEδ</i>	16
Figure 1.8	<i>Ribbon diagram of the β-sandwich fold of PDEδ</i>	17
Figure 1.9	<i>Structural details of the farnesyl binding to PDEδ</i>	18
Figure 1.10	<i>Superimposition of the crystal structures of F-Rheb–PDEδ and the PDEδ–Arl2-GTP complex</i>	20

Chapter 2

Figure 2.1	<i>The amide I band for secondary structure analysis of proteins</i>	25
Figure 2.2	<i>Diagram of the stopped flow setup</i>	27
Figure 2.3	<i>Fundamental elements of high-pressure stopped-flow spectrometer</i>	28
Figure 2.4	<i>Illustration of the high pressure autoclave (bomb) assembly</i>	29
Figure 2.5	<i>Lateral view of the high-pressure stopped-flow instrument</i>	30
Figure 2.6	<i>The construction of the windows mounts and HPSF observation cell</i>	31
Figure 2.7	<i>Schematic representation of the HPSF measurements</i>	33
Figure 2.8	<i>Schematic display of the fluorescently labeled lipid molecule β-DPH HPC</i>	34
Figure 2.9	<i>Principle of monitoring the PLA2 activity</i>	37
Figure 2.10	<i>Representative ITC data</i>	39
Figure 2.11	<i>Thermodynamic signatures of three different interactions with the same binding affinity</i>	40
Figure 2.12	<i>Generating and maintaining the standing ultrasound wave between transducers</i>	46
Figure 2.13	<i>U-shaped tube of a vibrating densitometer</i>	47

Chapter 3

Figure 3.1	<i>Schematic representation of a typical biomembrane</i>	54
Figure 3.2	<i>Schematic diagram of a phase-separated artificial lipid bilayer with raft and non-raft lipid domains</i>	55
Figure 3.3	<i>p, T-phase diagram for the anionic model raft mixture</i>	56

	<i>lipid hydrocarbon chains</i>	
Figure 3.4	<i>Increase of lipid bilayer thickness induced by pressure</i>	57
Figure 3.5	<i>Conformational changes in bvPLA2 upon pressurization</i>	65
Figure 3.6	<i>Pressure-induced changes in the second derivative amide I' spectra and curve fitting results of the FTIR data for bvPLA2</i>	66
Figure 3.7	<i>Curve fitting results of the FTIR data at 1 bar for bvPLA2</i>	68
Figure 3.8	<i>Model of a lipid vesicle binding bvPLA2</i>	69
Figure 3.9	<i>PLA2 binding to lipid membranes</i>	72
Figure 3.10	<i>Representative association curve of 0.35 μM bvPLA2 to liposomes of anionic raft-like and DOPC/DOPG bilayers at a 62.5 μM lipid concentration</i>	73
Figure 3.11	<i>Pressure-independent PLA2 association kinetics to lipid bilayers</i>	74
Figure 3.12	<i>Pressure dependence of the fluorescence intensity of the β-DPH-HPC fluorophore</i>	75
Figure 3.13	<i>PLA2 activity in the presence of lipid membranes</i>	77
Figure 3.14	<i>Effect of hydrostatic pressure on the rate of DBPC hydrolysis by bvPLA2</i>	80
Figure 3.15	<i>AFM visualization of lipid bilayers with coexisting l_o and l_d domains</i>	83
Chapter 4		
Figure 4.1	<i>A schematic illustration of free-energy and its components changes associated with the binding</i>	90
Figure 4.2	<i>A nonpolar molecule residing within an ice-like cage</i>	93
Figure 4.3	<i>ITC data for titration of farnesylated cysteine into PDEδ</i>	98
Figure 4.4	<i>Temperature dependence of the thermodynamic parameters for binding of PDEδ and farnesylated cystein</i>	100
Figure 4.5	<i>Illustration of Rheb (green) a protein member of Ras superfamily in complex with PDEdelta</i>	101
Figure 4.6	<i>Heat capacity (DSC profiles) for PDEδ (black) and the complex with farnesylated cysteine (red)</i>	103
Figure 4.7	<i>Thermal expansion coefficient, α, (PPC profiles) for PDEδ (black) and the complex with farnesylated cysteine (red)</i>	104
Figure 4.8	<i>Temperature dependence of K_S^0, the partial molar adiabatic compressibility</i>	106
Figure 4.9	<i>Temperature dependence of K_T^0, the partial molar isothermal compressibility</i>	107

Chapter 6

Figure 6.1	<i>Activation volumes, ΔV^\ddagger, and the binding volume, ΔV_{ES}, for an enzymatic reaction</i>	136
Figure 6.2	<i>Pressure induced acceleration of α-chymotrypsin-catalyzed hydrolysis</i>	138
Figure 6.3	<i>Combined effect of high hydrostatic pressure and kosmotropic cosolvent TMAO</i>	140

List of Tables

Chapter 3

Table 3.1	<i>Secondary Structure Content of BvPLA2 at Ambient Pressure as Determined by X-ray Diffraction in Comparison with the FTIR Spectroscopy Data Obtained in this Study (accuracy: $\pm 2\%$).</i>
------------------	--

Chapter 4

Table 4.1	<i>Thermodynamic Parameters Obtained from ITC Experiments for the Association of PDEδ and Farnesylated Cystein.</i>
Table 4.2	<i>Molecular Volumes, V_M, and Solvent Assessable Surface Areas, S_A, of Free PDEδ, the Complex of PDEδ and Farnesyl-Cystein, and Free Farnesyl-Cystein.</i>
Table 4.3	<i>Change in Partial Molar Volume, ΔV_{pr}^0, and Partial Molar Adiabatic Compressibility, ΔK_s^0, upon Binding Determined by Density and Ultrasound Velocimetry Measurements at 25 °C.</i>

List of Abbreviations and Acronyms

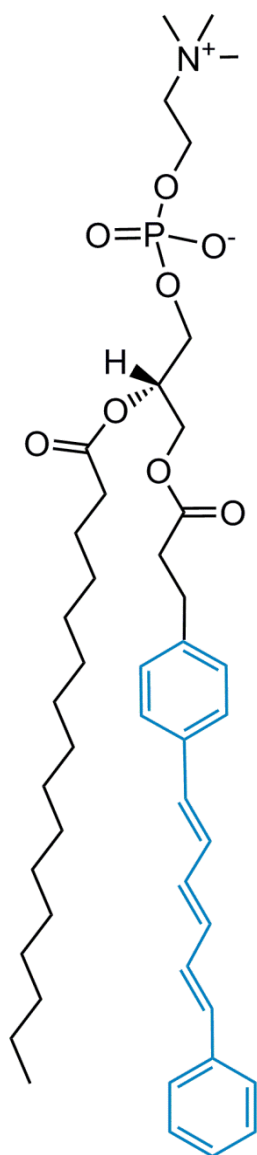
Å	Ångström (1 Å = 0.1 nm = 10 ⁻¹⁰)
α	Thermal expansivity coefficient
AFM	Atomic force microscopy
ASA	Solvent accessible surface area
β -DPH HPC	2-(3-(Diphenylhexatrienyl)propanoyl)-1-hexadecanoyl- <i>sn</i> -glycero-3-phosphocholine
bvPLA2	Bee venom phospholipase A2
Chol	Cholesterol
Da	Dalton
DAC	Diamond anvil cell
DBPC	1-O-(6-Dabacyl-aminohexanoyl)-2-O-(6-[12-BODIPY-dodecanoyl]amino-hexanoyl)- <i>sn</i> -3-glycerylphosphatidylcholine
DOPC	1,2-dioleoyl- <i>sn</i> -glycero-3-phosphocholine
DOPG	1,2-dioleoyl- <i>sn</i> -glycero-3-phospho-(1'- <i>rac</i> -glycerol) sodium salt
DPPC	1,2-dipalmitoyl- <i>sn</i> -glycero-3-phosphocholine
DPPG	1,2-dipalmitoyl- <i>sn</i> -glycero-3-phospho-(1'- <i>rac</i> -glycerol) sodium salt
DSC	Differential scanning calorimetry
FRET	Föster (fluorescence) resonance energy transfer
FSD	Fourier self-deconvolution
FTIR	Fourier transform infrared
ATR-FTIR	Attenuated total reflectance Fourier transform infrared spectroscopy
GAP	GTPase activating protein
GDI	GDP dissociation inhibitor
GDP	Guanosine diphosphate
GEF	Guaninenucleotide exchange factor
HHP	High hydrostatic pressure
HP	High pressure

HP-FTIR	High pressure Fourier transform infrared spectroscopy
HPSF	High pressure stopped-flow
l_d	Liquid-disordered
l_o	Liquid-ordered
IRS	Interfacial recognition surface
NMR	Nuclear magnetic resonance
PDE δ	Delta subunit of cyclic-guanosine-monophosphate phosphodiesterase
PDB	Protein data bank
PLA2	Phospholipase A2
PPC	Pressure perturbation calorimetry
Ras	Rat adeno sarcoma
Rheb	Ras homolog enriched in brain
Tris	Tris(hydroxymethyl)aminomethane
wt %	weight percent

List of Fluorophores

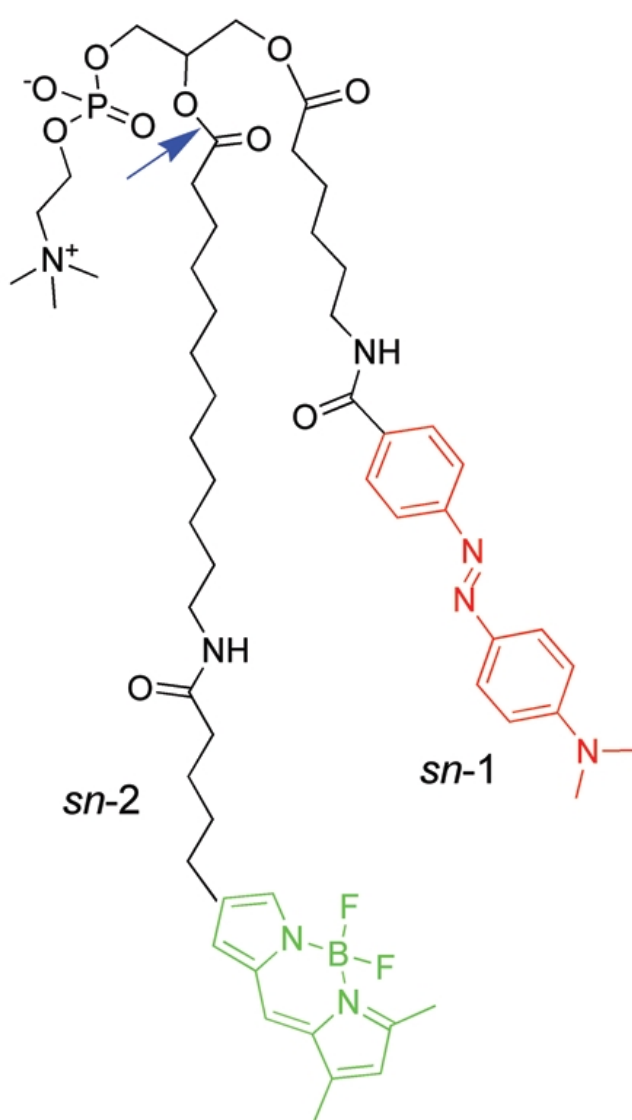
β -DPH-HPC

(2-(3-(Diphenylhexatrienyl)propanoyl)-1-hexadecanoyl- *sn*-glycero-3-phosphocholine)



DBPC

(1-O-(6-Dabcyl-aminohexanoyl)-2-O-(6-[12-BODIPY-dodecanoyl]amino-hexanoyl)-*sn*-3-glycerylphosphatidylcholine)



I

**Introduction
to
Phospholipase A2 and PDE δ**

1.1 Function and Structure of Phospholipase A2

1.1.1 The Phospholipase A2 Superfamily

Phospholipase A2 (PLA2s) are a class of enzymes that specifically hydrolyze the fatty acid from the *sn*-2 position of substrate phospholipids (Figure 1.1).¹ Different members of the PLA2 family play a number of important roles in diverse cellular processes including phospholipid metabolism and digestion, signal transduction and host defense.² At the cellular level, the hydrolysis products of this reaction, that is, free fatty acid, lysophospholipids and their derivatives, have numerous essential downstream roles in biological processes. For example, the *sn*-2 position of phospholipids frequently contains polyunsaturated fatty acids, after release, and these can be metabolized to form different eicosanoids. These compounds

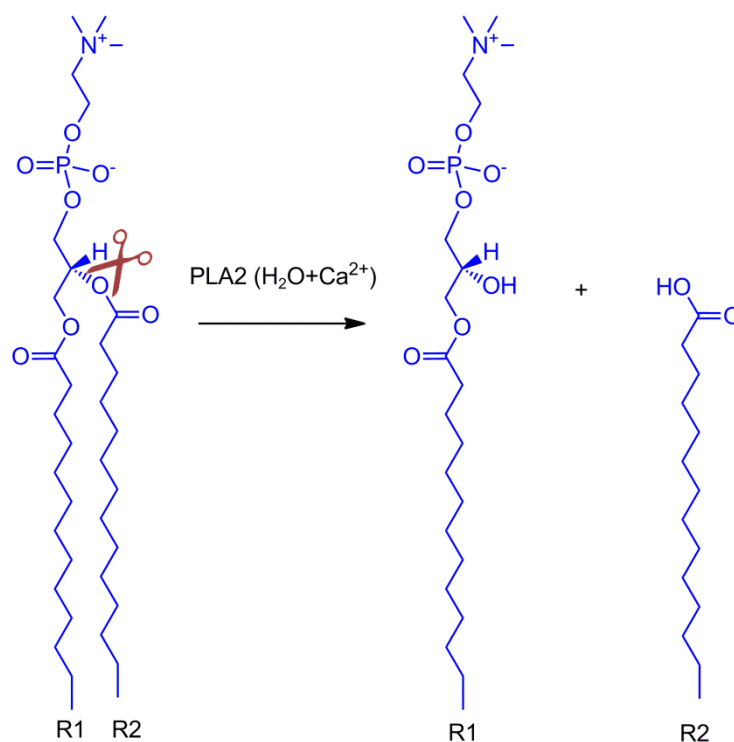


Figure 1.1: Reaction catalyzed by PLA2. Shown is the hydrolysis of the *sn*-2 ester of phospholipid to give free fatty acyl chain (R2) plus remaining lysophospholipid (R1).

are potent lipid mediators of inflammation³ and signal transduction.⁴ The other product of PLA2 action, lysophospholipid, serves as precursor of lipid derived mediators via G protein-

Chapter 1: Function and structure of Phospholipase A2

coupled receptors.⁵ Lysophospholipids also bind receptors and have various effects in regulation of cell physiology, specifically phospholipid remodeling and cell signaling.⁶

The action of PLA2 either changes the local composition of the membrane to remodel its architecture or to disrupt the cell structure entirely. These enzymes have likewise an important role in the degradation of damaged or aged cells.⁷ Interestingly, healthy cells that are naturally resistant to attack by sPLA2s become susceptible to hydrolysis in damaged or apoptotic cells.⁸⁻¹⁰ It has been suggested that physical changes to the cell membrane occurring upon apoptosis results in larger interlipid spacing that facilitates vertical migration of phospholipids into the active site of adsorbed enzyme.¹¹ Secretory PLA2 is also known to be overexpressed in colon, prostate and lung cancers.¹²⁻¹⁴ Since this enzyme is able to hydrolyze drug-encasing liposomes, a possible tool for targeted chemotherapy could be degradation of these liposomes specifically close to the tumor cells due to a high expression level of PLA2.^{15, 16}

The PLA2 superfamily represents a broad range of lipid (*sn*-2 ester bond) hydrolyzing enzymes diverse with regard to localization, sequence, structure, functional mechanism and role of divalent metal ions.¹ Secreted PLA2s (sPLA2s) are one of the major classes of PLA2. Its members are characterized as low molecular weight (13–15 kDa), water-soluble, Ca²⁺-dependent, highly disulfide bonded enzymes. These enzymes possess catalytic histidine and aspartate residues for hydrolysis.¹⁷ Secreted PLA₂s were found in venoms and pancreatic juices of different animals.¹ The pancreatic PLA2s clearly plays a role in the digestion of phospholipids in the stomach, while venom PLA2s are mainly involved in the toxicity of the venoms.² Traditionally, sPLA2s have been classified into three main groups, Group I, II, and III, and several subgroups based on their functional properties, location of their disulfide bridges and primary structure.¹⁸ The PLA2 discussed in this thesis is PLA2 from bee venom (Group III). Although this form has a similar catalytic mechanism to mammalian sPLA₂s,¹⁹ bee venom PLA2s (bvPLA2s) is unique in both its structure and sequence.² In addition to its catalytic activity, bvPLA2 is neurotoxic and binds specifically N-type (neuronal type) receptors, leading to molecular events responsible for neurotoxicity of this protein.^{20,21}

1.1.2 Structure of Bee Venom PLA2

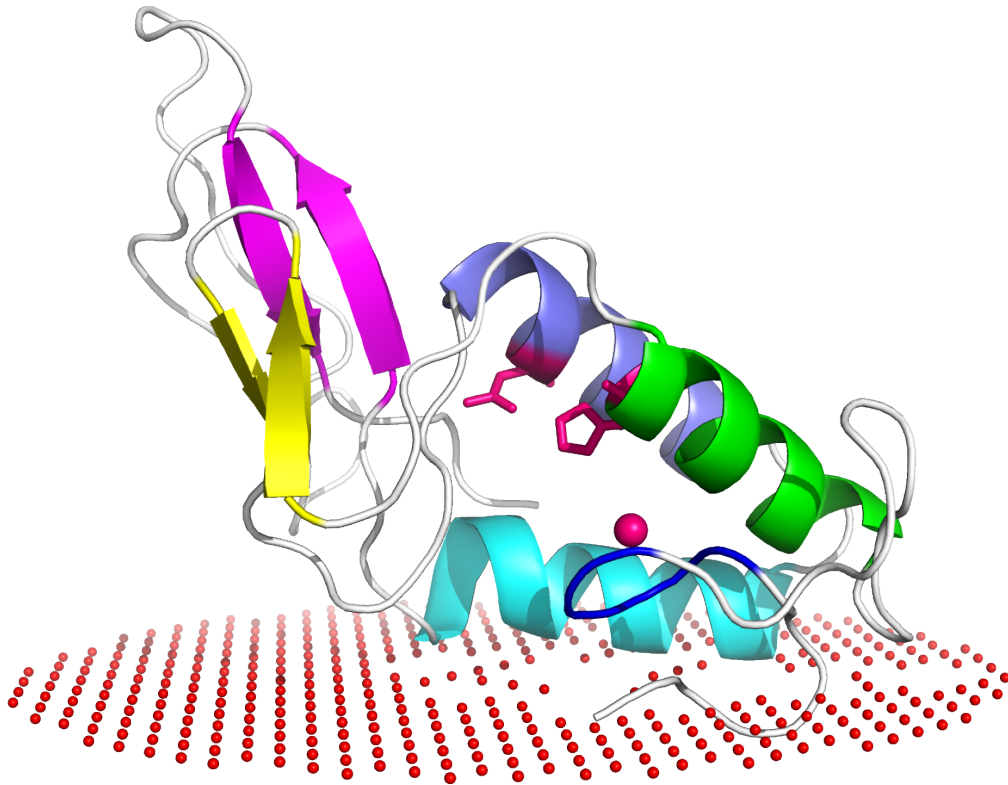


Figure 1.2: Ribbon drawing of bee venom phospholipase (apis mellifera) A2 from group III (PDB ID 1POC).²² This image displays secondary elements and the catalytic His-Asp diad (residues 34, 64, pink). The pink sphere represents the calcium ion that is bound to the protein via the calcium-binding loop (residues 8-12, blue). Two antiparallel alpha helices (residues 25-37, green and 61-74, violet) are main structural elements. They form a hydrophobic channel lined with hydrophobic amino acids that lead substrate phospholipids from the bilayer to the catalytic site.

The X-ray structure of bvPLA2, a 14 kDa, 134 amino acid protein, has been determined by Scott et al. (Figure 1.2).²² In the crystalline state, bvPLA2 possesses around 29% α -helices and 23% β -pleated sheet.²² The structure of phospholipase A2 is dominated by three α -helices, two of them (composed of residues 25-37, green and 61-74, violet) connected by an intermediate antiparallel β -sheet (yellow). These two disulfide-linked α -helices define a rigid scaffold to which the calcium binding loop (8-12, blue) and the C-terminal region including

Chapter 1: Function and structure of Phospholipase A2

antiparallel β -sheet (magenta) are covalently linked by disulfide bridges. Additionally, structural features of sPLAs also include the Asp-His dyad (34, 64, pink) catalytic site and the interfacial recognition surface (IRS), the region which forms direct contacts with the target membrane surface.²² The putative IRS of bvPLA2 is composed of residues that lie on one face of α -helix (residues 77-90, cyan) and of portion of N-terminal loop, containing the calcium binding region.²⁰ The protein IRS region, that is thought to anchor the enzyme to the membrane interface, is also responsible for binding enzyme to N-type receptors.^{20,21} The IRS and active site of PLA2 correspond to different regions of the protein. Thus, the interfacial binding of the enzyme to the membrane and the binding of a single substrate molecule to the catalytic site of the enzyme are considered as two distinct steps.²³

A central question is how the enzyme binds to a phospholipid molecule that is part of the membrane-water interface. The active site of the PLA2 is connected to the protein surface via an active site cavity, the so called hydrophobic channel. This channel is likely more open upon enzyme docking with a membrane. Phospholipid substrates one at a time move through the hydrophobic channel towards the active site of the enzyme. The active site is located at the top of a cavity in the center of the molecule (Figure 1.3). Several studies have shown that a substrate lipid molecule has to diffuse significantly from the membrane structure in order to fit into the active site.^{7,24} This protruded lipid configuration is stabilized by hydrophobic amino acid residues exposed along the sides of the hydrophobic channel. The estimated distance from the surface of the membrane plane to the active site of the enzyme is approximately 1.5 nm. This distance roughly corresponds to the half-length of an extended substrate lipid molecule.²⁵ As phospholipid moves into the channel, an enzyme bound Ca^{2+} ion (green on Figure 1.3) binds to the phosphate in the head group, thereby positioning the ester bond to be cleaved next to catalytic site.²⁶

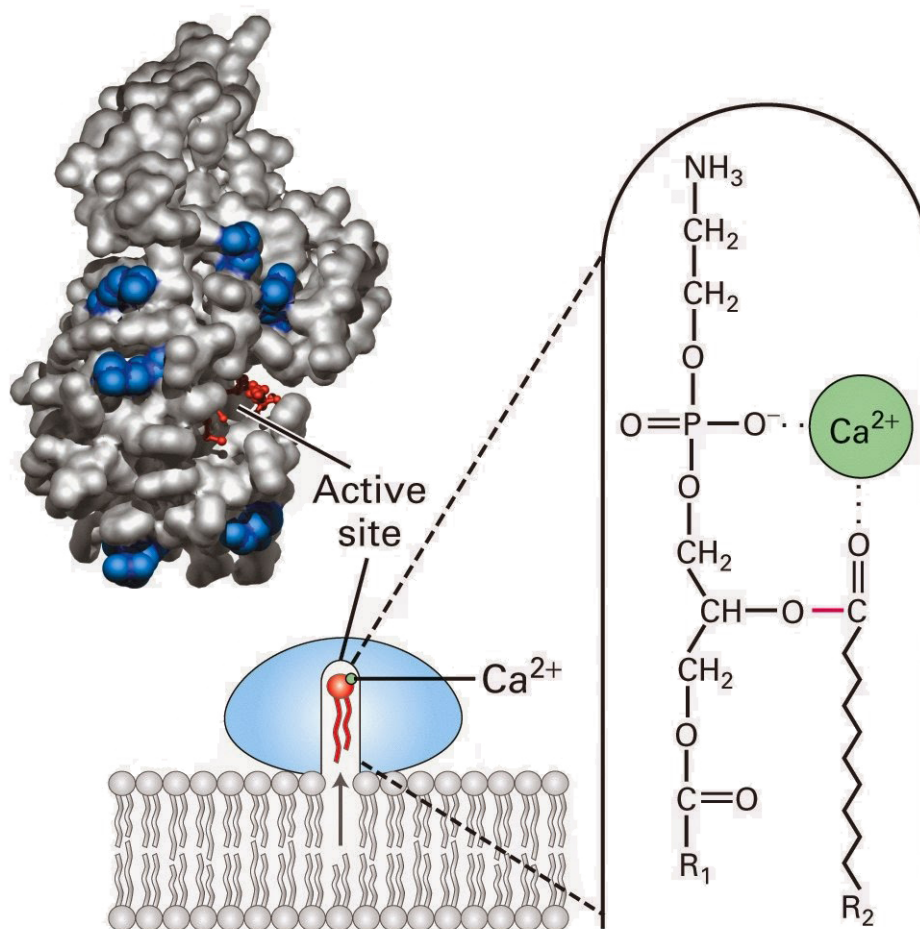


Figure 1.3: Interfacial binding and mechanism of PLA2 action. A small conformational change in phospholipase A2 induced by binding to the water-lipid interface opens the hydrophobic channel and fixes the protein to the phospholipid heads. The Ca^{2+} containing active site is buried in a channel enriched with hydrophobic amino acids that facilitate diffusion of a phospholipid from the bilayer to the catalytic site. Adapted from ref.⁷

1.1.3 Secretory PLA2 Interfacial Binding and Activity

The secreted PLA2 enzymes share the property to act optimally when the phospholipid substrate is present as a part of an interface, such as a micelle or membrane. This process, where the protein is activated by interaction with a phospholipid interface, is termed interfacial activation.²⁷ Understanding the mechanism of interfacial activation and the protein orientation upon lipid binding has long been an aim of mechanistic studies of the secreted PLA2s.¹⁷

Unfortunately, it is extremely hard to acquire crystals of PLA2 in the presence of interfacial phospholipid. Up to this point, it has only been possible to obtain high-resolution X-ray crystal structures with nonhydrolyzable monomeric substrate analogues. Two different, but complementary models have been proposed to clarify the interfacial activation phenomenon. According to the “enzyme model”, the enzyme is activated by means of a structural change upon binding at the lipid-water interface.²⁸ In contrast, the “substrate model” recommends that the physicochemical properties of the lipid membrane are key determinants for the enzyme activity.²⁹ These properties of the membrane interface include surface charge, structural defects, phase separation, curvature, membrane fluidity and lipid packing densities.³⁰ One example would be a significant increase in PLA2 activation in the presence of vesicles with gel-liquid crystalline phase transition regions. In this case, the irregularities between the phases allow the protein to penetrate smoothly into the lipid surface.²⁹ These results provide evidence that the undergoing changes in the bilayer physicochemical state are controlling the action of the phospholipase. Furthermore, most X-ray studies on sPLA2s revealed similar structures of these enzymes with and without bound inhibitory substrate analogs. This additionally finding contradicts the enzyme model of PLA2 activation.

On the other hand, small structural differences are still found by X-ray crystallography between the free and complexed forms of a type II PLA2. Structural analyses showed that the N-terminal helix and the Ca²⁺-binding loop are shifted towards each other in the presence of substrate analog.³¹ In addition, NMR studies revealed that in the free enzyme the N-terminus and catalytic residues His and Asp are flexible; but they adopt a fixed conformation upon complex formation between the enzyme and substrate micelles.³² It has been suggested that conformational changes upon membrane binding, switch protein from an inactive to a catalytically active state. Eventually, Tatulian using the ATR-FTIR spectroscopy method described a direct correlation of the membrane’s physical properties with the enzymatic structural changes upon membrane binding.²⁷ This finding unified the enzyme and substrate hypothesis of interfacial activation of PLA2 and implied that both membrane and enzyme factors are synergistic and complementary determinants of the activation of membrane-attached PLA2.²⁷

Structural analyses uncovered that sPLA2s have an identical catalytic motif (hydrophobic channel in conjunction with a Ca²⁺ binding loop),³³ but vastly diverse interfacial recognition surfaces that regulate their binding affinity for various types of phospholipid vesicles.²⁶ It has

been demonstrated that 10-20 amino acids of PLA2 bind to tens of phospholipids on the outer monolayer surface of the membrane.³⁴ The exact amount of phospholipids forming one binding site for an enzyme is about 20–40 phospholipids in the membrane interface, depending on the PLA2 isoform. There is an ongoing debate over what types of interactions, including electrostatic, hydrogen bonding, and hydrophobic interactions, modulate the effective interfacial binding^{34,35} In general, the interface of sPLA2s contains hydrophobic residues and two or more cationic Arg (arginine) and Lys (lysine) residues. As a result of these charged residues, the interfacial binding site of sPLA2s has a positive electrostatic potential which explains the high affinity of some isoforms for anionic interfaces.²⁶ However, the relative importance of electrostatic and hydrophobic interactions in interfacial binding must ultimately depend both on the physicochemical composition of the membrane and on the structure of the interfacial recognition site (IRS).²⁶ PLA2s containing a Trp (tryptophan) in their lipid binding surface display the highest activity towards neutral lipid substrates. In contrast, PLA2s with an excess of basic residues in their lipid binding surface display the highest activity toward negatively charged surfaces.³⁶

Electron paramagnetic resonance (EPR) experiments on bvPLA2 have determined the orientation of the enzyme with respect to the membrane-aqueous interface. It was shown that in contrast to most PLA2s, bvPLA2 sits on the membrane surface rather than digging into the membrane.³⁷ Furthermore, the study revealed that the six basic residues on the face of the enzyme, except one (K14), are not in close contact with the membrane interface. The residues that are in direct contact with the interface are hydrophobic. These hydrophobic residues are not deeply inserted into the hydrophobic interior of the bilayer but “somehow” provide a micro-interfacial environment that drives interfacial binding to the polar phospholipid head groups.³⁷ Subsequent studies have confirmed that bvPLA2 binds with a non-electrostatic mechanism^{34,38} and does not penetrate significantly into the membrane like other PLA2s.³⁹

The kinetics involved in the action of the protein towards substrate aggregates can be analyzed using the classical Michaelis-Menten theory adopted for the action of enzymes at interfaces.⁴⁰ The action of phospholipase A2 is plotted in Figure 1.4.

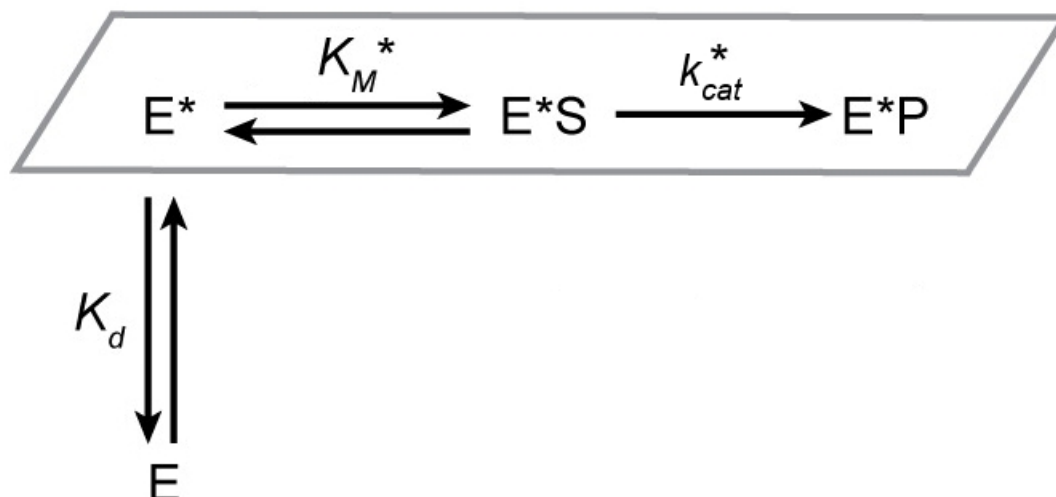


Figure 1.4: Schematic representation of the binding and catalysis by PLA2 at the water–lipid interface. The parallelogram frame displays the steps occurring on the membrane. K_M^* is the interfacial Michaelis constant while k_{cat}^* represents the interfacial turnover number. E is the free enzyme in the aqueous phase, E^* represents the “activated” form of the enzyme which is formed upon the interaction of the enzyme with the membrane interface. E^*S is PLA2 attached to the water-lipid interface with the active site occupied by a single substrate phospholipid (E^*S is similar to the well-established Michaelis complex, ES , for an enzyme operating in a homogeneous, fluid environment). E^*P represents the enzyme attached to the interface with the hydrolysis products (fatty acid and lysophospholipid) in the active site.²³

It has been suggested that the initial step includes a more general reversible binding of the enzyme (E) to the interface, but not to individual phospholipid molecules. This creates an interfacially activated enzyme (E^*), which afterwards binds a phospholipid substrate (S) as displayed in Figure 1.4. Thus, the enzyme bound to the membrane can exist with its active site devoid of bound substrate (E^* state), containing bound substrate (E^*S), which is a classical Michaelis complex, or containing bound product (E^*P). Kinetic proof for these distinct enzyme states comes from the observation that, in particular cases, multiple catalytic cycles can occur without the desorption of the enzyme into the aqueous phase (scooting mode catalysis). This happens when binding of the enzyme to the interface is sufficiently tight, usually in the presence of a large fraction of anionic lipids.⁴¹ The substrate specificity of a PLA2 is controlled by a composite of two factors.⁴² The first is the ability of the enzyme to bind to the membrane surface (E^* to E equilibrium dissociation constant, K_d in Figure 1.4). Second, once bound, the relative rate of the hydrolysis of different substrate species by E^* is controlled by the relative interfacial specificity constant (k_{cat}^*/K_M^* in Figure 1.4).

1.1.4 Mechanism of the sPLA2 Reaction

Initially, the catalytic mechanism of the chemical reaction of bvPLA2 was proposed by Scott et al.⁴³ Their study revealed that sPLA2s catalyze the hydrolysis through the same mechanism of abstraction of a proton from a catalytic water molecule followed by a nucleophilic attack on the *sn*-2 bond of phospholipids.⁴³ Later studies proposed alternative mechanisms wherein two active site water molecules (instead of one) participate in the formation and subsequent breakdown of the tetrahedral intermediate (Figure 1.5).^{44,45} In this model, the water molecule involved in the formation of the tetrahedral intermediate is mediated by Ca²⁺, whereas the water molecule involved in the breakdown is activated via H-bonding by His (histidine). These two water molecules are bridged, correlating Ca²⁺ and the catalytic His. The role of His as a proton acceptor is to stabilize the associated water required for the proton donation during the decomposition of the tetrahedral intermediate. This process is assisted by negatively charged Asp residue (aspartate). In addition to coordination of a catalytic water molecule, Ca²⁺ ion, orients and polarizes the *sn*-2 carbonyl oxygen group of phospholipids, which eventually results in formation and stabilization of tetrahedral intermediate of the PLA₂ reaction. Subsequently, a fatty acid and a lysophospholipid are released as a result of the collapse of the tetrahedral intermediate, which is suggested to be the rate-limiting step of the reaction.⁴⁴

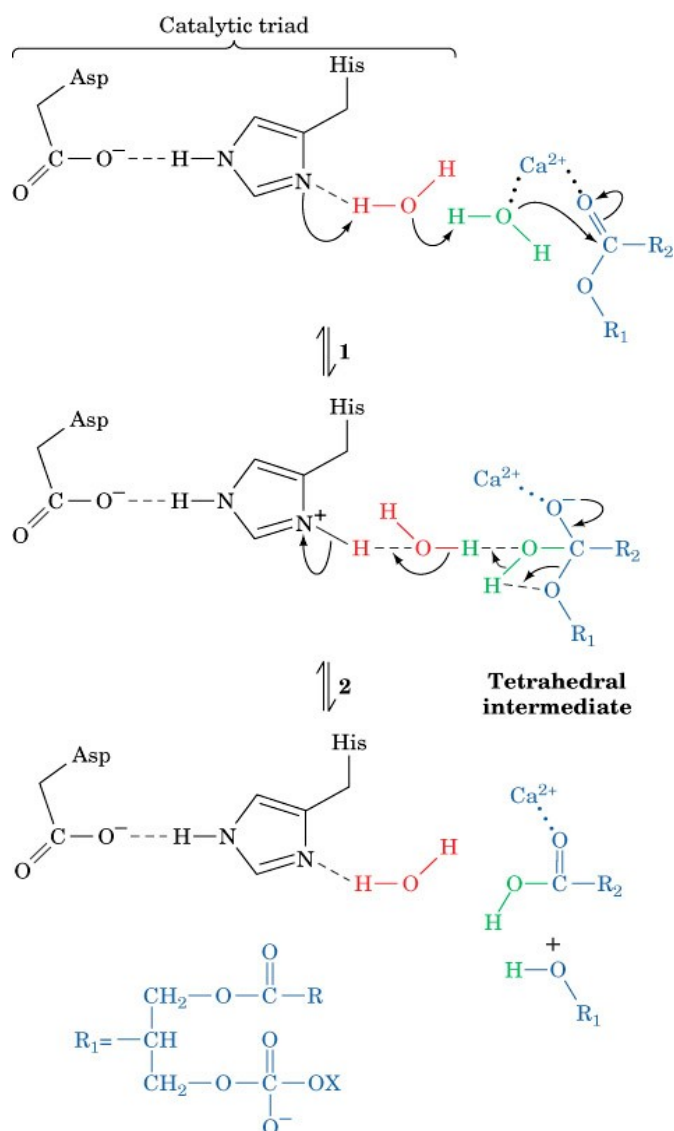
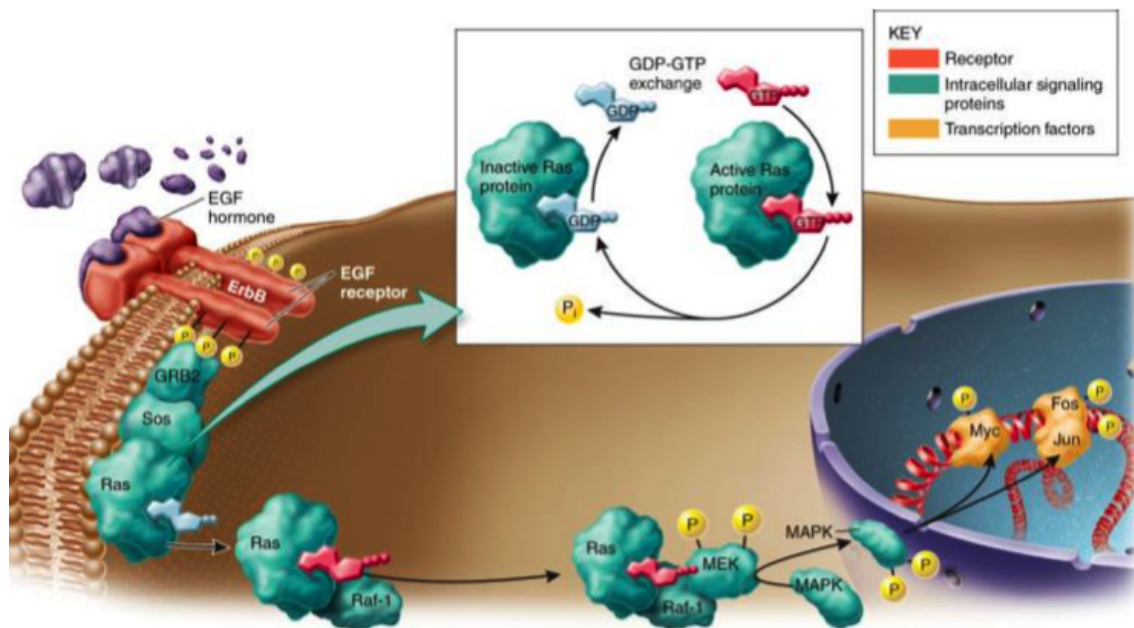


Figure 1.5: Water-assisted catalytic mechanism of sPLA2.⁴⁴ A calcium-coordinated water molecule (w5) is proposed as the attacking nucleophile; while the proton exchange of the second water (w6) linked to catalytic His is proposed to contribute to the formation and breakage of the tetrahedral intermediate.

1.2 Structural and Functional Aspects of PDE δ , a Cytosolic Carrier for Farnesylated Ras Proteins

1.2.1 GTP Binding Proteins

Ras-like small GTPases belong to GTP binding proteins (G proteins), which together with their associated regulators and effectors are key to signal transduction pathways.⁴⁶ For instance, Ras proteins through a signaling Ras/MAPK pathway can receive multiple signals from outside cells surface receptors and relay the signal to the nucleus. This results in regulation of vital cellular processes such as normal cell growth, development and apoptosis in response to external signals. In order to control complex cellular processes, Ras proteins act as molecular switches by cycling between an inactive GDP-bound “off” and an active GTP-bound “on” conformational states. This cycle is illustrated in Figure 1.6.



Active Ras promotes cell division – its normal activation pathway (shown above) is by GTP binding. In some cancers, the Ras gene has sustained mutations that make it continuously activated, thus continuously stimulating cell division.

Figure 1.6: The proto-oncogene, Ras, acts as a molecular switch.⁴⁷

In response to the activation of cell surface receptors, Ras proteins switch to an "on conformation" by binding to GTP. This allows activated Ras proteins to interact with high

Chapter 1: Functional and Structural Aspects of PDEδ

affinity to downstream effectors, which generate specific responses until GTP hydrolysis switches the protein back into the “off-conformation”. Activation of Ras proteins is further regulated by (1) guanine nucleotide exchange factors (GEFs), which trigger the release of (GDP) and subsequently permit binding to GTP, and (2) GTPase activating proteins (GAPs) that stimulate hydrolysis of Ras-bound GTP (Figure 1.6).⁴⁸ Members of the Ras family of GTPases also play a role in oncogenesis. Oncogenic Ras mutations suppress their deactivation often by inhibiting GAP-induced GTP-hydrolysis. Hence, the Ras protein is in a constant "on-conformation" and the persistent transitions of deregulated signals to the cell nucleus causes uncontrolled cellular growth, which eventually leads to cancer. In fact, Ras mutations, including those of K-Ras, H-Ras and N-Ras, are found in many tumor types, including roughly half of all colon cancers and 90% of pancreatic carcinomas.⁴⁹

The function of certain members of the Ras superfamily is critically dependent on their association with membranes and their cellular compartmentalization. The majority of Ras superfamily members carry a CAAX motif (C denotes the cysteine; AA, two saturated aliphatic residues; and X, any residue) at their C-terminus that target them to a specific subcellular location. In fact, many RAS proteins are post-modified at their cysteine(s) located in the CAAX box by the addition of one or more farnesyl or geranylgeranyl lipid tails. Prenylation with such 15-20-carbon hydrophobic membrane anchors allow association with the inner surface of the plasma membrane, where Ras proteins perform their normal, as well as their cancer associated, signaling activity.⁵⁰ The corresponding prenyl-cysteine thioether bond is catalyzed by farnesyltransferase (FTase) and geranylgeranyltransferase 1 (GGT1) enzymes, respectively.⁵¹ Protein prenylation is common and found in approximately 2% of all proteins expressed in eukaryotic cells.⁵²

Furthermore, Ras proteins necessitate a carrier GDI protein (guanine nucleotide dissociation inhibitor) for effective subcellular compartmentalization. The primary function of a GDI is to modulate the cycling of Ras proteins between the cytosol and membranes. GDIs solubilise Ras proteins into the cytosol by forming a high affinity complex, in which the Ras prenyl group(s) is deeply buried into the hydrophobic pocket of the immunoglobulin-like β sandwich of the GDI. Thus, prenylation and membrane trafficking offers further activation and regulation essential for certain Ras proteins for proper localization at the plasma membrane.⁵³

1.2.2 PDE δ as a Regulatory Molecular Chaperone

The 17 kDa PDE δ is a prenyl binding protein, which was originally identified as soluble delta subunit of the retinal rod phosphodiesterase PDE δ .⁵⁴ However, later studies revealed that PDE δ is a binding partner for various prenylated G proteins of the Ras sub-family like Rac, Rap, Rho, Rheb, RhoA, RhoB, and RhoG.^{55,56} Furthermore, the PDE δ protein sequence is highly conserved all through the animal kingdom, with 50% sequence homology among invertebrates and at least 70% sequence identity within vertebrates.⁵⁶ According to the sequence similarity search, mouse, bovine, and human PDE δ share over 97% sequence identities.⁵⁷ The broad pattern of PDE δ expression implies that PDE δ could be involved in various key cellular functions.⁵⁸ One of the most interesting properties of PDE δ is its contribution to deliver prenylated proteins to the plasma membrane. For instance, an in vitro study suggests that PDE δ protein delivers farnesylated K-Ras to the model membrane vesicle and then releases it upon membrane contact, which finally leads to membrane attachment of K-Ras.⁵⁹ The property of PDE δ to contribute to the delivery of prenylated Ras proteins to plasma membranes, where signaling is initiated, became of particular interest for the development of PDE δ -Ras targeted anticancer agents.⁶⁰

Unfortunately, intensive efforts within the last three decades to inhibit Ras signaling through various strategies have had disappointing results. The main strategies of "drugging" the Ras-related cancers included direct targeting the GTP binding site of Ras or to inhibit Ras signaling through preventing posttranslational modifications needed for association with the plasma membrane. In the first instance, GTP is present intracellularly at micromolar concentrations and bind to Ras proteins with picomolar affinity, and thus, the design of drugs with higher affinity is challenging.⁴⁶ In the second case, farnesyltransferase inhibitors were reported to successfully block membrane association of H-Ras but they were ineffective against other Ras members. For instance, K-Ras was still able to attach to the inner side of the plasma membrane through geranylgeranylation with geranylgeranyltransferase-I, which modifies Ras with a geranylgeranyl, instead of a farnesyl group.⁶¹ On the other hand, tumors caused by Ras mutations are also difficult to treat because Ras proteins lack well-defined surface pockets suitable for a small molecule binding with high affinity. An earlier study found that suppression of PDE δ levels disrupts Ras association with the plasma membrane and decreases the growth of Ras depended mutant tumour cells.⁶² Later, cellular experiments demonstrated how K-Ras localization, and thus, signaling is controlled by PDE δ together

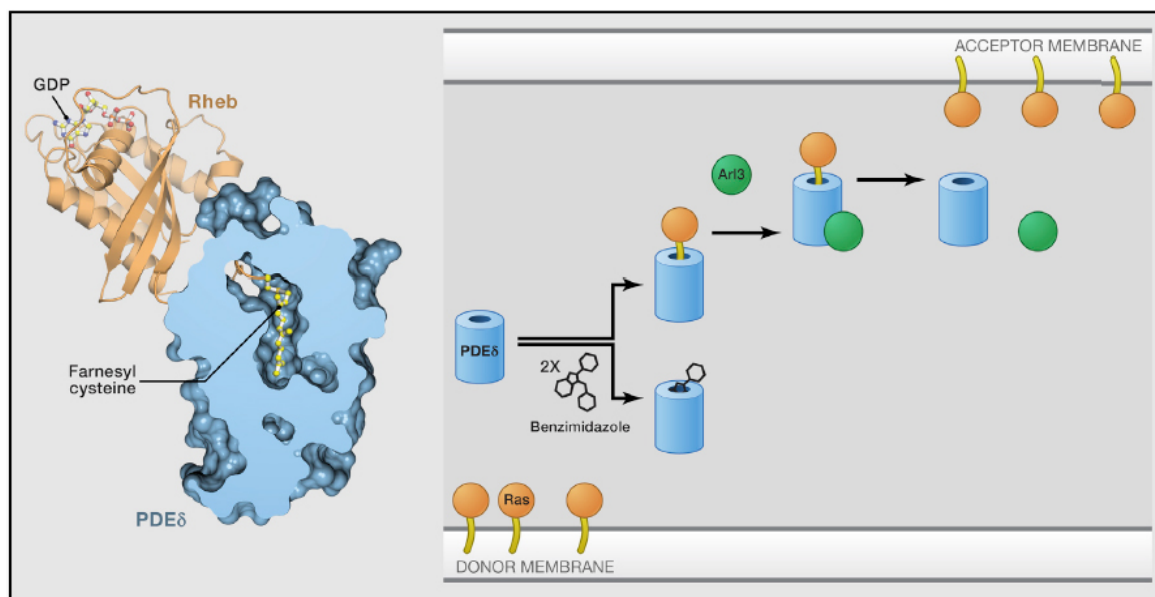


Figure 1.7: Regulation of GTPase trafficking by PDE δ . In order to prevent proper cellular localization of K-Ras (or Rheb) and suppress signaling, benzimidazole-based compounds were developed that inhibit the Ras-PDE δ interaction by plugging the farnesyl-binding cavity (right).⁶¹

with the release factor Arl2.⁶³ Considering the importance of PDE δ for proper Ras signaling, interaction between PDE δ and Ras was targeted for the development of a new approach for anticancer therapy.⁶⁰ In this regard, structural-based small-molecules were designed that bind to the farnesyl-binding pocket of PDE δ and inhibit its binding to the K-Ras isoform.⁶⁰ Fluorescence lifetime imaging microscopy-based FRET measurements demonstrate that interruption of the coupling of farnesylated K-Ras and prenyl binding protein PDE δ results in solubilization and relocation of K-Ras aside from the plasma membrane to intracellular membranes and therefore suppresses K-Ras activity (Figure 1.7). Thus, this approach may provide a novel opportunity to disrupt the oncogenic Ras signaling pathway. Moreover, the PDE δ inhibitor significantly reduced tumor volume in KRAS-mutant PDAC xenografts relative to control animals.⁶⁰ This innovative study initiated a new drug discovery campaign on drugging the farnesyl binding pocket of PDE δ to disrupt plasma membrane localization of RAS GTPases. Therefore, the K-Ras–PDE δ interaction became an important therapeutic target. The thermodynamic description of driving forces behind Ras–PDE δ interaction in combination with structural data is of particular importance for the optimization of structure based design of a inhibitors that target Ras oncoactivity.

1.2.3 Structure of PDE δ

The structure of PDE δ features an immunoglobulin-like β -sandwich fold forming a large hydrophobic pocket into which the C-terminal farnesyl (C15) or geranylgeranyl (C20) prenyl side chains of diverse interacting proteins/peptides may insert.^{64,65} A hydrophobic pocket is formed between strands β 1, β 2, β 4, β 7 on one side and β 3, β 5, β 6, β 8, β 9 on the other. The N-terminal region forms an α -helix (α 1) and the loop connecting β 7 and β 8 is disordered (not revealing an ordered structure due to high flexibility).⁶⁵ Due to the similarity in folding it was

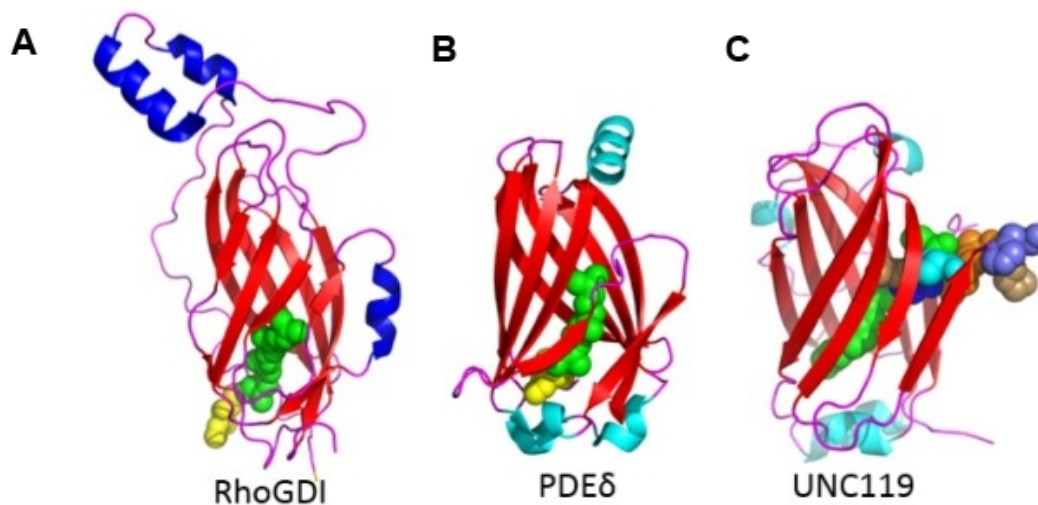


Figure 1.8: Ribbon diagram of the β -sandwich fold of (A) RhoGDI, (B) PDE δ , and (C) UNC119 structures.⁵⁶

proposed that the action of PDE δ is similar to that of Rho guanine nucleotide dissociation inhibitors (GDIs), which also use a β sandwich fold to recognize the geranylgeranyl moiety of the Rho GTPase.⁶⁶ Additionally, the β -sandwich fold of PDE δ is closely related to other lipid-binding proteins, such as, Uncoordinated 119 (UNC119).⁶⁷ Despite the striking structural similarities between these polypeptides, the overall sequence homology is rather low. Sequence alignments of human PDE δ reveal approximately 20% amino acid sequence identity with RhoGDI and 24 % sequence similarity with UNC119. Major structural differences among these three proteins consist of the loop lengths and structures connecting β -sheet and the N-terminal regions (Figure 1.8).⁶⁵ A common feature of these lipid-binding proteins is that they solubilize lipidated proteins, thereby modulate the cycling of GTPases

between cytosol and membranes. While PDE δ and RhoGDI both preferentially interact with prenyl groups, UNC119 transports myristoylated proteins in the cell.^{67,68}

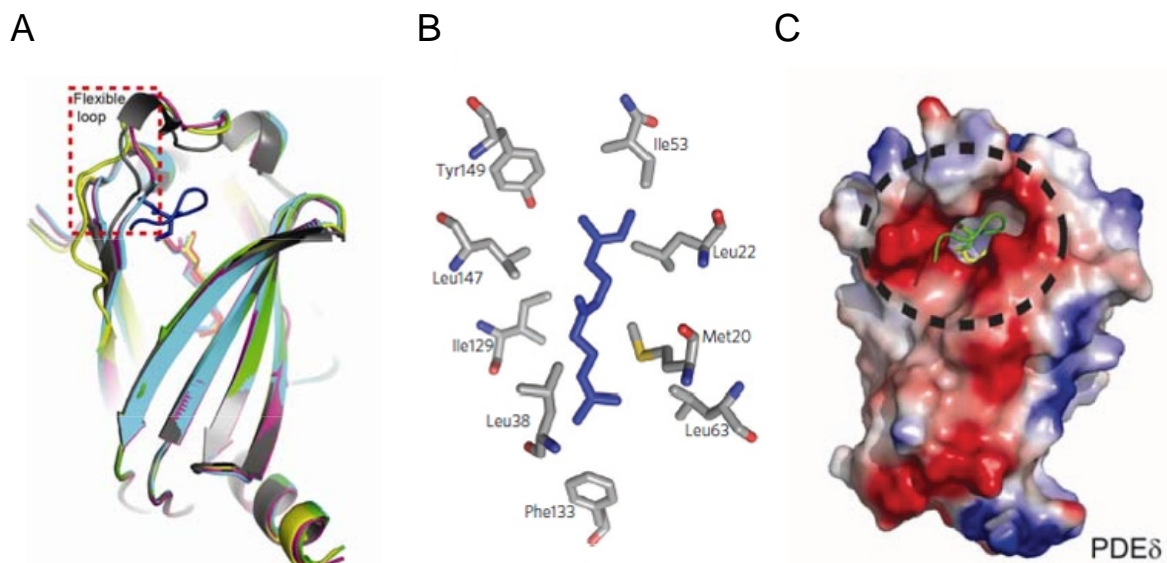


Figure 1.9: Structural details of the farnesyl binding to PDE δ . (A) Superimposition of four molecules to reveal the flexible loop of PDE δ . (B) Residues forming the PDE δ hydrophobic pocket around the farnesyl. (C) Surface charge distribution of PDE δ . Red color represents negative charge; blue represents positive charge; and white color represents neutral charge.⁶⁴

The 1.7-Å crystallized structure of PDE δ in complex with farnesylated Rheb (Ras-like homolog expressed in brain) demonstrates that the farnesyl group of Rheb deeply buried in a hydrophobic pocket formed by PDE δ , which constitutes 80% of the total buried surface area, implying that an interaction occurs almost exclusively via the *S*-farnesylated C-terminus.⁶⁴ Rheb C-terminal residues contact PDE δ by means of main-chain atoms with a buried surface area of 1,007 Å² that incorporates a PDE δ flexible loop. This flexible loop is missing in the crystal structure of PDE δ in complex with Arl2 protein and can adopt distinctive conformations, as revealed by superimposing diverse molecules of the F-octapeptide–PDE δ complex (Figure 1.9 A). The flexibility of this loop together with main-chain predominantly polar interactions support the concept of broad specificity of PDE δ .⁵⁵ Several hydrophobic residues constitute the nonpolar binding pocket for farnesylated cysteine (Figure 1.9 B). Substitution of one of those hydrophobic residues, Met20 to lysine, diminishes the binding affinity of the mutant by a factor of 18 in comparison to that of the wild type.⁶⁴ The hydrophobic pocket of PDE δ does not require a contribution from Rheb, which explains the nucleotide-independent binding of G proteins to it.⁶⁴ Therefore, since PDE δ in the absence of

polypeptide chains forms stable complexes with prenyl side chains⁵⁸ the interaction between these proteins can be mimicked for simplicity by farnesylated peptides of different lengths/sequences or prenyl side chains.⁶⁹ However, the interaction of PDE δ with domains of the prenylated protein may strengthen or weaken the interaction.⁵⁸ The PDE δ surface close to the Rheb C terminus is negatively charged (Figure 1.9 C), that may facilitate binding to the positively charged C terminus of G proteins, for example K-Ras.

In contrast to RhoGDIs that use a second domain to contact the switch regions of the GTPase, the nucleotide-bound state of the G protein is not sensed by PDE δ , thus the interaction between the two proteins is regulated by other mechanisms.⁶⁴ When bound to Rheb, the hydrophobic binding pocket of PDE δ is in an “open” conformation to be able to accommodate prenyl side chains. The structural and biophysical analysis suggests that the binding of Arl2-GTP or Arl3-GTP to the PDE δ -Ras complex forms a short-lived ternary complex, both *in vitro* and in cells that allosterically induces PDE δ to release farnesylated cargo at a specific location in the cell,^{64, 65} establishing that GTP-bound Arl proteins act as GDI displacement factors (GDFs) (Figure 1.10).^{64,68} Lipid-independent binding of nonprenylated Arl proteins to PDE δ is enabled by parallel inter-protein β -sheet interactions. The interface between ARL2-GTP and PDE δ is formed basically by the β 7 of PDE δ and β 2 strand from ARL2 constituting switch regions. The binding site of Arl2/3 on PDE δ is therefore distinct from the binding site of farnesylated proteins. In complex with Arl2-GTP, residues of PDE δ 's hydrophobic pocket, for example, Met20, Ile129 and Arg61, are moved toward the inside of the pocket and confront with the farnesyl group.⁶⁴ PDE δ associates particularly with ARL2 and ARL3 only in the GTP-bound form. GDFs serve as a displacement factors for small prenylated G proteins from their lipid binding proteins, preventing further interaction by stabilizing the “closed” form of the GDI, as for PDE δ .⁵⁷ Interestingly, ARL3-GTP additionally assists cargo release from UNC119, however by a completely distinctive mechanism in which the β -sandwich opens to discharge lipidated protein cargo.^{68, 70}



Figure 1.10: Superimposition of the crystal structures of F-Rheb–PDE δ (PDB 3T5I) and the PDE δ –Arl2-GTP complex (PDB code 1KSJ). This reveals Arl controlled conformational change of PDE δ between open and closed conformations for binding or release of a farnesyl group, respectively.⁶⁴

II

Experimental Procedures & Biophysical Methods

2.1 MATERIALS

2.1.1 Phospholipids and Reagents

Products	Manufacturer
DOPC	Avanti Polar Lipids, USA
DOPG	Avanti Polar Lipids, USA
DPPC	Avanti Polar Lipids, USA
DPPG	Avanti Polar Lipids, USA
Cholesterol	Sigma-Aldrich, Germany
β -DPH HPC	Setareh Biotech, USA
DBPC	Echelon Biosciences, USA
Phospholipase A ₂	Sigma-Aldrich, Germany
S75 column	GE Healthcare, Germany
Glutathione Agarose Beads	Sigma-Aldrich, Germany
N-acetyl-S-farnesyl-L-cysteine	Cayman Chemical, USA

Instruments and Software

Instrument	Manufacturer
Nicolet 6700 IR spectrometer	Thermo Fisher, USA
High pressure FTIR cell	Diamond Optics, USA
SX. 18MV Stopped-flow apparatus	Applied Photophysics, USA
HPSF-56 HP Stopped-flow system	TgK Scientific, UK
Atomic Force Microscopy	Digital Instruments, USA
VP-ITC Calorimeter	Microcal Inc., USA
VP-DSC Calorimeter	Microcal Inc., USA
VP-PPC Calorimeter	Microcal Inc., USA
Ultrasonic resonator	TF Instruments, Germany
DMA 5000 densitometer	Anton Paar, Austria

Software	Manufacturer
Origin 9.0	Origin Labs, USA
GRAMS 8.0	Thermo Fisher, USA
Kinetic studio 4.07	TgK Scientific, UK
Chem Draw 12.0	Perkin Elmer, USA

2.1.2 PDE δ Expression and Purification

The expression construct for full length PDE δ in pGex-5t was a kind gift from Prof. A. Wittinghofer (Max Planck Institute of Molecular Physiology, Dortmund). Glutathione S-transferase (GST)-tagged recombinant PDE δ was expressed in *Escherichia coli* BL21 cells.⁵⁸ Overnight cultures were diluted 1 in 20 and grown at 37 °C in a bubbling system for highly parallel protein expression until an A600 \approx 2.5 was reached, cooled to 20 °C and induced with 0.1 mM isopropyl- β -D-Thiogalactopyranoside (IPTG) for about 16 h. GST-tagged PDE δ was affinity purified using glutathione-agarose beads, and eluted from the beads by cleavage of the GSTtag by TEV protease prior to gel filtration on a S75 column.

2.2 Spectroscopic Methods

2.2.1 Fourier-Transform Infrared (FTIR) Spectroscopy

Infrared (IR) spectroscopy is one of the traditional experimental techniques, which is a popular tool for elucidation of the secondary structure of polypeptides and proteins.⁷⁰ The fundamental advantages of FTIR over other methods are that spectra can be recorded for proteins in a large variety of environments, requiring relatively little time and sample quantity. The amide I band (1700-1600 cm⁻¹) is the most sensitive and prominent spectral region to the protein secondary structure of the backbone, which is mainly induced by C=O stretch vibrations of the peptide linkages. Deuterium oxide (D₂O) is often used as a solvent in IR experiments, due to the strong water absorption in the most critical spectral region at around 1640 cm⁻¹. The frequency of the amide I band components are in close correlation with the individual secondary structural elements of the protein.⁷¹ The most well established approach to acquire the secondary structure is fitting the amide I band with component bands

after identifying their position with band narrowing techniques.⁷² A typical example of such curve fitting results is displayed in Figure 2.1 (A).

Instrumentation, spectral collection and analysis

The pressure-dependent FTIR spectra were recorded using a Nicolet 6700 IR spectrometer equipped with a liquid nitrogen cooled MCT (HgCdTe) detector (Thermo Fisher Scientific). The infrared light was focused by a spectral bench onto the pin hole of a diamond anvil cell (with type IIa diamonds from Diamond Optics) as described previously (Figure 2.1 B).⁷³ High pressure in a diamond anvil cell is generated by application of a moderate force on a small area. For pressure estimation, calibrant barium sulphate was placed in the hole of the steel gasket of the diamond anvil cell. Consequently, the changes in pressure were quantified by

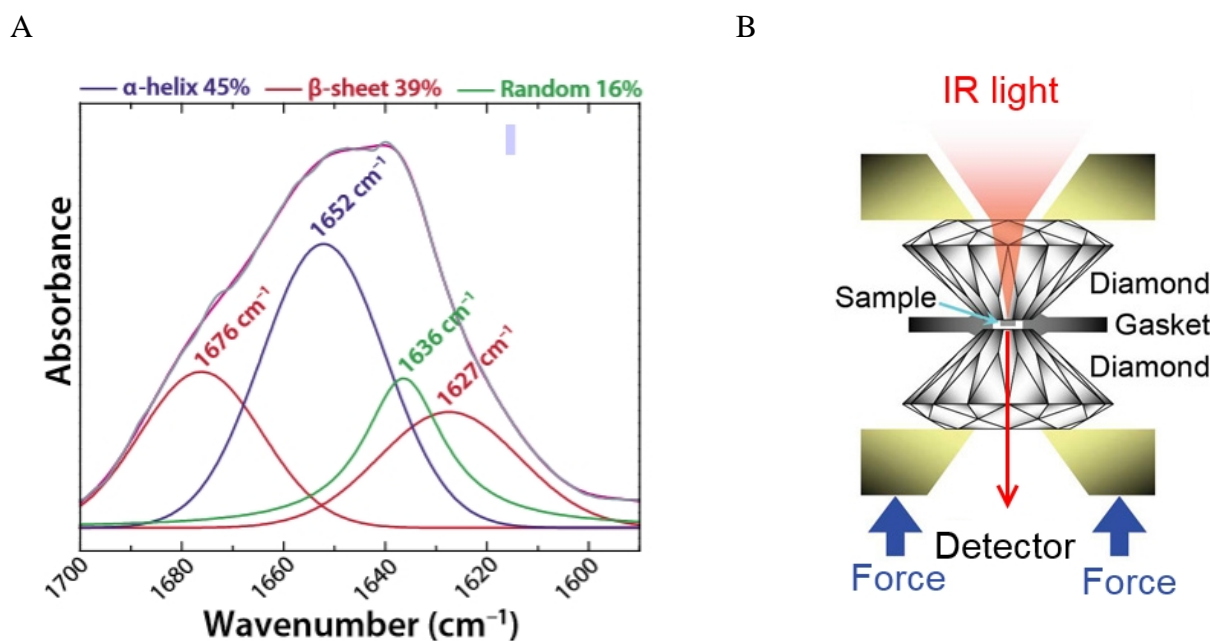


Figure 2.1: (A) An amide I band for secondary structure analysis of proteins. The underlying component bands are assigned to the designated secondary structures: alpha-helix (blue), beta-sheet (red), random coil (green).⁷⁴ (B) A schematic representation of the diamond anvil cell for high pressure generation in the infrared spectroscopy setup.⁷⁵

the shift of the barium sulphate stretching vibration at 983 cm^{-1} .⁷⁶ FTIR measurements have been carried out in D₂O as the solvent to avoid spectral overlap of the amide I band with the bending mode of H₂O. For H/D exchange, bvPLA2 was kept in pure D₂O for 5 hours. Following lyophilization, protein (2 wt%) was hydrated with 20 mM bis-Tris buffer, pD = 8.0, 100 mM NaCl, 15 mM KCl, 2 mM CaCl₂ or 0.5 mM EGTA in the presence of lipid vesicles (protein to lipid molar ratio 1:40). Large unilamellar vesicles, after five freeze-thaw-vortex cycles, were formed by extrusion through polycarbonate membranes of 100 nm pore size at 65 °C.⁷⁷ Spectral analysis was carried out using Grams software.

After the spectra collection, several processing steps need to be employed, including background buffer signal subtraction and spectral baseline correction. The spectra were normalised by setting the area between 1700 and 1600 cm^{-1} to 1 to allow for a quantitative analysis of the secondary structure of proteins, in the free and membrane bound form. Secondary structure estimation from normalised FTIR spectra was performed by fitting subbands to the amide I band, whose peak wavenumbers are characteristic for the secondary structure elements, and areas are proportional to their fractions. Initial peak wavenumbers for the fitting analysis were taken from commonly used band narrowing techniques, second derivative spectra and Fourier self-deconvolution (FSD). The corresponding subband positions were assigned to the protein secondary structures according to literature data.⁷⁸

2.2.2 Ambient and High-Pressure Stopped-Flow Measurements

Experimental design of the stopped flow setup

The stopped-flow technology in combination with spectroscopic signal recording is used to follow kinetic changes of reactions in solution on timescales of milliseconds to seconds (Figure 2.2). Reactants are initially placed in separate syringes. After a pneumatic drive rapid push, equal amounts of both solutions simultaneously enter a mixing chamber and then a small-volume (~ 20 µl) observation cell, after which the flow is stopped in the system by a stop syringe, which triggers a detection unit and the instrument starts data acquisition instantly.

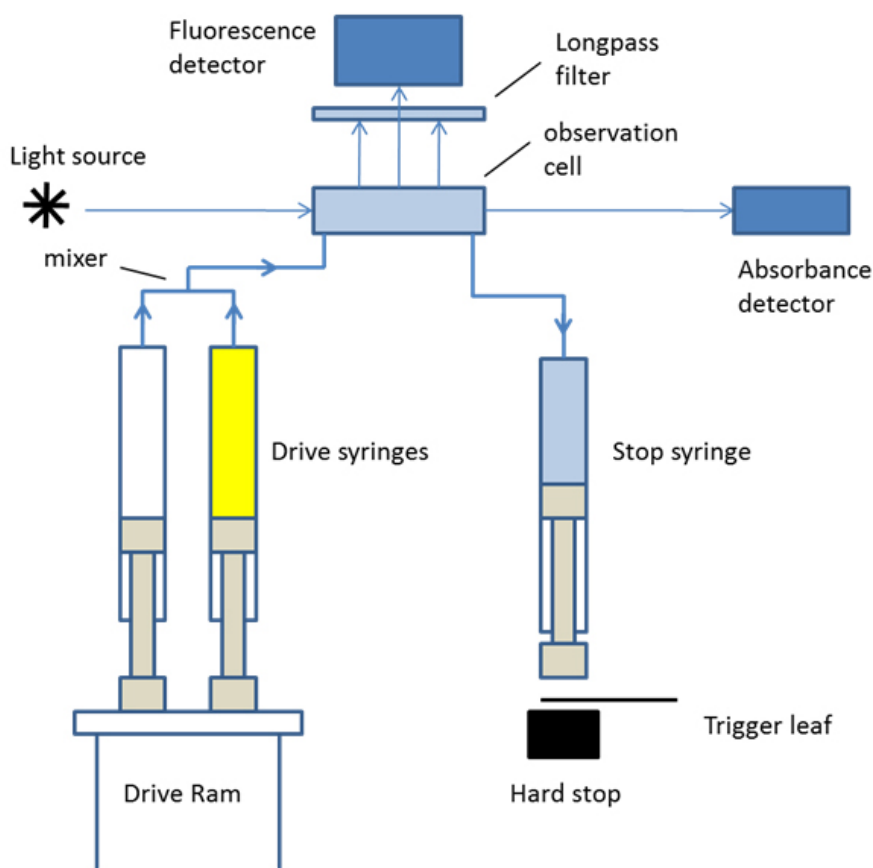


Figure 2.2: Schematic representation of the stopped-flow setup (from Applied Photophysics, www.photophysics.com).

The dead time between the mixing of reagents in the observation cell and the start of the measurement usually is approximately 1 ms. For the present work described in this thesis, the fluorescence intensity as a function of pressure was tracked to observe the kinetics of PLA2-vesicle interactions and PLA2 enzymatic activity. For spectroscopic signal detection, stable light from a xenon or mercury-xenon lamp is guided through a monochromator in order to select the desired wavelength. The light beam passes through an observation cell, and a suitable optical cut-off filter that enables the fluorescent signal to be detected by a photomultiplier. Other elements of the stopped-flow spectrometer are discussed in the following chapter together with the high pressure stopped-flow (HPSF) set up.

High-pressure stopped flow (HPSF-56) apparatus

Any stopped-flow spectrometer consists of the following components (Figure 2.3): 1) a light source to produce intense emission over a large wavelength range; 2) the monochromator to select the desired light wavelength; 3) a sample handling unit to ensure rapid mixing into an observation cell and coordination of stopping the flow with the start of detection; 4) a detection system that can be a photomultiplier or a photodiode array detector; 5) a data acquisition system, including computer and control software to adjust parameters of the measurement or for data analysis; 6) a temperature controlled water bath to regulate the temperature of the observation cell.

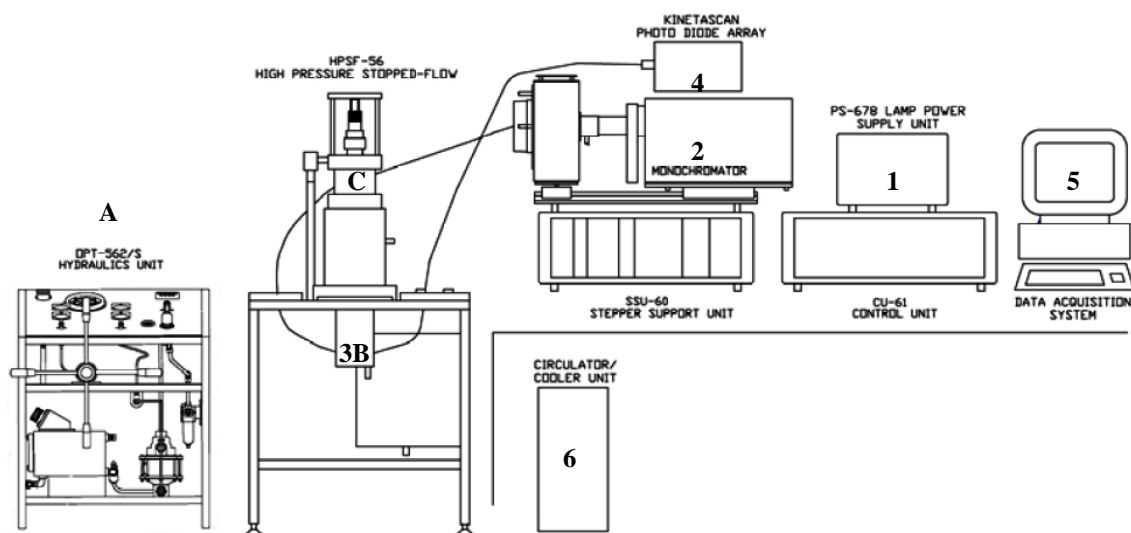


Figure 2.3: Fundamental elements of the HPSF spectrometer (adapted and modified from TgK Scientific user manual).

Additional components of the HPSF-56 instrument can be subdivided into the following three parts: a) a high-pressure control unit; b) the HP resistant autoclave vessel termed as “bomb”, including a sample handling unit of the stopped-flow circuit, wherein the sample can be mixed under controlled pressure and temperature conditions (Figure 2.4) and c) the drive mechanism to cause the mixing which is provided by a pneumatic cylinder which is positioned over the bomb during driving, and which is moved to the backward position to allow access to the bomb for introducing the reagents prior to the experiment (Figure 2.5).

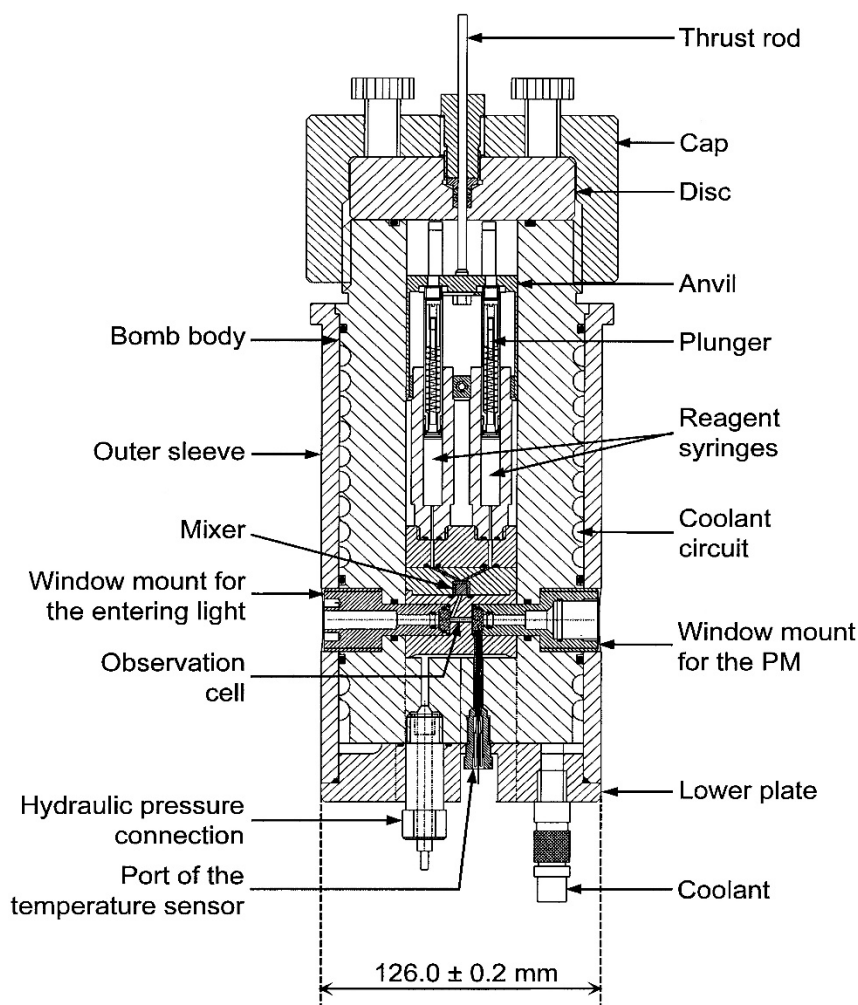


Figure 2.4: Illustration of the high pressure autoclave (bomb) assembly.⁷⁹ During a single injection, the thrust rod pushes the anvil, which consequently pushes the plungers of the syringes to initiate mixing of the two reagents.

The autoclave is made of an empty cylinder with an inner 5 cm and an outer 11 cm diameter. The autoclave is covered at the top with a steel disk, which is firmly fixed with six big screws of the cap to secure the disk in place and the thrust rod goes through the disk. Two reagent syringes and a collection syringe which belong to the dynamic component of the HPSF unit are screwed to the static cylindrical autoclave underside by four long screws. Three hole ports equipped with silicon O-rings (to ensure the sealing of syringe assembly to the autoclave base) are constructed into the lower part of the hollow cylinder (4.9 cm from the bottom of the autoclave, slightly above the mixer), where the sample goes through the thin cylinders wall, then the mixer mount and capillary hole to end up at the observation cell. The cell is

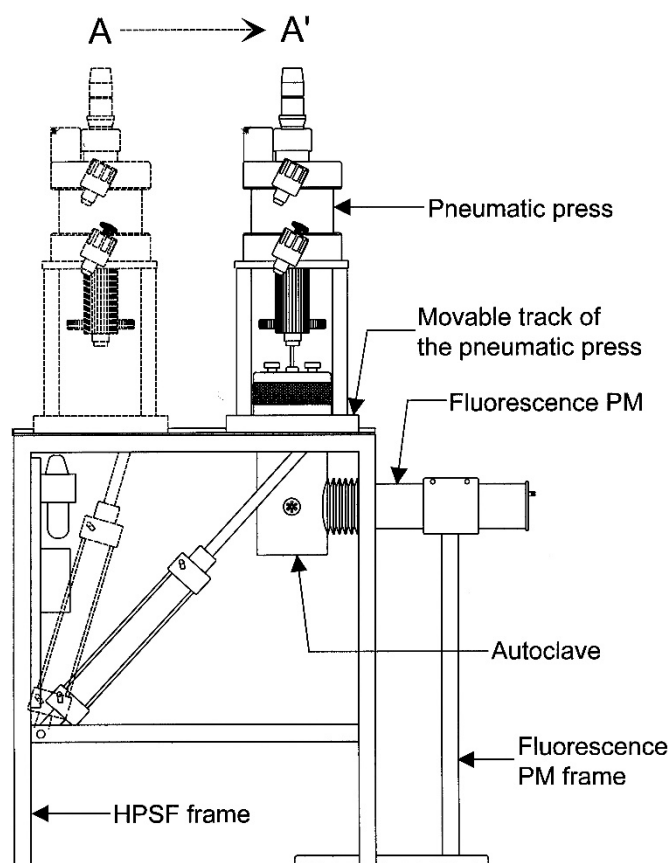


Figure 2.5: Lateral view of the HPSF instrument. After loading of the samples into the pressure autoclave, the pneumatic press is moved from position A to A' and vice versa at the end of an experiment to easily disassemble the entire syringe assembly.⁷⁹

incorporated into the vessel block and contains three sapphire windows in special high-pressure sealing mounts, one for the incoming light beam and the others are for output signal detection of the absorbance or the fluorescence measurements within the bomb (Figure 2.6). The observation cell is $2 \times 2 \times 10 \text{ mm}^3$ in dimension, with path lengths of 10 mm for the absorbance and 2 mm for the fluorescence measurements, respectively. A fluorescence detection window is placed at a 90° angle to the incident light relative to the center of the observation cell.

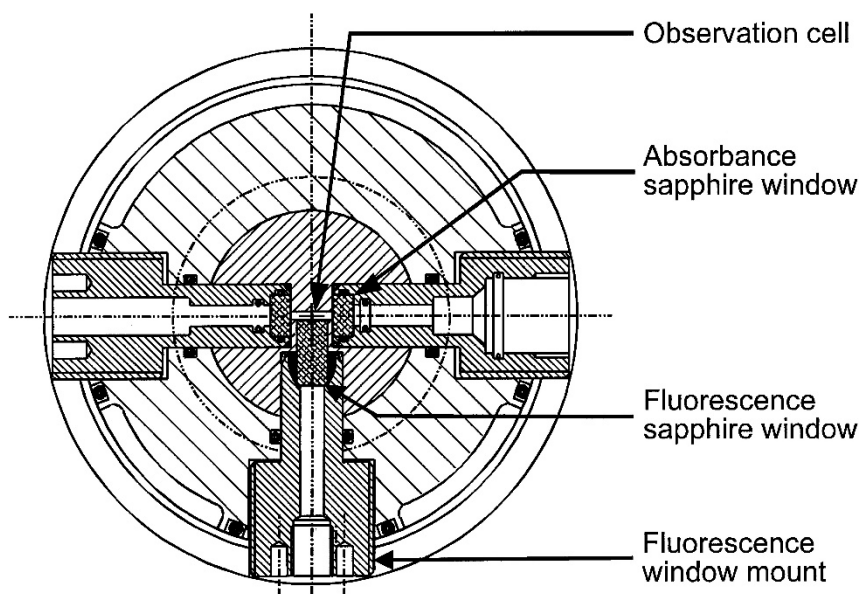


Figure 2.6: The construction of the windows mounts and HPSF observation cell.⁷⁹ There is provision for three sapphire windows in special high pressure sealing mounts that allow for absorbance and fluorescence observation. The rectangular cuboid observation cell within a vessel body has dimensions of $2 \times 2 \times 10 \text{ mm}^3$ and a hence a volume of $40 \mu\text{L}$.

The sapphire windows are pressure resistant below 8000 bar and operate well within a wavelength range of 200 to 850 nm. In order to optimize the sensitivity and accuracy of the HPSF measurement, the absorbance photomultiplier and the light source via flexible light fibers (Hellma UK Ltd) are placed on the detection sapphire window, which on the other side are in direct contact with the sample solution, resulting in improved optical system performance, because the light does not pass through the pressurizing fluid, as is often the case with other HP instruments.

During each measurement, the thrust rod is driven down by quantified increments with the help of a pneumatic drive cylinder press (Festo DC) onto an anvil that moves the reagent syringe plungers inside the autoclave. The pneumatic press along with carriage assembly is placed on a track to conveniently change the position either backwards from the bomb while dismantling (removal/fitting of the stopped-flow syringe assembly unit from/to the container) or centered over the bomb while conducting the experiments (Figure 2.5). The pneumatic

Chapter 2: Spectroscopic methods – stopped-flow

drive requires a single compressed air supply rate of 8-10 bar which usually comes from a nitrogen tank, routed to the inlet of the pneumatic control box.

A temperature sensor (platinum resistance, Pt 100) is placed close to the cell; but the sensing element does not come into direct contact with the pressurizing medium. This sensor is connected to a digital thermometer (2024T, Digitron instrumentation Ltd, Hertford, UK) through a port in the base of the bomb. The autoclave has an integrated cooling system in the form of a double helical groove, which has been constructed onto the surface of the bomb to ensure good temperature control, with a minimal temperature gradient throughout the autoclave.

The hydrostatic pressure in the system is applied by an external pressure intensifier (Hydratron Ltd, Cheshire, UK). The pressure generator consists of two pumps, a liquid tank and five gates, connected to each other and to the underside connection of the autoclave bomb by steel capillary tubes (Novaswiss). Applied pressure is measured by a piezoelectric manometer. The typical choice of hydraulic fluid is distilled water. A pressure is usually applied using an electric pneumatic pump for the larger increment, and then using a manual pump for smaller changes to adjust more accurately the pressure to the desired value.

A simplified representation of HP stopped-flow measurements is displayed in Figure 2.7, further details can be found in the HPSF-56 user manual from Tgk Scientific or ref.⁷⁹ The main characteristics of the HPSF apparatus are: the measurements can be performed in the pressure range 1 to 2000 bar, over a broad temperature usage range between -40 and $+100$ °C. The dead volume is about 65 μL , while the cell volume equals 40 μL . Thereby, sample syringes can be loaded with enough reagents for 20-25 experimental shots (including several “dummy” shots) without disassembling the high-pressure unit.

Furthermore, it is possible to measure simultaneously in both the absorbance and fluorescence mode in the wavelength range from 220 to 850 nm. The estimated empirical dead time has been found to be independent of the applied pressure to the system and is less than 10 ms in aqueous solution and at room temperature up to 2000 bar (HPSF-56 user manual).

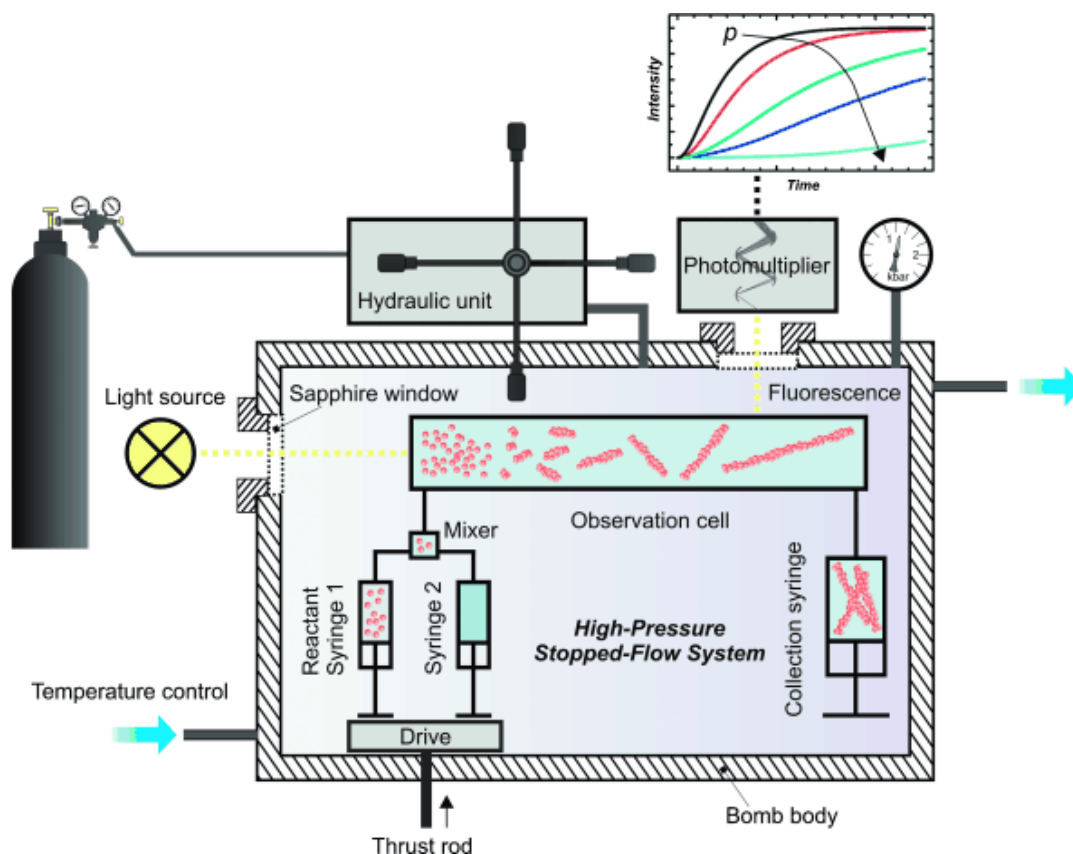


Figure 2.7: Schematic representation of the HPSF measurements.⁸⁰

Data collection

Rapid reaction pressure-dependent kinetic experiments of binding and activity were both monitored by means of a Hi-Tech Scientific HPSF-56 high-pressure stopped-flow spectrophotometer at pressures between 1 and 2000 bar. The syringe assembly of the high-pressure stopped-flow unit was held inside a high-pressure vessel that has pressure-stable sapphire windows for the (excitation) entering and fluorescence light. Measurements of the enzymatic activity were carried out under conditions that confer to a pseudo-first-order reaction kinetic behavior by using $0.35 \mu\text{M}$ bvPLA2 and $98.2 \mu\text{M}$ lipid vesicles. Typically, 3–6 reaction traces were measured at each pressure condition with an interval of 400 bar. We confirmed that the application of pressure had an insignificant effect on the emission of released BODIPY upon hydrolysis, and the pressure-induced minor increase in the initial baseline signal of the lipid vesicles was corrected for in the final data analysis.

2.2.3 Fluorogenic Assays for Studying PLA2-Membrane Interactions and Enzyme Kinetics

Fluorescence (Förster) resonance energy transfer (FRET) is a process describing a non-radiative transfer of energy from an excited state donor fluorophore to an acceptor chromophore to monitor molecular interactions, since the energy transfer efficiency is very sensitive to the spatial proximity of the two fluorophores in use. The distance at which 50 percent of the donor excitation energy is transferred to the acceptor for a given donor-acceptor pair is called Förster radius. For example, the Förster radius for tryptophan and 1,6-diphenyl-1,3,5-hexatriene (DPH) equals to 40 Å.⁸¹ The efficiency of energy transfer is given by Equation 1 and depends on the donor-to-acceptor distance with an inverse 6th power law:

$$E_{\text{FRET}} = \frac{1}{1 + \left(\frac{R}{R_0}\right)^6}, \quad (1)$$

where E_{FRET} = efficiency of energy transfer, R = separation between the two fluorophores, the donor and the acceptor (a distance sufficiently close for molecular interactions to occur within a range of 10-100 Å), R_0 = Förster radius.

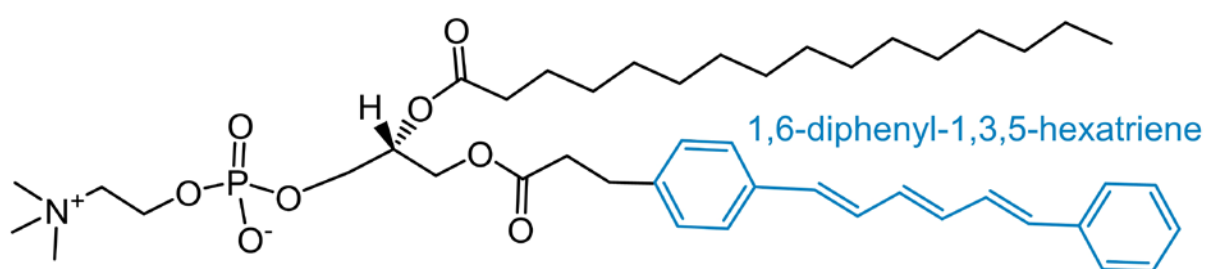


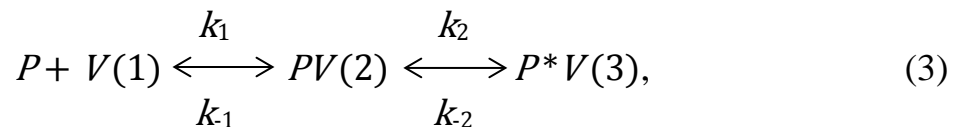
Figure 2.8: Schematic display of the fluorescently labeled lipid molecule β -DPH HPC [2-(3-diphenylhexatrienyl) propanoyl]-1-hexadecanoyl-*sn*-glycero-3-phosphocholine]

The protein-membrane binding kinetics was studied by observing FRET between tryptophans in PLA2 and the fluorescently labeled phospholipids β -DPH HPC (Figure 2.8) incorporated in the lipid vesicles. Fast kinetics measurements of bvPLA2 membrane binding and activity at atmospheric pressure were performed using an ambient and high pressure stopped-flow spectrometers by rapid mixing of 0.35 μ M bvPLA2 with liposomes of varying concentration. Fluorescence of the intrinsic tryptophans of bvPLA2 was excited at 280 nm filter using a slit width of ± 1 nm. Fluorescence emission of the lipid β -DPH HPC dye resulting from FRET with bvPLA2 was recorded through a 420 nm cut-off filter. Typically, 5-8 single injections were accumulated for each experimental condition, monitored over 2 s binding reaction time. Unless indicated otherwise, all binding measurements were performed at 37 °C in buffer containing 20 mM Tris/HCl, pH 8.0, 0.5 mM EGTA to avoid vesicle hydrolysis during the fluorescence measurements. The observed association rate constants were obtained from fits assuming multiphasic exponential processes; typically, a biphasic time course displayed a sufficient approximation of the experimental data (equation 2).

$$F(t) = F_{max} + \sum_{i=1}^n A(i)_{obs} e^{(-k_{(i)obs}t)}, \quad (2)$$

where $F(t)$ = fluorescence at a time t , $A(i)_{obs}$ = amplitude of i -th exponential, $k_{(i)obs}$ = rate constant of the i -th exponential function, n = number of exponential function; for a bi-exponential function, $n = 2$

The binding of PLA2 to vesicles can be described by the reaction displayed below. Bi-exponential curve fitting indicated a two step binding mechanism, which corresponds to a first initial attachment of the protein to the membrane followed by structural rearrangements of PLA2 on the membrane surface.



where P = protein, V = fluoroscently labeled vesicles, P^* = protein in an activated state.

The lipid concentration was chosen to be much higher ($> 100x$) than the concentration of the protein, to be able to analyze the data in terms of a pseudo-first-order association model in which the phospholipid concentration is rate-determining. Furthermore, the first equilibrium step of the reaction is much faster than the equilibrium step (2) $\xrightleftharpoons[k_{-2}]{k_2}$ (3). On an average the observed rate constant for the second step which describes isomerization of the protein is slower by a factor of 10. The observed rate constant for the fast phase, k_{1obs} , is given by equation 4, which can be simplified considering a slower second binding phase.

$$k_{1obs} = k_{-1} + k_1 * [V] + k_2 + k_{-2} \approx k_{-1} + k_1*[V], \quad (4)$$

The second rate constant, considering the strong preference of the system to a condition (2) over condition (1) is given by

$$k_{2obs} \approx k_2 + k_{-2}. \quad (5)$$

The obtained rate constants k_{1obs} and k_{2obs} were plotted against the vesicle concentration. A simplified version of equation 4 corresponds to a linear equation, and a linear regression of data points provides k_{on} (slope) and k_{off} (the intersection with y-axis) for the fast phase.

In the catalysis experiment, a fluorogenic analog of the PLA₂ substrate PC, named DBPC (1-*O*-(6-DABCYL-aminoheptanoyl)-2-*O*-(12-(5-BODIPY-entanoyl)aminododecanoyl)-*sn*-glyceryl phosphatidylcholine), was used.⁸² In this fluorescence dequenching assay, the DBPC molecule, containing the quencher DABCYL, quenches the emission of the excited BODIPY fluorescent dye when the phospholipid substrate is not hydrolyzed hydrolyzed via intramolecular energy transfer. The loss of this intramolecular spatial correlation of the two fluorophores in DBPC by hydrolysis of the *sn*-2 acyl chain results in a strong enhancement of fluorescence of BODIPY attached to the released lyso-fatty acid analogue (Figure 2.9). This increase of fluorescence emission of the BODIPY dye resulting from the release of the reaction product was recorded for 100 s through a 530 nm cut-off filter, after excitation at 488 nm. All enzyme activity measurements were performed at 37 °C in buffer containing 20 mM Tris/HCl, pH 8.0, 5 mM MgCl₂, 2 mM CaCl₂.

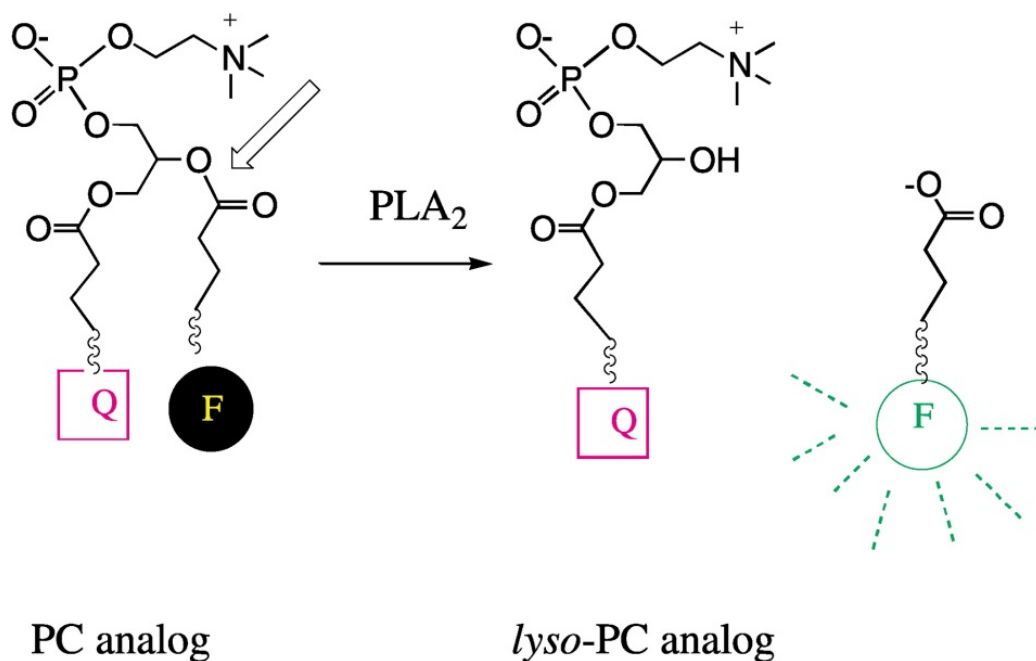


Figure 2.9: Principle of monitoring the PLA₂ activity. In the real time fluorogenic probe DBPC, a fluorescence quencher DABCYL is in close proximity to the BODIPY fluorophore and absorbs a photon emitted by an excited BODIPY group, without fluorescing. The typical distance between these two fluorophores is in the low end of this range 10–100 Å. As a result of PLA₂ induced *sn*-2 acyl chain disruption, DABSYL and BODIPY become separated and the reaction can be monitored by observing BODIPY fluorescence as a function of time.⁸²

2.3 Atomic Force Microscopy (AFM)

Instrumentation and experimental details

The preparation of the supported lipid bilayers and the AFM setup is described in detail in refs.^{83, 84} For the enzyme–membrane interaction studies, 250 μL of PLA2 ($C_{\text{PLA2}} = 0.35 \mu\text{M}$) in Tris buffer (20 mM Tris, 7 mM MgCl_2 , 2 mM CaCl_2 or 0.5 mM EGTA, pH 7.4) were injected into the AFM fluid cell and allowed to incubate for 1 h at room temperature. Measurements were performed at room temperature using a MultiMode scanning probe microscope with a NanoScope IIIa controller (Digital Instruments (now Bruker), Santa Barbara, USA) and a J-Scanner (scan size 125 μm). Images were obtained by applying the tapping mode in liquid with sharp nitride lever (SNL) probes mounted in a fluid cell (MTFML, both Veeco (now Bruker), Mannheim, Germany). Tips with nominal force constants of 0.24 N m^{-1} were used at driving frequencies around 9 kHz and drive amplitudes between 200 and 400 mV; scan frequencies were between 1.0 and 2.0 Hz. The images with resolutions of 512×512 pixels were analyzed using the image analysis and processing software NanoScope version 5 and 6 (Veeco (now Bruker), Mannheim, Germany) and Origin 8.6 (OriginLab, Northampton, USA).

Lipid vesicles were prepared from stock solutions of 10 mg mL^{-1} lipid (DOPC, DOPG, DPPC, DPPG, and Chol) in chloroform/methanol 4:1 for DPPG and in chloroform for all other lipids and mixed to obtain 1.94 mg of total lipid with the composition of DOPC/DOPG/DPPC/DPPG/Chol 20:5:45:5:25 (mol%). After removal of the solvent by drying under vacuum overnight, the dry lipids were resuspended in 1 mL of 20 mM Tris, 7 mM MgCl_2 , 2 mM CaCl_2 , pH 7.4 (hydrolysis expected) and in 1 mL of 20 mM Tris, 7 mM MgCl_2 , 0.5 mM EGTA, pH 7.4 (negative control experiment: no hydrolysis expected) for the AFM experiments to yield a total lipid concentration of 3 mM. All buffers were filtrated and sonicated.

2.4 Calorimetric and Volumetric Methods

2.4.1 Isothermal Titration Calorimetry (ITC)

A complete thermodynamic characterization of the binding interaction can be derived from ITC measurements. These include the binding free energy (ΔG), enthalpy (ΔH), entropy (ΔS), and heat capacity change (ΔC_p). A titration system injects a small portion of reactant into the sample cell. ITC uses a heat effect associated with the binding of a macromolecule to its ligand to study the interaction.⁸⁵ In ITC, the temperature inside the sample and the reference cells is maintained at a constant value. Consequently, heat of reactant binding, generating an imbalance between these two cells, is compensated by modulating the power applied to cell heaters.⁸⁶

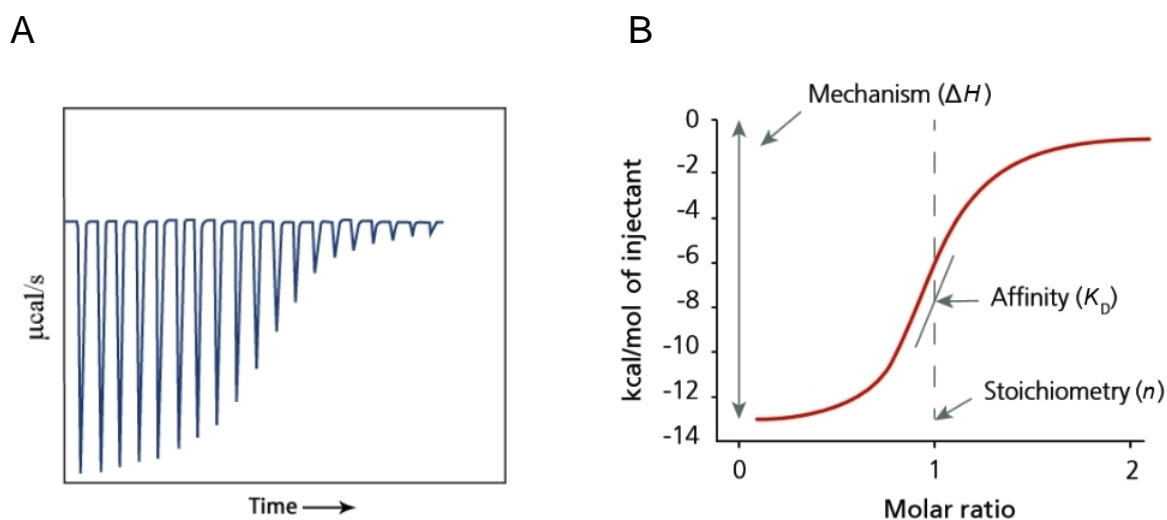


Figure 2.10: Representative ITC data. (A) Output of ITC measurements. (B) The thermodynamic profile of interaction is obtained by integration of reaction heats. Binding affinity (K_d), stoichiometry (n) and enthalpy (ΔH) changes are determined from fitting to an appropriate binding model. Using these parameters and basic thermodynamic relationships, the changes in (standard) binding free energy (ΔG) and binding entropy (ΔS) are estimated. Adapted from the MicroCal ITC brochure.

Figure 2.10 (A) displays representative ITC experimental data, where power is plotted as a function of time. After a series of programmed equal injection steps, the peaks reach the saturated baseline. More specifically, the area of each peak represents the heat of reaction for

each reactant injection. Subsequently, when the ligand binding site becomes saturated, accompanied heat effect of interaction decreases significantly. The right panel displays transformation of the raw ITC data into the binding isotherm obtained by a fit to a particular binding model (Figure 2.10 B). This binding isotherm directly yields the binding enthalpy, stoichiometry and the binding constant.

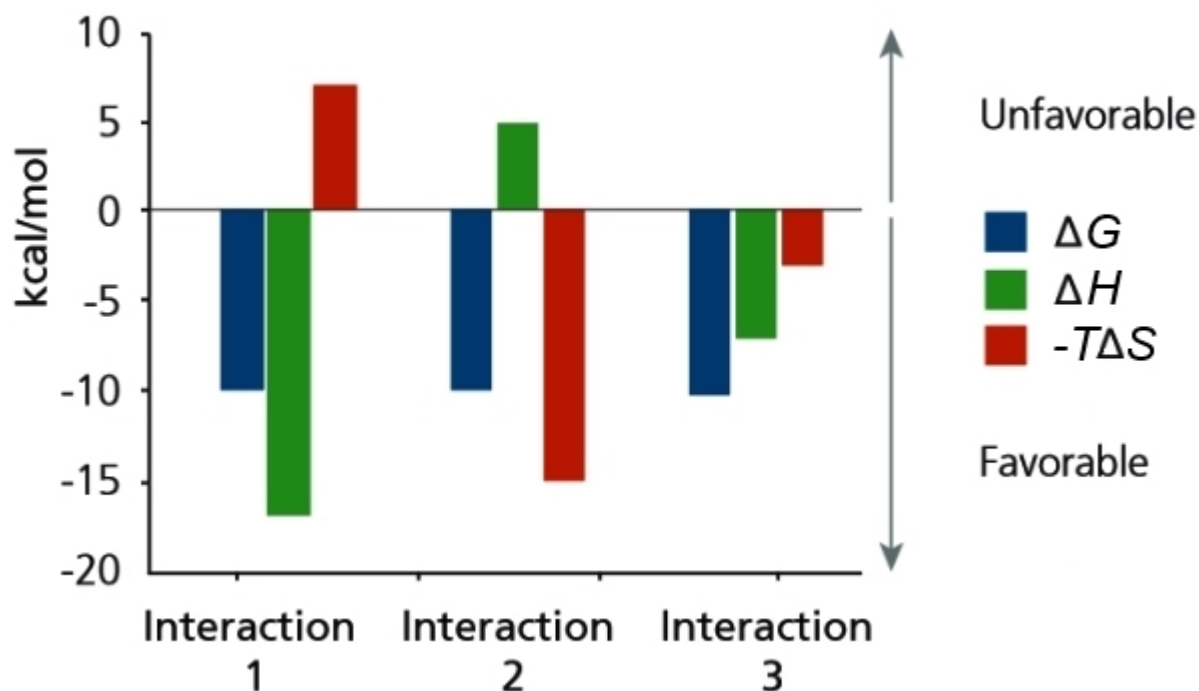


Figure 2.11: Thermodynamic signatures of three different interactions with the same binding affinity. The binding affinity is related to the Gibbs energy and is a combined function of the binding enthalpy (ΔH) and the binding entropy (ΔS). Adapted from MicroCal ITC brochure.

Due to the fact that the binding free energy comprise of both enthalpy and entropy components, several combinations of ΔH and $T\Delta S$ values are possible that yield the same ΔG value (Figure 2.11). Enthalpic contributions reflect generally the strength of ligand binding interactions with the protein (e.g via hydrogen bonds, van der Waals interactions) relative to solvent binding. Interestingly, the binding enthalpy is not straightforwardly dependent on the number of hydrogen bonds formed but mainly results from the quality of the hydrogen bonds within the binding pocket.⁸⁷ Favorable entropic contributions to the free energy are primarily due to changes in solvent entropy resulting from burial of hydrophobic groups of ligand to its binding site and release of water upon ligand binding.⁸⁸

2.4.2 Differential Scanning Calorimetry (DSC) and Pressure Perturbation Calorimetry (PPC)

DSC is a useful method to explore thermally driven reactions in the sample. DSC monitors the difference in the input energy of a sample relative to a reference as the temperature of both cells is raised identically in a precisely controlled manner.⁸⁹ The thermal induced changes of macromolecules in the sample cell cause a temperature imbalance between the cells. Therefore, in order to match the temperature of the sample to that of the reference, power to the heaters on the cells brings them back into balance. The raw data represents compensation power versus temperature. Power is a fundamental physical quantity, which can be easily converted to energy units of calories or joules.⁹⁰ Protein denaturation in aqueous solution generates an endothermic peak in the thermogram, where the heat capacity of the protein is displayed as a function of temperature. The transition temperature (T_m) and the enthalpy change (ΔH_u) of the unfolding reaction are derived by integration of the transition curve. Protein denaturation is thermodynamically coupled to a ligand binding reaction. Preferential binding of the ligand to the native folded state increases its unfolding temperature and stabilize the protein.⁹¹ The magnitude of the shift in thermal stability is a direct function of the binding affinity, hence, thermal denaturation DSC experiments can yield additional thermodynamic information about binding processes.⁹²

Pressure perturbation calorimetry (PPC) is a yet largely unutilized calorimetric technique that has become available in recent years in a form suitable for studying dilute samples in solution.⁹³ This calorimeter has basically the same architecture as a power-compensation differential scanning calorimeter (DSC), but measures the heat flow into or out of a sample upon small isothermal pressure changes (of typically ± 5 bar). PPC measurements are generally carried out on a differential scanning calorimeter equipped with a pressure perturbation accessory. An equal pressure-jump of about ± 5 bars is applied to both the reference and sample cells using (nitrogen) gas in the isothermal mode of the calorimeter. Pressure-induced differences in heat uptake between the sample and reference cells needed to maintain equal temperature is used to obtain the coefficient of thermal expansion of the partial volume of the solute, $\alpha = (1/V)(\partial V / \partial T)_p$, defined as the relative change of the partial volume with temperature at constant pressure.⁹³ After measurement at a particular

temperature T , the calorimeter is automatically heated or cooled to the subsequent desired temperature followed by the next two (compression/decompression) pressure-jumps, etc.. The output from the PPC experiment is a plot showing expansivity as a function of temperature. Upon structural or phase changes, peaks of $\alpha(T)$ indicate accompanying negative or positive volume changes. The integrated area over the peak after appropriate baseline correction allows calculation of the relative volume change at the transition, $\Delta V/V$. Volume changes in proteins upon unfolding are generally found to be very small, less than 0.5 % of the total volume.^{94, 95} The development of PPC enables accurate measurements of volume changes that are not easily possible using densimetric methods. Moreover, α , is strongly affected by the interaction of the biomolecule with the surrounding solvent. Thus, PPC can provide useful information about hydration properties of the solute.^{96, 97}

The expansivity of a solute in the PPC experiment is determined from a solute/buffer run with respect to that of buffer, and the buffer expansivity is obtained from a buffer/water scan with reference to water. In order to account for minor differences in the design of the sample and reference cell, corresponding water/water and buffer/buffer scans are subtracted from the buffer/water and solute/buffer scans, respectively. Therefore, four scans, i.e. water/water, buffer/water, buffer/buffer, and solute/buffer are necessary for each PPC experiment to obtain the coefficient of thermal expansion of the solute. The amount of heat, Q , absorbed or released by the solution, at temperature T , inside the calorimetric cell of volume V_{cell} , upon the pressure change Δp is related to the coefficient of thermal expansion, α , of the solution by:

$$Q = -TV_{\text{cell}}\alpha\Delta p. \quad (6)$$

PPC software of the manufacturer generally includes α -values of water determined from precise density measurements for calibration. Thus, the heat released or absorbed upon pressure-jumps for the calorimetric cell containing water is known. The measured differential heat between buffer and water filled cells is used to calculate the heat exchange and the expansivity of the buffer solution given by eq. (6). Following the same procedure for the dilute solution of the solute in the sample cell and the corresponding buffer in the reference cell, taking into account the volume occupied by the solute molecules inside the sample cell,

leads us to the final formula for determining the coefficient of thermal expansion of the solute:⁹³

$$\alpha = \alpha_0 - \frac{\Delta Q}{Tmv^0\Delta p}. \quad (7)$$

ΔQ is the heat difference between the sample and reference cells, resulting from pressure-jumps Δp ; m is the mass of the solute; α_0 is the expansibility of the solvent (buffer) which is determined in a separate PPC experiment, with buffer in the sample cell and pure water in the reference cell.⁹⁸

Instrumentation and data collection of calorimetric data

Isothermal titration calorimetry (ITC) experiments were carried out on a VP-ITC instrument as described in ref.⁸⁵ *N*-Acetyl-*S*-farnesyl-*L*-cysteine (800 μ M) was titrated with 6 μ L increments into the sample cell (1.5 mL) containing PDE δ protein (50 μ M) in 20 mM Tris, 50mM NaCl, and 1 mM tris(2-carboxyethyl)phosphine (TCEP) (pH 7.5). In order to minimize differences in buffer composition, protein samples were dialyzed with two buffer changes at 4 °C and *N*-Acetyl-*S*-farnesyl-*L*-cysteine was dissolved directly in buffer after lyophilization. Experimental data were fitted to a single-site binding model in the Origin script provided by the VP-ITC manufacturer. For the single-binding site model, we obtain⁸⁶

$$Q = \frac{nC_{pr}\Delta H V_0}{2} \left(A - \sqrt{A^2 - 4 \frac{C_{lig}}{nC_{pr}}} \right), \quad (8)$$

where Q is the integrated heat at each injection point, $A = 1 + C_{lig}/(nC_{pr}) + 1/(nK_a C_{pr})$, n (= 1 here) is the stoichiometry, C_{pr} is the total molar concentration of the protein in the ITC cell with volume V_0 , C_{lig} is the total molar concentration of the ligand solution in the cell, and K_a is the binding (association) constant. Fitting of the data to the binding model results in the stoichiometry (n), equilibrium binding constant (K_a), and enthalpy change upon complex formation (ΔH).

Chapter 2: Calorimetric methods

DSC experiments were performed on a VP-DSC calorimeter at a scan rate $1.5\text{ }^{\circ}\text{C min}^{-1}$ as described in ref.⁸⁹ The protein concentration was 0.8 mg mL^{-1} . The protein solutions were dialyzed against 20 mM glycine at pH 3.5 using 3.5 kDa cutoff membranes (Spectra/Por). The partial molar heat capacity of the protein, $C_{p,\text{pr}}^{\circ}$, was obtained from the experimentally measured apparent heat capacity difference, ΔC_p^{app} , between the sample and reference (buffer) cells using the equation:⁹⁹

$$C_{p,\text{pr}}^{\circ} = \frac{C_{p,\text{buf}}^{\circ}}{V_{\text{buf}}^{\circ}} V_{\text{pr}}^{\circ} - \frac{\Delta C_p^{\text{app}}}{m_{\text{pr}}M}, \quad (9)$$

where V_{pr}° is the partial molar volume of the protein (here we will not discriminate between partial and the measured apparent values). $C_{p,\text{buf}}^{\circ}$ and V_{buf}° are the partial molar heat capacity and partial molar volume of the buffer, respectively, m_{pr} is the mass of the protein in the DSC cell, and M is the molar mass of the protein.

The PPC measurements were carried out between 5 to $90\text{ }^{\circ}\text{C}$ using a MicroCal VP-DSC instrument with a PPC attachment.⁹⁶ The concentration of the protein used for the PPC experiments was 3 mg mL^{-1} . In order to obtain the temperature dependence of the thermal expansion coefficient of the protein, $\alpha_{\text{pr}}(T)$, differential temperature dependent heats were acquired from water/water, buffer/water, buffer/buffer and protein/buffer scans, respectively, yielding:⁹³

$$\alpha_{\text{pr}} = \alpha_{\text{H}_2\text{O}} - \frac{\Delta Q_{\text{H}_2\text{O}/\text{buf}}}{T\Delta pV_0} - \frac{\Delta Q_{\text{pr}/\text{buf}}}{T\Delta pV_0c_{\text{pr}}v_{\text{pr}}^{\circ}}. \quad (10)$$

where $\Delta Q_{\text{H}_2\text{O}/\text{buf}}$ and $\Delta Q_{\text{pr}/\text{buf}}$ are the differential heat changes during a water/buffer and protein/buffer scan, respectively, caused by a small pressure-jump (Δp); v_{pr}° is the partial specific volume and c_{pr} is the specific concentration of protein inside the cell.

The enthalpy change upon unfolding and the transition temperature as derived from the DSC data, and the relative volume change deduced from the PPC experiments were obtained using a special script in the Origin software provided by MicroCal.

2.4.3 Ultrasonic Resonator Technology (URT)

Ultrasonic high-resolution measurements were carried out by using the ultrasonic device Resoscan from TF Instruments. This instrument is based on resonance technique and measures the ultrasound velocity, u , through a given aqueous sample. Generally, a high-frequency acoustical wave propagation through sample media induces compression or decompression density areas, and also causes oscillations of the sample's molecular structure.¹⁰⁰ The ultrasonic velocity is determined by the elasticity of the medium and the density. The speed of sound (u) is directly related to the mechanical property adiabatic compressibility (β_s) and thermodynamic property density (ρ) via the Newton Laplace equation:

$$u = \sqrt{\frac{1}{\beta_s \rho}}. \quad (11)$$

The ultrasonic resonator is equipped with a temperature-controlled, independent, twin sample and reference cells, with a path length of 7 mm. The instrument determines the ultrasonic velocity in both cells and the software calculates the difference (Δu). Differential ultrasound velocity measurements, of sample solution versus buffer reference, can provide the relationship between the propagation of the sound and vital mechanical properties of the sample. The closed lids prevent evaporation of the sample. The measurement cells can be heated or cooled (between 5 to 85 °C), via a Peltier-thermostat with a temperature stability of 0.001 °C. The resolution of the ultrasound velocity experiments is 0.001 m s⁻¹, while typical values for the velocity of sounds in various liquids vary in the range of 800-2000 m s⁻¹.

The observation cells serve as ultrasonic resonators in which a standing sound wave is created between two parallel piezo electric transducers (Figure 2.12). The generated electronic signal by the piezotransducer is converted into the ultrasonic wave traveling through the sample. The second piezotransducer, which also serves as a reflector, transform the received ultrasonic wave into an electronic signal for analysis. Consequently, the

ultrasonic velocity, u , is determined from the lowest resonance (fundamental) frequency, f , and the path length of the sample cells, d :

$$u=2df. \tag{12}$$

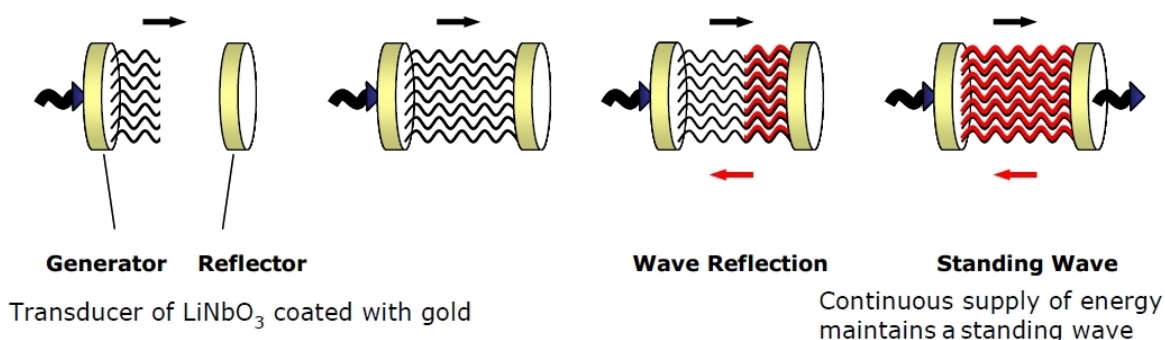


Figure 2.12: Generating and maintaining the standing ultrasound wave between transducers (TF Instruments training course).

2.4.4 Densitometry

The densities of the liquid samples were obtained by a high-precision DMA 5000 density meter, with a precision of $\pm 5 \times 10^{-6} \text{ g cm}^{-3}$. The working principle of this vibrating densitometer is based on the change of the resonance frequency of a hollow U-tube when filled with different fluids. The measuring cell consists of an oscillator formed by a hollow U-shape borosilicate glass tube that comprises about 0.7 mL of solution (Figure 2.13). The measurement of the respective period of the U-tube oscillation allows the determination of the density value of the liquid sample. More specifically, a U-shaped glass tube of known volume and mass, filled with sample liquid, is excited electronically via Piezo-elements to oscillate continuously at its resonant frequency f . The period of oscillation ($\tau = 1/f$) is recorded using optical measuring transducers.

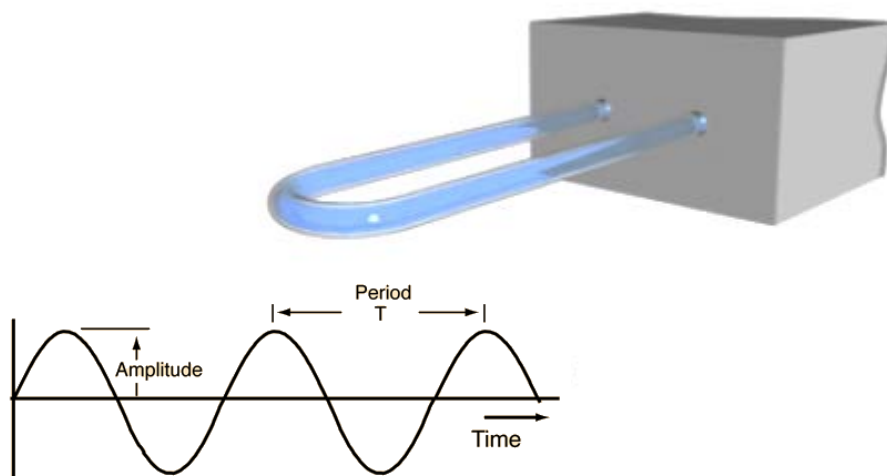


Figure 2.13: U-shaped tube of a vibrating densitometer (Anton Paar).

The relationship between sample density and the measured oscillation period, τ , can be characterized by mass-spring model equations:

$$\tau = 2\pi \sqrt{\frac{\rho V + M}{K}}, \quad (13)$$

Where ρ is the sample density, V the cell volume, M the hollow cell mass and K the spring constant. Correspondingly, the density dependence of the period is expressed by:

$$\rho(T) = \frac{\tau^2 K}{4\pi^2 V} - \frac{M}{V} = A(T)\tau^2 - B(T). \quad (14)$$

Where constants $A = \frac{K}{4\pi^2 V}$ and $B = \frac{M}{V}$ are temperature dependent parameters derived from calibration of each individual oscillator.

2.4.5 Calculation of the Adiabatic Compressibility, Isothermal Compressibility and Relative Volume Fluctuations

The compressibility data and volume fluctuations were obtained from molecular acoustics and calorimetry measurements as described previously.¹⁰¹ The measurements of the density

and the ultrasound velocity of the solution, provide the partial volume and adiabatic compressibility of the solute. Thereby, combinations of these data with calorimetric measurements provide a full characterization of the thermodynamics of the solute, including information about the fluctuation parameters of the system.⁹⁸

The acoustic measurements were performed on an ultrasonic resonator device ResoScan (TF Instruments GmbH) using a single-crystal lithium niobate transducer of a fundamental frequency of 9.5 MHz. Both sample and reference cells were filled with 200 μL of the sample and buffer solutions, respectively. The sound velocity of the protein solution was determined relative to that in the buffer solution at the same temperature in terms of the molar sound velocity number, $[u]$:

$$[u] = \frac{u-u_o}{u_o C_{\text{pr}}}, \quad (15)$$

where u and u_o are the sound velocities in the solution and neat solvent, respectively. C_{pr} is the molar concentration of the protein inside a sample cell.

The density measurements presented here were performed using a high-precision density meter DMA 5000 (Anton Paar) based on the mechanical oscillator principle, which automatically corrects for sample viscosity-induced errors.¹⁰² The densities of the solution, ρ , and the buffer solution, ρ_o , were used for evaluation of the partial molar volume V_{pr}^o of the protein in solution:¹⁰¹

$$V_{\text{pr}}^o = \frac{M}{\rho_o} - \frac{\rho - \rho_o}{\rho_o C_{\text{pr}}}, \quad (16)$$

The adiabatic compressibility coefficient of a medium is a function of the sound speed propagation in the medium, u , and the density, ρ , and can be directly obtained from combined ultrasound velocity and density measurements:

$$\beta_s = -\frac{1}{V} \left(\frac{\partial V}{\partial p} \right)_S = \frac{1}{\rho u^2}, \quad (17)$$

Where V , p and S are the volume, pressure, and entropy, respectively.

The partial molar adiabatic compressibility, K_S^o , of a protein in diluted solution is given by:¹⁰³

$$K_S^o = \left(\frac{\partial V_{pr}^o}{\partial p} \right)_S \cong \beta_{s,o} \left(2(V_{pr}^o - [u]) - \frac{M}{\rho_o} \right), \quad (18)$$

here $\beta_{s,o}$ ($= \beta_{s,buf}$) is the coefficient of adiabatic compressibility of the buffer.

K_S^o can be subdivided into two terms, an intrinsic contribution, K_{SM} , and a hydration term, K_h .¹⁰⁴

$$K_S^o = K_{SM} + K_h. \quad (19)$$

The hydration contribution to the partial molar adiabatic compressibility can be estimated according to ref.¹⁰⁵ Particularly, the authors provide average hydration contributions for 1 Å² solvent accessible area of various surface groups of proteins in the temperature range from 18 to 55 °C.¹⁰⁵

$$K_h = B_c S_c + B_p S_p + B_n S_n, \quad (20)$$

where B_c , B_p , and B_n are the compressibility contributions of the solvent accessible surface areas of the charged, polar and nonpolar atomic groups per Å², and S_c , S_p and S_n are the corresponding solvent accessible surface areas of the charged, polar and nonpolar atomic groups, respectively, which can be obtained from crystallographic data. The B_c , B_p , B_n values were taken from the literature.¹⁰⁵ According to eq. 19, this analysis allows determination of the intrinsic coefficient of adiabatic compressibility, $\beta_{SM} = K_{SM}/V_M$, which similarly to the intrinsic coefficient of isothermal compressibility, $\beta_{TM} = K_{TM}/V_M$ (see below, eq. 23), is a measure of intraglobular interactions and reflects the tightness of intrinsic packing.¹⁰³

Chapter 2: Calorimetric and Volumetric methods

The mean square volume fluctuations of the protein molecule, $\langle \Delta V_M^2 \rangle$, are directly proportional to the intrinsic coefficient of isothermal compressibility, β_{TM} , which reflect the global dynamic properties of the protein:¹⁰³

$$\langle \Delta V_M^2 \rangle = RT\beta_{TM}V_M, \quad (21)$$

where R is ideal gas constant and V_M the actual intrinsic molar volume of the protein, which represents the geometric volume of its solvent-inaccessible interior.

Accordingly, the relative volume fluctuations, $\delta V_M/V_M$, of the solute molecules can be calculated from:

$$\frac{\delta V_M}{V_M} = \sqrt{\frac{\langle \Delta V_M^2 \rangle}{V_M^2}} = \sqrt{\frac{RT\beta_{TM}}{V_M}}. \quad (22)$$

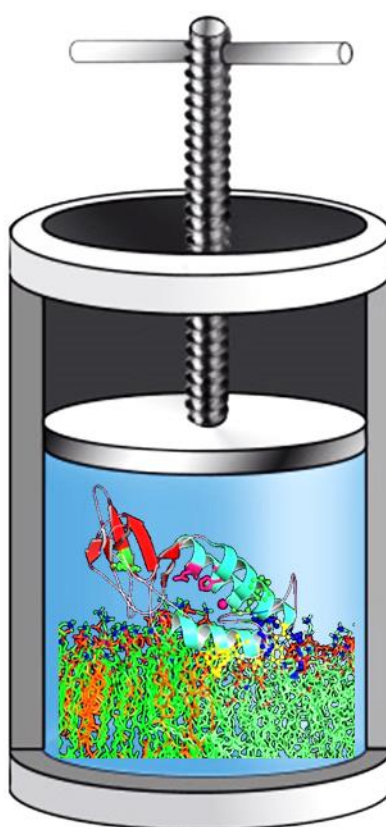
The partial molar isothermal compressibility, K_T^o , of the solute can be calculated from:¹⁰⁶

$$K_T^o = K_S^o + \frac{T\alpha_{buf}^2}{\rho_0 c_{p,buf}^o} \left(2 \frac{E^o}{\alpha_{buf}} - \frac{C_{p,pr}^o}{\rho_0 c_{p,buf}^o} \right). \quad (23)$$

where α_{buf} and $c_{p,buf}^o$ are the thermal expansion coefficient and the partial specific heat capacity of the solvent (buffer), and E^o is the partial molar expansibility of the protein. The E^o and $C_{p,pr}^o$ values were obtained using the calorimetric methods PPC (eq. 10) and DSC (eq. 9), respectively.

III

Pressure Modulation of the Enzymatic Activity of Phospholipase A2



* The work herein described has been published and subsequently reprinted in parts with permission from Suladze, S.; Cinar, S.; Sperlich, B.; Winter, R. (2015). Pressure Modulation of the Enzymatic Activity of Phospholipase A2, A Putative Membrane-Associated Pressure Sensor. *J. Am. Chem. Soc.* 137 (39), 12588–12596.

3.1 Background and Overview

3.1.1 Biomembranes and Lipid-Protein Interactions

Biological membranes constitute one of the central functional and structural elements of all living cells. Most fundamentally, they are complex structures which are responsible for the entity of cytosolic organelles and cells. Besides having a structural role, membrane components also play a key role in communications between the extra- and intracellular environments, e.g., serving as messengers in signal transduction and recognition processes.

The main constituents of biological membranes lipids and proteins co-exist together mainly held by non-covalent interactions. The absence of covalent interactions between lipids within membranes underscores the highly dynamic properties of these assemblies. Lipids are amphipathic molecules that self-assemble into a continuous double layer arrangement in the aqueous environment, where the polar head groups have a tendency to interact with the water, while hydrophobic moieties self-associate via hydrophobic interactions (Figure 3.1). Although phospholipid molecular species vary greatly in eukaryotic cell membranes, they predominantly belong to four main lipid types: Phosphatidylcholine (PC), phosphatidylserine (PS), phosphatidyl-ethanolamine (PE) and sphingomyelin (Sph). The asymmetric distribution of lipid components between extra-cellular and intra-cellular leaflets can differ significantly, in an organelle or cell type-dependent manner.¹⁰⁷ This molecular heterogeneity can lead to the formation of membrane microdomains in both model and natural membranes. Microdomain areas have distinct physicochemical properties and lipid compositions in comparison to neighboring regions.^{108,109} In addition, regularity of the bilayer arrangement relies on the presence of integral and peripheral proteins inducing changes in the membrane dynamics and topography.¹¹⁰

Proteins participate in virtually every step of biological processes. The changes in lipid properties (different surface electrostatics, local curvature, spatial arrangement or motional freedom), depending on the environmental conditions, may induce recruitment of specific proteins/enzymes from the cytosol. Thus, there is increasing evidence demonstrating the role of lipids in regulating the localization and activity of membrane-associated proteins.¹¹⁰ Particularly, membrane domains may serve as spatio-temporal platforms for interacting signaling proteins.¹¹¹ A good example to illustrate how proteins may influence membrane

local structure, and vice versa are G proteins.¹¹⁰ On the one hand, co-/post-translational lipid modifications (addition or removal of fatty acids or isoprenoid moieties) of these proteins contribute to their membrane attachment and modulation of the membrane-local structure.^{83,112} On the other hand, local lipid domains formed within membranes enable clustering of specific G proteins.¹¹³

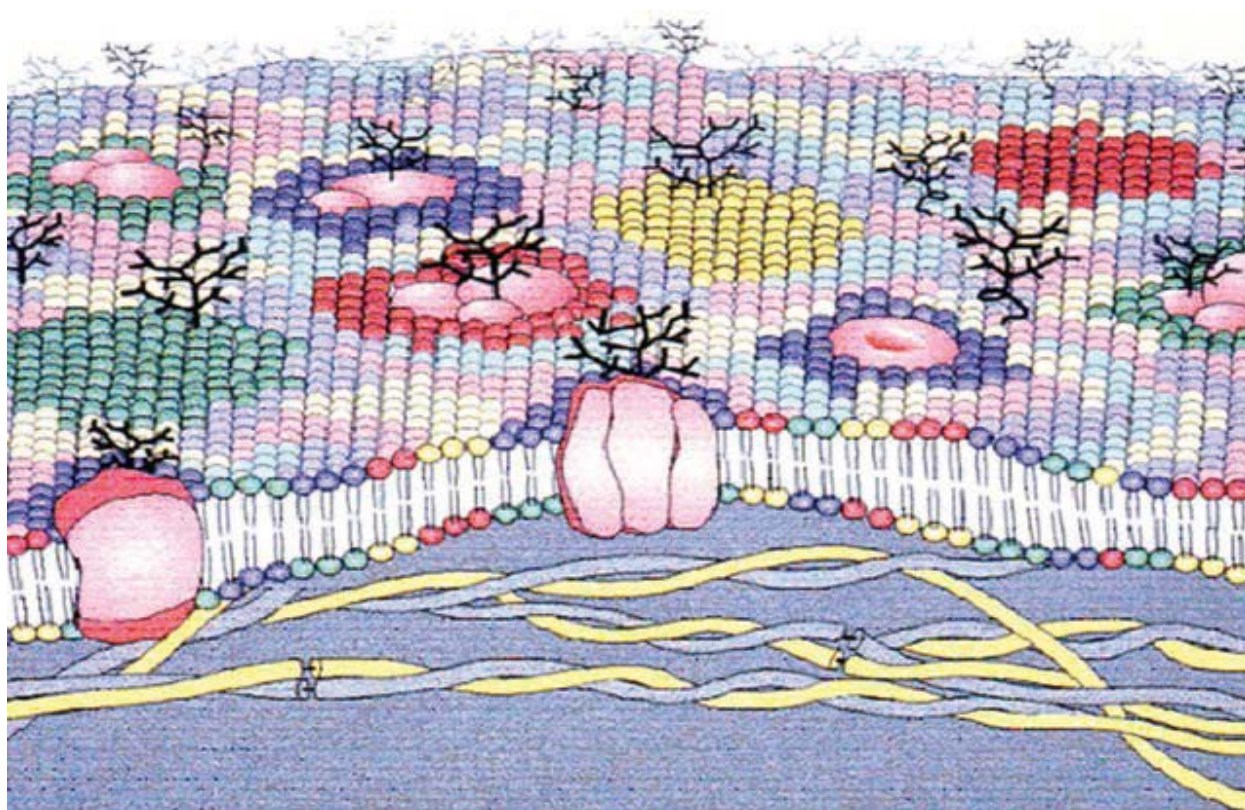


Figure 3.1: Schematic representation of a typical biomembrane, displaying membrane lipid asymmetry and in addition microdomains enriched in particular lipids caused by the presence of membrane proteins.¹¹⁰

The large variety of the biological lipids and proteins and their interactions with intra- and extra-cellular matrices render direct investigations into the protein-membrane interactions rather complex. Therefore, well-established model membranes serve as idealized platforms to characterize specific interactions and to obtain fundamental physicochemical insights into the same. For instance, AFM studies showed that the peripheral membrane protein phospholipase A2 (PLA2) experiences an increased activity towards membranes with structural defects induced by the interfacial boundary between lipid domains.²⁹ Extraordinarily, PLA2 activity within natural biological membranes of erythrocytes was also found to be governed by the

same membrane properties as for liposomes.¹¹⁴ These results indicate that general principles learned from studies with artificial model membranes may very well apply to biological systems.

Irregularities of the membrane surface in artificial membranes are usually modeled by multiple lipid systems that exhibit phase segregation into distinct membrane domains, forming lipid rafts. Lipid rafts are nanometer-scale membrane domains rich in saturated lipids, cholesterol and particular proteins.¹¹⁵ The presence of lipid rafts mainly arises due to difference in chain length between phases made of a high- and a low-melting temperature lipid and cholesterol.¹¹⁶ A ternary lipid mixture composed of DPPC–DOPC–Chol at ambient conditions separates into the following domains: the liquid-ordered (l_o) and liquid-disordered (l_d) phase lipids.¹¹⁷ A schematic illustration of such phase separation is displayed in Figure 3.2.

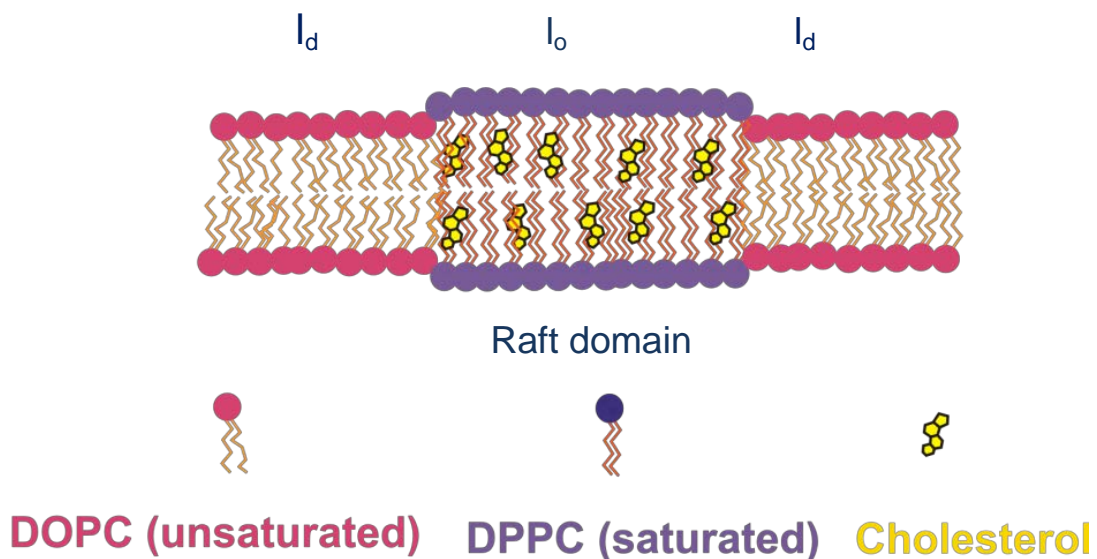


Figure 3.2: Schematic diagram of a phase-separated artificial lipid bilayer with raft and non-raft lipid domains.

Liquid-ordered (l_o) phase domains or the so-called lipid rafts in artificial membranes can be constructed by mixing high concentrations of cholesterol (25-30 mole %) with saturated sphingomyelin, or other lipids containing at least one saturated acyl chain.¹¹⁸ Raft domains disperse in the liquid-disordered (l_d) phases mainly composed of lipids with unsaturated chains. Structures and phase diagrams of these domains have been intensively characterized. In l_o phases cholesterol induces conformational ordering of the neighboring nonpolar chains.

This results in extended lipid chains, although the translational mobility required for membrane function is still preserved.¹¹⁹ Higher affinity of certain proteins to raft lipids or phase boundaries indicate that raft domains might be a meeting point for particular proteins to increase their activity level.¹¹⁵ Besides heterogeneity, biological membranes are negatively charged and many proteins bind membranes with strong electrostatic interactions.¹²⁰ In order to closely mimic the matrix of the heterogeneous biological membranes, Winter and colleagues have characterized a multicomponent anionic model membrane system.⁷⁷ This anionic lipid raft mixture displays coexistence of l_o and l_d phases over a wide temperature and pressure range (Figure 3.3).⁷⁷ For this reason, it provides an excellent system for studying the interaction of the lipid membrane with signaling proteins.⁵⁹ Visualization of such phase-separated membrane domains is possible by means of the AFM technique or confocal fluorescent microscopy.

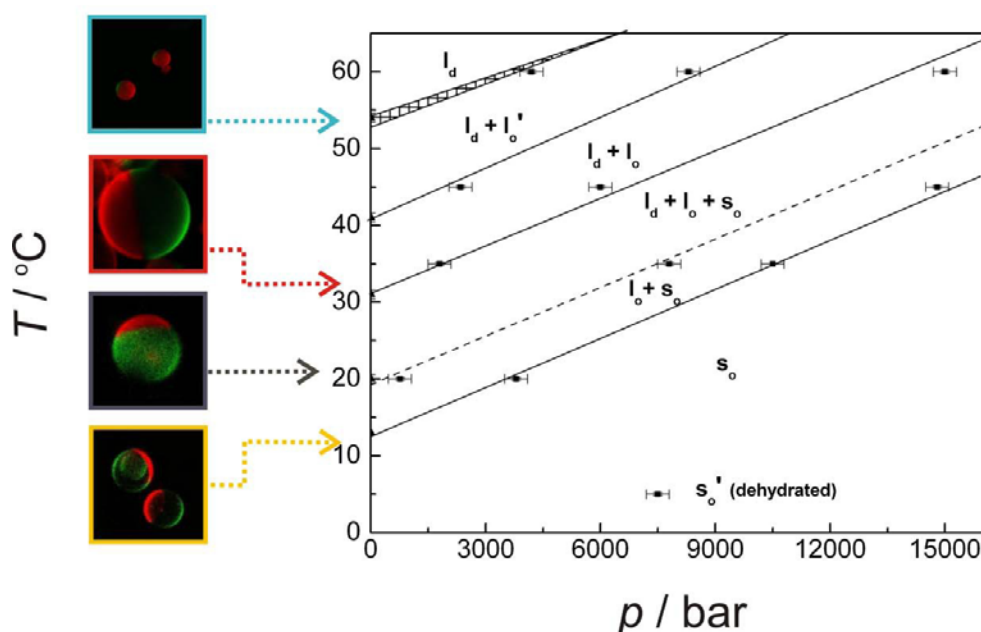


Figure 3.3: p , T -phase diagram for the anionic model raft mixture composed of DOPC/DOPG/DPPC/DPPG/Chol (15:10:40:10:25. mol%). The solid-ordered s_o -phase is observed in the low-pressure, low-temperature region of the phase diagram; the liquid-ordered (l_o)-liquid-disordered (l_d) phase regions appear at relatively higher temperatures. The left panel describes temperature-dependent confocal fluorescence microscopy images at ambient pressure. The l_d domains of the membrane are displayed in red, whereas l_o domains in green.⁷⁷

3.1.2 Pressure Effects on Membrane Organization

Pressure is an important environmental variable extensively used in examining the structure and dynamics of biologically important macromolecules. High-pressure studies are also essential for understanding the physiology of deep-sea extremophilic organisms (living in cold-and high-pressure habitats). Microorganisms are discovered even at the bottom of the Mariana Trench (11 km underneath sea level), reaching pressure values in excess of 1 kbar (100 MPa).¹²¹ Compared to other biomolecules, biological membranes are the most pressure sensitive (compressible) subcellular structures.^{122,123} Hence, one of the general mechanisms to ensure survival of organisms living under high pressure (HP) conditions is to adjust their lipid membranes by altering their lipid composition (also known as Homeoviscous Adaptation). Another HP adaptation hypothesis suggests the incorporation of additional molecules into the cell membranes to keep their mechanical properties intact and maintain the vital fluidity required within bilayer structure.¹²⁴ Nevertheless, regulatory mechanisms of HP adaptation are still vague and are the subject of great scientific interest.¹²²

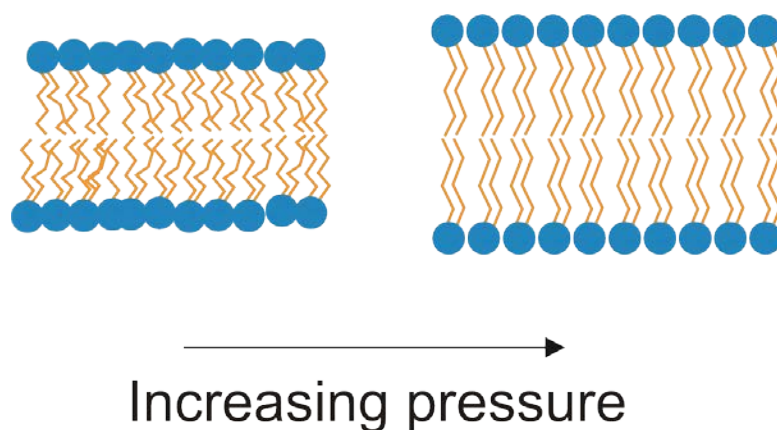


Figure 3.4: Increase of lipid bilayer thickness induced by pressure.

The response of any structure to high pressure is mainly governed by the Le Chatelier's principle, which states that pressure always favors a smaller-volume condition of the system. For instance, when the transition state volume is smaller than that of the ground state of reactants, increasing pressure results in a higher reaction rate of such a process.¹²⁵ For lipid assemblies, pressure increases the ordering within the hydrocarbon chains by diminishing

their partial molar volume. The major pressure effect on homogenous membranes is the increase in its chain length in the direction parallel to the lipid chains (Figure 3.4), which is accompanied by a decrease of the chain cross-sectional area.¹²⁶

In the phase separated heterogeneous membrane, pressure reduces the tendency of the l_o phase lipids to phase separate since the physical properties of the phases become increasingly similar with pressure. Nevertheless, this phenomenon is not observed when the lipid raft domains are composed mainly of cholesterol. The reason for such a behavior is the hydrocarbon rings of cholesterol that are not anticipated to pack well against cis-unsaturated lipids. Therefore, pressure may reduce the presence of l_o raft phase simply by causing the surrounding regions to become more ordered, but phase separation still remains. For instance, temperature-pressure phase diagram of anionic lipid raft mixtures suggest coexistence of l_o and l_d phases under pressure in the 1-2000 bar range at 37 °C (Figure 3.3).⁷⁷

In general, the structure adopted by a hydrated lipid assembly depends strongly on the preferred curvature of the lipids. Additionally, other more indirect effects involve the interplay between chain packing, elastic stress and curvature,¹²⁷ and all of these factors are perturbed by pressure. As the lipid head group region is relatively incompressible compared to the hydrocarbon interior, pressure affects membrane function essentially by increasing the lipid packing density. In heterogeneous membranes, pressure may induce changes in lateral organization of lipid domains.^{77,128} Stronger compression of hydrocarbon interior causes also the pressure induced increment of the curvature towards the hydrocarbon chain region. In many cases, membrane curvature will promote protein binding. For example, curvature is thought to coordinate the routing of vesicles through the cell and the binding of proteins during fusion events.¹²⁹ Till now, studies of the effect of pressure-induced curvature on protein membrane association events are not well explored. More studies that directly compare the rates of binding of proteins, particularly those proteins whose binding are curvature-sensitive, are needed to fully address the role of curvature in the pressure dependence of protein-membrane interactions.¹²⁸

It should be noted that the effect of increasing pressure on a lipid bilayer is qualitatively similar to the effect of decreasing temperature, such as ordering of the lipid arrangement and diminishing the number of gauche conformers.¹²² However, in certain cases additional phases are observed upon pressurization, which do not exist otherwise at atmospheric

pressure and at any temperature. A typical illustration is the arrangement of an additional gel phase, with interpenetrating hydrocarbon chains of the opposing monolayers leaflets.¹³⁰ There is compelling experimental evidence that the impact of pressure on the bilayer surface charge groups as well as hydration is negligibly small.^{131,132} Explicit details regarding these and other possible effects of high pressure on lipid systems can be found in a number of outstanding reviews.^{127,133}

3.1.3 Pressure Effects on the Structure and Enzymatic Activity of Membrane-Associated Proteins

Generally, pressure acts on the structure and dynamics of biomolecular systems through changes in specific volume, that are largely due to changes in hydration or packing efficiency. Thus, high hydrostatic pressure (HHP) is uniquely well suited for studying the role of solvation in folding, dynamics and interactions of proteins and other biomolecules. High hydrostatic pressure investigations remain relatively underrated and often less utilized because of technical limitations of these studies. There are some advantages of utilizing high hydrostatic pressure as a variable in probing the structure, dynamics and function of biological assemblies over other structure-change inducing triggers, for example, temperature and chemical denaturants. These advantages include, a) an exceptionally rapid propagation of pressure (~ speed of sound) which leads to a fast equilibration process throughout the sample, permitting detection of fast structural changes, b) rather mild perturbation of the spatial, i.e. secondary, tertiary, quaternary, and supramolecular structures of biomacromolecules (below 20 kbar) by changing intermolecular distances and conformations.¹³⁴ c) Finally, the high reversibility of pressure-induced conformational and structural changes.

High hydrostatic pressure causes a gentle thermodynamic perturbation of the native protein structure, because of a small volume change of the system upon unfolding. The volume change of unfolding is the sum of different effects, such as disruption of noncovalent bonds, change in protein hydration and conformational changes. The predominant pressure effect on proteins comes from the volume change due to internal cavities exposed to the solvent upon unfolding. For example, studies on different cavity variants of the SNase protein demonstrated that the differences in volume between the conformational states of the proteins mainly emerge from variations in their solvent excluded void volumes.¹³⁵ In spite of the fact

that the interior of native proteins is generally quite well packed, this packing is not perfect. Some of this empty space inside proteins can be filled with water in partially unfolded states or upon complete unfolding, resulting in a lower specific volume of these unfolded states. Interestingly, high pressure may also increase the population of so-far undetected excited states (e.g., conformational and functional protein substrates with a lower partial volume) and allows for modulating biochemical processes, thereby enabling determination of reaction constants which otherwise are difficult to obtain. More specifically, profound conformational fluctuations that are unnoticed at ambient pressure can be detected by using high pressure NMR or FTIR spectroscopy.¹³⁶

The net effect of pressure on the catalytic activity of an enzyme critically depends on the magnitude and sign of the volume changes accompanying the binding and consequent catalytic steps. The functional relationship of the fundamental parameters in enzymatic conversion reactions, K_M and k_{cat} , with pressure can either be linear or non-linear.¹³⁷ From the current literature, it is evident that enzymatic reactions may be reversibly enhanced or retarded by pressure due to changes of the substrate specificity or by influencing the rate limiting molecular steps. Pressure may consequently influence a rate-determining step of an overall enzyme reaction by changing the enzyme, substrate or product composition.¹³⁸ This could be the main reason for the usually observed non-linear concave curves ($\ln k_{cat}$ versus p) for the pressure dependence of the rate of enzymatic reactions.

As mentioned above, membrane associated proteins play an exceptionally active role in cellular processes and signaling events. The overall structural response of membrane proteins to external influences such as pressure is likely to result from the close coupling of changes in both the lipids and the proteins, as well as their interactions. A key feature that should be considered in studying the impact of pressure on peripheral membrane associated proteins is to determine the pressure range that will allow proteins to remain stable on the membrane surface. The membrane-binding potential of a particular protein is governed primarily by its packing efficiency with the membrane surface and its ability to change its conformation under pressure. When the protein is not packed well with the interface of the membrane, applied pressure simply favors dissociation by pushing water into voids between the interacting macromolecules.¹²⁸ Furthermore, pressure can affect membrane-associated processes by modulation of the membrane protein's conformational sub-states and altering interactions of these proteins with membrane components, ligands and receptors.^{136,139}

There are only very few data available on the effect of pressure on proteins binding to membranes and the enzymatic activity of membrane bound proteins. One key example is the inhibition of the activity of (Na,K)-ATPase under pressure, which is dictated by the decrease of the membrane fluidity, impeding conformational transitions associated with rate-limiting steps of the enzymatic activity of the (Na,K)-ATPase reaction.¹⁴⁰ Another case of changes in the activity of a membrane-associated protein upon hydrostatic pressure application is the enzyme phospholipase C δ_1 . This enzyme exhibits a substantial increase in the hydrolysis rate under high pressure conditions. This result has been explained by two possible factors. First, it was demonstrated that phospholipase C δ_1 does not significantly penetrate the membrane surface, thus, the impact of pressure on chain packing does not play a role, and second, the product created has an extra ionic group allowing for a huge volume reduction due to the electrostriction effect.¹³²

3.2 Introduction and Objectives

Biomembranes play an essential role in regulating an extensive variety of cellular processes by providing an active two-dimensional lipid framework within which biochemical reactions can occur. The lateral dynamics and structure of these membranes selectively modulates the activity of membrane associated proteins, such as receptors and channels.^{141–143} One important class of membrane associated proteins are phospholipases.²³ On the basis of their cellular location, phospholipases are generally divided into two groups: 14–16 kDa secretory PLA2 (sPLA2) and 80–85 kDa intracellular PLA2s.¹ The structure of sPLA2 is dominated by three α -helices, two of them coupled by an antiparallel β -sheet. This assembly forms a hydrophobic channel that extends from the surface of the molecule to the active site, allowing incorporation of a lipid substrate molecule to access the catalytic site. The protein's main structural features also include the catalytic Asp-His dyad, the calcium binding loop, and the interfacial binding site with its hydrogen bonding network, which is responsible for the attachment of the protein to the lipid membrane.²² For phospholipid hydrolysis, PLA2s require to bind to the membrane-water interface. The rates of interfacial activation and hydrolysis are influenced by the membrane's physical–chemical properties, including membrane curvature, compressibility, lateral diffusivity, surface charge, and hydration.^{27,29} In contrast to varying interface binding surfaces of the enzymes across sPLA2 members,³⁵ the active site structure, residues involved in calcium binding and catalysis, as well as orientations of the catalytic water are highly conserved,²² implying common modes of their reaction. While PLA2s are attractive targets for pharmacological applications,¹⁴⁴ the relationship between their mechanistic action and physiological function remains still poorly characterized.¹⁴⁵

Using pressure modulation of the activity of PLA2 and of the membrane's physical–chemical properties, one aim of this work was to reveal novel kinetic and mechanistic information about the membrane association process and subsequent reaction. In fact, the interest in using, next to temperature and chemical potential (or activity), pressure as a thermodynamic and kinetic variable has been largely growing in physical–chemical studies of biological systems in recent years.^{122,146} Generally, pressure acts on the structure and dynamics of biomolecular systems through changes in specific volume that are largely due to changes in hydration or packing efficiency. Thus, high hydrostatic pressure (HHP) is uniquely well suited for studying the role of solvation in folding, dynamics and interactions of proteins and

other biomolecules. Moreover, high pressure may increase the population of so far undetected excited states (e.g., conformational and functional substates) and allows modulating biochemical processes, thereby enabling determination of reaction constants which otherwise cannot be obtained.¹³⁶

Besides the general physical–chemical interest in using high pressure as a tool for understanding the structure, phase behavior and energetics of biomolecules, HHP is also of biotechnological (e.g., for steering enzymatic processes by pressure modulation, for which the term baroenzymology has been coined) and physiological (e.g., for understanding the physiology of deep-sea organisms living in cold and high-pressure habitats) interest. Interestingly, though the biological membrane seems to be one the most pressure sensitive biological system,^{122,123,136,147–149} pressure effects on binding and activity changes of membrane associated proteins are largely unknown. In particular mechanisms how external pressure stress is sensed and how this information is transferred in organisms being exposed to high pressure stress are still largely unknown. Membrane stretch-activated sensors, membrane-localized proteins whose activities are modulated by mechanical forces generated in the membrane, appear to be promising candidates for the role of detecting changes in external stress.^{139,150-153} Various kinds of environmental stresses, such as temperature stress, osmotic and hydrostatic pressure stress, cause severe alterations in the physical properties of the membrane lipids in model membranes and in living cell membranes. In particular, dynamic properties and the membrane's lateral organization are significantly altered upon compression.¹³³ Hence, promising candidates for the role of detecting changes in external stress, such as pressure, include mechanosensitive ion channels and membrane-localized enzymes such as phospholipase A2 (PLA2). The activity of PLA2 is sensitive to packing of the lipid bilayer of the cell and is responsive to osmotic changes, i.e., will be a prime candidate to look into pressure effects as well. As the rates of interfacial activation and hydrolysis will be significantly influenced by the membrane's physical–chemical properties, marked pressure effects can be envisioned.^{141–143} As the lipid head groups region is relatively incompressible compared to the hydrocarbon interior, pressure affects membrane function essentially by increasing the packing density and order parameter of lipid chains and, for heterogeneous membranes, their lateral organization.^{77,128} Furthermore, pressure can affect membrane-associated processes by modulation of the membrane protein's conformational substates and altering interactions of these proteins with membrane components, ligands and receptors.^{136,139}

Phospholipases A2 superfamily enzymes are involved in regulatory processes as they interact directly with the membrane by altering both its chemical composition and physical state by hydrolysis of the sn-2 ester bond of phospholipids to produce free fatty acids (arachidonic acid) and lysophospholipids, which take part in cell signaling, immune system responses against bacterial infections and stimulation of inflammations.^{1,2,154–156} As they play an important role in membrane remodeling processes as well as in cellular signaling cascades, they should be able to serve as effective pressure sensor. Hence, as a second aim of this study, we set out to explore the pressure sensitivity of bee venom phospholipase A2, bvPLA2, and study its binding process and enzymatic activity upon HHP stress using appropriate model biomembrane systems. To this end, we used a rapid mixing high-pressure stopped-flow spectroscopy platform, which enabled us to obtain new structural, thermodynamic and kinetic information on the action of PLA2 in various model biomembrane systems at HHP conditions. Moreover, our results deepen our understanding of membrane-associated pressure effects in deep-sea organisms, where pressures up to the kbar-level are encountered.

3.3 Results and Discussion

3.3.1 Effect of Pressure on the Conformation of BvPLA2 in Bulk Solution and upon Membrane Binding

In an attempt to better understand the structural-functional relationship of multifunctional PLA2s, including conditions of harsh environmental conditions such as high pressure, we explored the structure, binding and activity of the membrane-associated protein at atmospheric and high-pressure conditions by means of various biophysical methods.

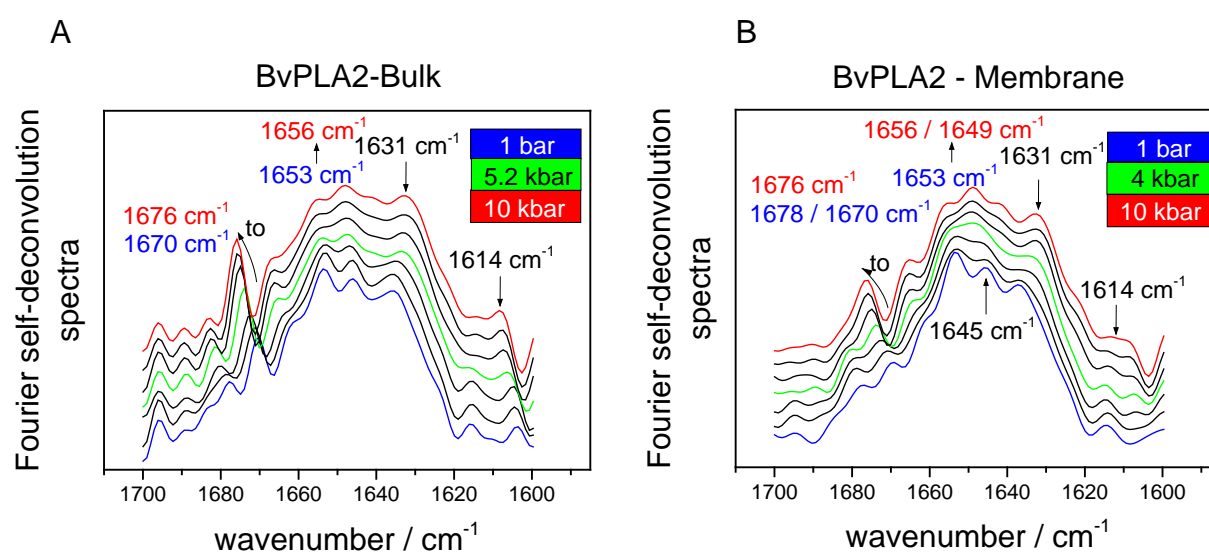


Figure 3.5: Conformational changes in bvPLA2 upon pressurization at 37 °C (A) in bulk buffer solution and (B) in the presence of the lipid bilayer in the pressure range from 1 bar to 10 kbar.

To reveal the pressure stability of the enzyme first, we measured high-pressure FTIR spectra of bvPLA2 in the pressure range from 1 bar to 10 kbar and analyzed the pressure-induced changes in the amide I' spectral region of the protein (Figure 3.5). The second derivative spectra of the amide I' band allow a better visualization of the changes occurring and are shown here in Figure 3.6 (A-B) for the protein in bulk solution and in the presence of a lipid bilayer. BvPLA2 displays an amide I' band contour with similar contents of stable α -helices and β -sheets as well as β -turns and random coil secondary structures, in good agreement with the X-ray crystal structure data (Table 3.1, Figure 3.7).

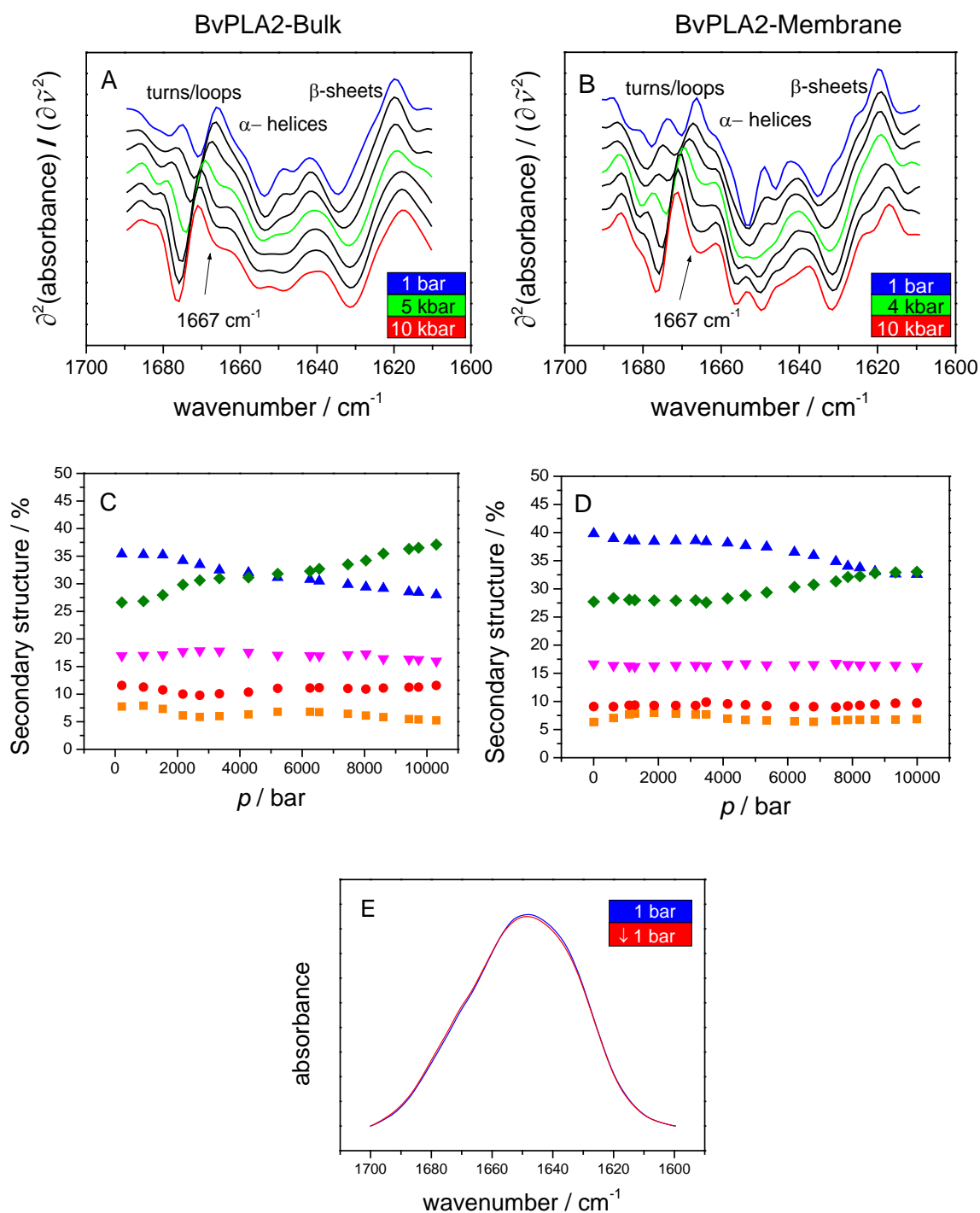


Figure 3.6: Pressure-induced changes in the second derivative amide I' spectra and curve fitting results of the FTIR data for bvPLA2 (A) in bulk solution and (B) in the presence of the lipid bilayer. Secondary structural changes (\blacktriangle α -helices, \blacklozenge β -sheets, \blacktriangledown random structures, \bullet & \blacksquare turns and loops) of bvPLA2 as a function of pressure at 37 $^{\circ}\text{C}$ in (C) bulk solution and (D) in the presence of the lipid bilayer. (E) Comparison of amide-I' spectra of bvPLA2 in bulk solution at 1 bar before and after pressurization, indicating full recovery of the native protein structure.

The bvPLA2 protein maintains its compact tertiary structure even at high pressures of 10 kbar, indicating a high pressure stability of this protein. Linear pressure-induced frequency shifts (elastic effects) are frequently observed as a result of pressure-induced compression of the chemical bonds equivalent to changes of the force constant. All secondary structural elements except β -sheets exhibit this blue shift. The band position for intramolecular β -sheets observed at 1635 cm^{-1} remains constant throughout the entire pressure range, indicating the absence of solvent exposed β -sheets up to 10 kbar.¹³⁶ Only small, but reversible changes in spectral shape are visible upon pressurization (Figures 3.6 A-B, E), which renders bvPLA2 a very attractive model for detailed high-pressure enzymological studies of membrane associated proteins. For bvPLA2 in bulk solution, we notice a small decrease is the observed α -helical content upon compression with a concomitant increase of β -sheets, but the contribution of unordered secondary structure elements does not increase. At pressures above ~ 5 kbar, a subband appears at 1667 cm^{-1} , suggesting pressure-induced formation of solvated turns/loops.¹⁵⁷ The pressure-induced secondary structural changes can be more easily monitored by means of a quantitative fit analysis of the amide I' band region using mixed Gaussian and Lorentzian line shapes for deconvolution. As can be deduced from Figure 3.6 (C-D) the α -helix content decreases by about 7%, and intramolecular β -sheets increase concomitantly by about 10% altogether. Hence, these data indicate a minor pressure-induced shift toward more β -sheets at the expense of α -helices in the high-pressure state of the protein.

Members of the sPLA2s are activated by attaching to the plasma membrane, thereby rendering the membrane interaction of the bvPLA2 proteins crucial for their function. Therefore, the effect of membrane binding on the pressure-induced conformational changes needs to be explored and compared with the bulk solution behavior. FTIR amide I' spectra were recorded for bvPLA2 bound to the anionic model raft membrane DOPC/DOPG/DPPC/DPPG/Chol 20:5:45:5:25 (molar ratio) under noncatalytic conditions. We observe small secondary structural changes in the protein upon membrane binding at ambient pressure (Figure 3.7). Changes are mainly observed in the α -helical regions when compared to the bulk behavior, suggesting their involvement in membrane binding. This result is consistent with earlier observations by Pande et al., showing that bvPLA2 predominately exhibits membrane interaction through the helical region that is lying at the lipid interface (Figure 3.8).³⁹

Table 3.1. Secondary Structure Content of BvPLA2 at Ambient Pressure as Determined by X-ray Diffraction²² in Comparison with the FTIR Spectroscopy Data Obtained in this Study (accuracy: $\pm 2\%$). Please note that owing to differences in transition dipole moments of the different secondary structure elements, full agreement of the X-ray and FTIR data cannot be expected. Rather, relative pressure-induced changes will essentially be discussed.

Secondary structure element	BvPLA2 from X-ray diffraction (1POC)	BvPLA2 in bulk solution from FTIR	BvPLA2 in the presence of membrane from FTIR
α -helices	29.1 %	35.4 %	39.8 %
β -sheets	22.4 %	26.6 %	27.7 %
turns	31.3 %	19.4 %	15.4 %
unordered/random	17.2 %	18.6 %	17.1 %

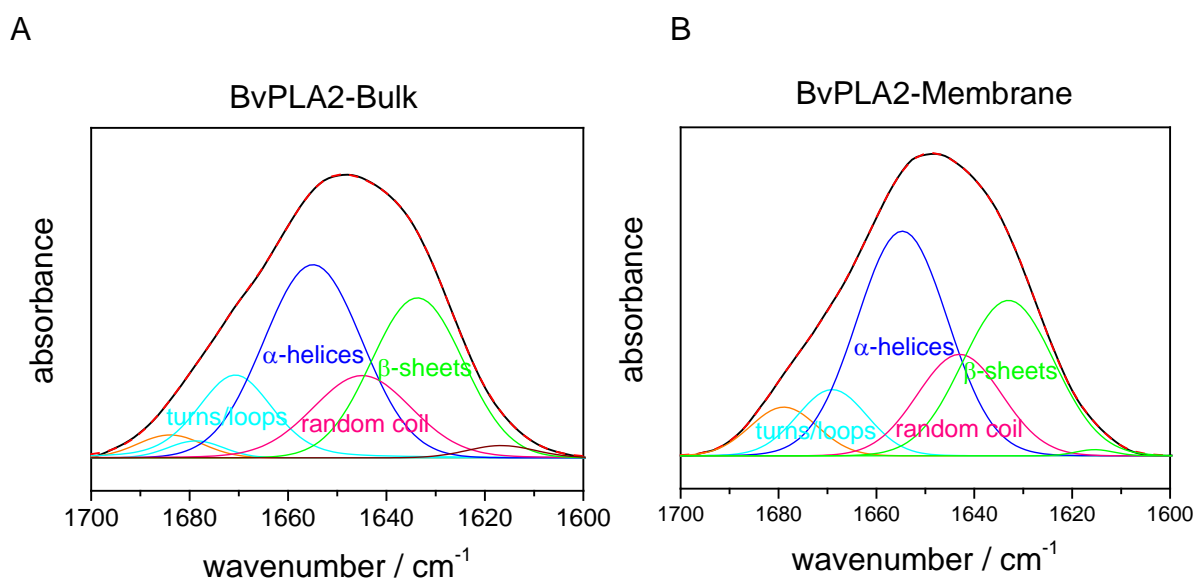


Figure 3.7: Curve fitting results of the FTIR data at 1 bar for BvPLA2 in bulk solution (a) and in the presence of the lipid bilayer (b). The raw FTIR spectrum is shown in black, the fitted spectrum in red, and the component bands assigned to the secondary structure elements are marked as well according to the assignment given in Table 3.1.

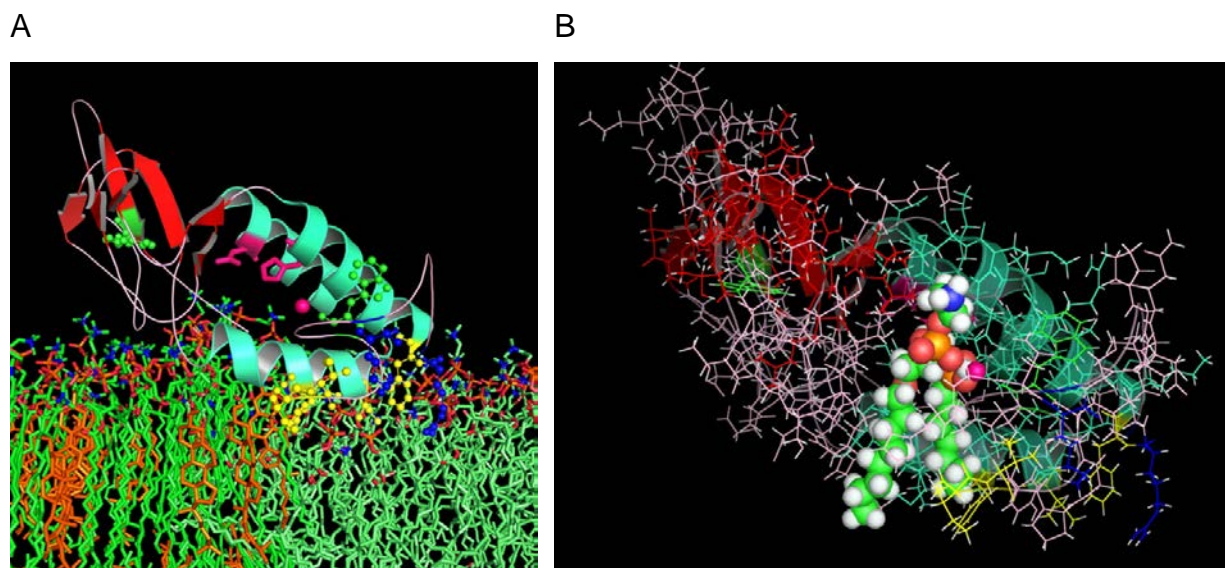


Figure 3.8: (A) Model of a lipid vesicle binding bvPLA2. The hydrophobic residues surrounding the substrate binding cleft and involved in membrane anchoring, Ile-1, Ile-2, Phe-24, Ile-78, and Phe-82, are colored in yellow, and the cationic residues that support membrane binding by ionic and/or H-bonding interactions with the lipid polar groups, Lys-14, and Arg-23, are colored in blue. Trp-8 and Trp-128 are colored green (ball and stick format). The active site residues, the His-34 Asp-64 diad, and the bound Ca^{2+} are shown in magenta. BvPLA2 orientation to the membrane-water interface and the depth of insertion is accessed from.^{37,39} (B) Bee venom phospholipase A2, bvPLA2, with a phosphonate transition-state analogue (1-O-octyl-2-heptylphosphonyl-*sn*-glycero-3-phosphoethanolamine) in the active site (pdb entry 1POC).²² Atoms of the transition-state analogue are represented by colored spheres: C (green), H (white), O (red), P (gold), and N (blue).

The α -helical peak at 1651 cm^{-1} has also been found to split into two subcomponents at ~ 1650 and $\sim 1658\text{ cm}^{-1}$ in the presence of POPC/POPG lipid vesicles, the latter supposed to be due to a flexible, more dynamic α -helix.²⁸ A subband for solvated turns/loops at 1667 cm^{-1} (minimum in the second derivative spectra) in the presence of membrane appears at rather low pressures, which becomes more clearly visible at higher pressures. This small difference compared to the bulk solution structure can be linked to formation of a more flexible conformation of the PLA2 upon membrane binding due to disruption of a few intrahelical hydrogen bonds and formation of such bonds between the enzyme and the phosphate, carbonyl, and hydroxyl groups of membrane lipids. These data are in agreement with findings of Tatulian et al., who showed that the free enzyme in solution displays more resistance to amide $^1\text{H}/^2\text{H}$ exchange than the membrane-bound enzyme, suggesting an increase in flexibility in α -helical regions induced by snake venom PLA2 binding to lipid

bilayers.²⁸ It has been proposed that more flexible helices are formed at the expense of disruption of a few intrahelical hydrogen bonds for membrane attachment and enzyme-substrate hydrogen bonding, leading to transition-state complex stabilization for efficient catalysis.^{28, 158}

Figure 3.6 (D) displays the variation of the secondary structural contents of membrane-bound bvPLA2 with increasing pressure. For membrane-bound bvPLA2, upon compression, the helix content decreases by about 7%, similar to the bulk behavior, with a concomitant increase in β -sheets by 6%, whereas observed changes for unordered structures and turns/loops are less than 1%, i.e., insignificant within the accuracy of the experiment. Interestingly, these pressure-induced small conformational changes appear for the membrane associated protein at much higher pressures (>4 kbar) compared to the bulk (>~1.5 kbar), indicating strong stabilization of the conformation of bvPLA2 in its membrane-bound form (Figure 3.6 C-D).

3.3.2 Membrane Association of BvPLA2

Secretory PLAs are water soluble enzymes that must adsorb to the substrate membrane interface for phospholipid hydrolysis to occur.²³ Even though the secreted enzymes exhibit similar catalytic mechanisms, for example with respect to the orientation of the catalytic water and the active site histidine and aspartate residues which are very similar in bvPLA2 and porcine pancreatic PLA2,²² the mechanism of interfacial activation and specificity to membrane components upon binding seems to vary significantly. PLA2s with an excess of basic residues on the lipid binding surface display the strongest affinity toward negatively charged lipid surfaces, and PLA2s containing a tryptophan in the lipid binding surface display strong affinity towards neutral lipid substrates.³⁶ It has been suggested that binding of bvPLA2 to phospholipids occurs predominately in a non-electrostatic fashion with hydrophobic interactions together with hydrogen-bonding providing a major portion of the interfacial binding energy.^{34,38} Hydrophobic and basic residues of bvPLA2 involved in membrane anchoring are depicted in Figure 3.8. Additionally, interfacial activation is affected by membrane fluidity and curvature,^{159,160} which are known to be largely affected by temperature and pressure.^{127,133} Interestingly, the activity of bvPLA2 appears to be less sensitive to membrane fluidity. Substitution of DOPC with the more rigid POPC decreases

the activity by only 8% in contrast to a 51% reduction of porcine pancreatic PLA2.¹⁶¹ The reason might be that bvPLA2 does not penetrate as deep into the hydrocarbon core of the lipid bilayer like other PLA2s such as porcine pancreatic or human PLA2s do.^{39,162} It has been suggested that isoform-specific differences in membrane-binding modes between PLA2s are likely related to their mechanistic differences.³⁹

In order to study the association of PLA2 with liposomes, we used a fluorescence-based assay for the kinetic analysis of this interaction.¹⁶³ The spatial approximation of bvPLA2 to liposomes was detected by Förster resonance energy transfer (FRET) from the intrinsic protein tryptophans to a PC-based fluorescent dye (β -DPH HPC) embedded in the lipid bilayer, allowing emission to be observed in the range of 420-520 nm. The 15-kDa bvPLA2 protein has 2 tryptophan residues, at positions 8 and 128. Detected changes in the intensity of the fluorescent signal upon PLA2-liposome binding were in the range of 10-40% (Figures 3.9 A-B).

The time course of the association process could be described by a bi-exponential function, implying that the bvPLA2-membrane interaction occurs in at least two steps. The fast step should involve the initial attachment of the enzyme upon binding to the lipid vesicles, while the slower second phase is expected to represent the reorientation of the enzyme at the lipid interface in a catalytically productive manner, involving structural rearrangements of α -helical regions of the bvPLA2 as observed in the FTIR measurements. From a bi-exponential fit of the association curves at different lipid concentrations, the corresponding observed rate constants, $k_{\text{obs},1}$ and $k_{\text{obs},2}$, were derived and the binding kinetics quantified. For the interaction of 0.35 μM bvPLA2 with 62.5 μM lipids in unilamellar vesicles at 37 °C, the fast association process for the phase-separated anionic raft-like membrane, exhibiting liquid-ordered (l_o)/liquid-disordered(l_d) domain coexistence, revealed a rate, $k_{\text{obs},1}$, of about 39 s^{-1} , which is almost 10 times higher than that of the slower process with a rate, $k_{\text{obs},2}$, of about 3.0 s^{-1} . The second process contributed approximately 40% to the entire FRET signal increase, A. (Figure 3.10). Increasing the lipid concentration stepwise from 31.3 to 125 μM , with the concentration of PLA2 kept constant at 0.35 μM , displayed a marked increase of the fast association rate as a function of lipid concentration, ranging from 30 to 50 s^{-1} . The slower component, however, remained approximately constant at 3.0 s^{-1} , i.e., is essentially independent of the lipid concentration.

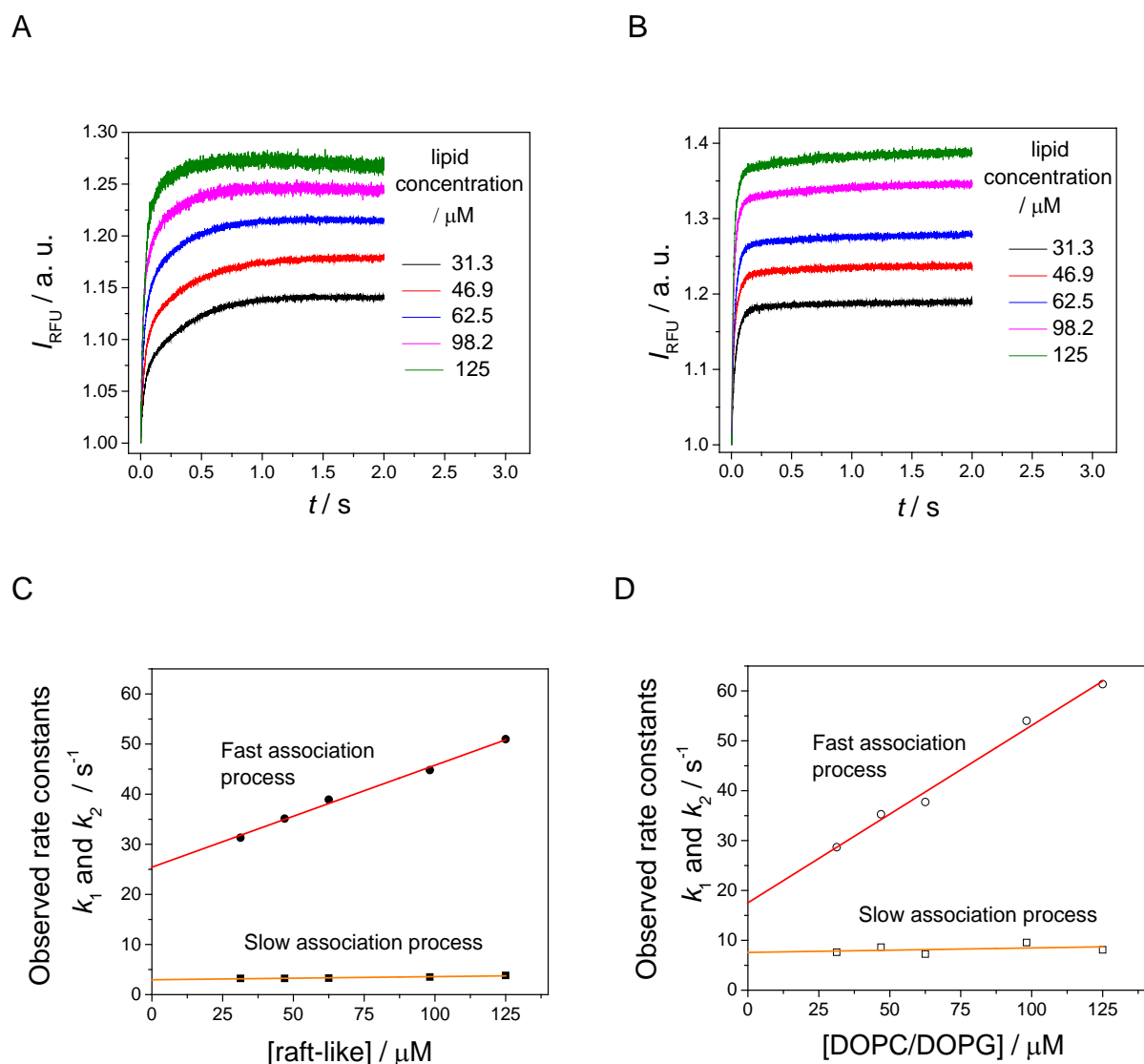


Figure 3.9: PLA2 binding to lipid membranes. Association curves expressed in relative fluorescence units (I_{RFU}) of a stopped-flow kinetic experiment with 0.35 μM bvPLA2 and increasing concentrations of liposomes, (A) anionic raft-like vesicles DOPC/DOPG/DPPC/DPPG/Chol/DPH-HPC 19/5/43/5/24/4 mol% and (B) DOPC/DOPG/DPH-HPC 86/10/4 mol%. The FRET measurements reveal a fast concentration-dependent and a slower concentration-independent association process for (C) the anionic raft-like and (d) the DOPC/DOPG lipid vesicles.

In a second experimental series, we studied bvPLA2 binding to the homogeneous anionic membrane DOPC/DOPG (lipid bilayer with a molar ratio 90/10) which exhibits an all-fluid (l_d) phase, only. We found that, in contrast to that of raft-like phase separated membranes, binding of PLA2 to vesicles composed of the DOPC/DOPG mixture displays an about 2-fold faster rate constant for $k_{\text{obs}2}$ (about 7.5 s^{-1}), and this slower second process contributes only

10% to the entire FRET signal increase (Figure 3.10). The fast component $k_{\text{obs}1}$ is of similar magnitude at low to medium lipid concentrations. A careful analysis of the slow binding

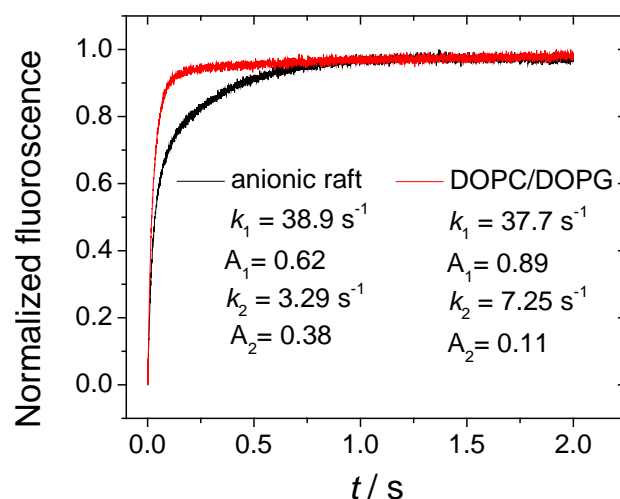


Figure 3.10: Representative association curve of 0.35 μM bvPLA2 to liposomes of anionic raft-like and DOPC/DOPG bilayers at a 62.5 μM lipid concentration.

kinetics of bvPLA2 to the heterogeneous anionic raft-like membrane with respect to the homogeneous DOPC/DOPG membrane reveals a more complex behavior, which might be due to effects of changes in localization and/or lipid sorting to reach a favorable fluid environment which is required for PLA2 function.

A linear fit to the observed rate constants ($k_{\text{obs}} = k_{\text{on}} [\text{Lipid}] + k_{\text{off}}$) allowed the calculation of the dissociation constant, $K_{\text{d},1} = k_{\text{off},1}/k_{\text{on},1}$, for the fast binding step 1. Taking into account that one bvPLA2 molecule is surrounded by about 20 lipids forming its binding site,³⁸ an apparent second-order association rate constant for the first rapid phase, k_{on} , was obtained from the slope of the plot shown in Figures 3.9 (C-D), yielding a value of $k_{\text{on}} = (0.203 \times 10^6 \text{ M}^{-1} \text{ s}^{-1} \times 20) = 4.07 \times 10^6 \text{ M}^{-1} \text{ s}^{-1}$ for the raft mixture, and the dissociation rate constant, k_{off} , from the intercept with the ordinate, amounts to 25.4 s⁻¹, which corresponds to a first-order rate constant for the reverse reaction. Hence, the fast membrane binding phase of bvPLA2 to raft-like lipid vesicles is associated with a $K_{\text{d},1}$ value of 6.2 μM . Following the same considerations, a $K_{\text{d},1}$ value of 2.5 μM was obtained for DOPC/DOPC vesicles. The overall

process including the fast and slow phases of binding bvPLA2 to these model membranes is expected to proceed with a dissociation constant in the submicromolar range ($K_d < 1 \mu\text{M}$).³⁴

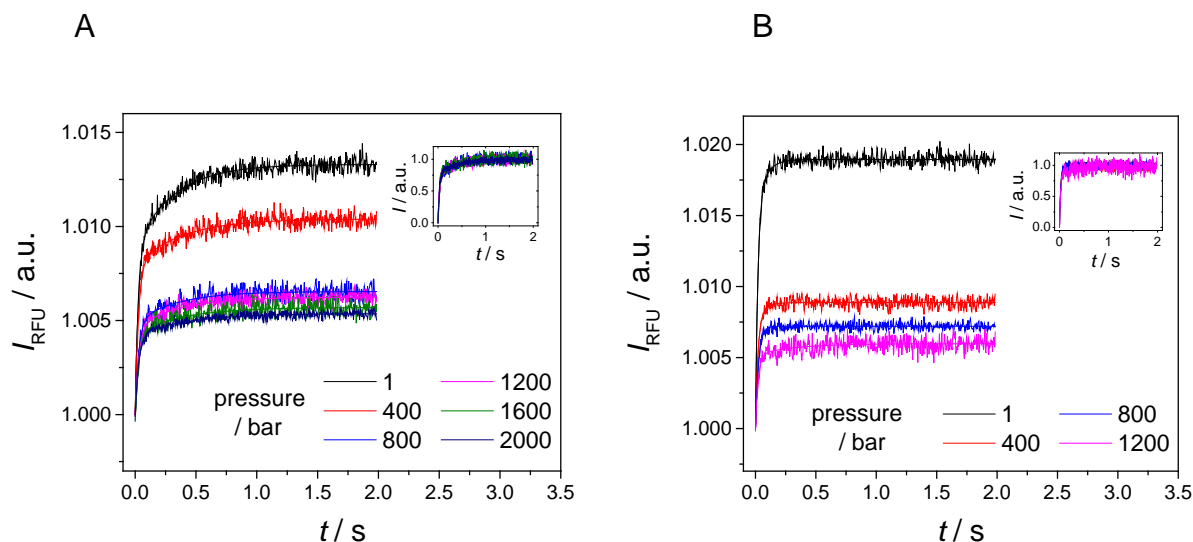


Figure 3.11: Pressure-independent PLA2 association kinetics to lipid bilayers composed of (a) the anionic raft-like and (b) DOPC/DOPG lipid vesicles. Thin solid lines represent double-exponential fits to the experimental data. The inset shows the intensity-normalized fluorescence curves.

Figure 3.11 displays the binding reaction of bvPLA2 to model membranes under HHP conditions, measured using the high-pressure stopped-flow technique with fluorescence detection. Interestingly, pressure has a minor effect on the binding rate constant of PLA2 to the lipid membranes. The observed fast association rate observed in this high-pressure setup is in excellent agreement with the ambient-pressure stopped-flow data (Figure 3.10), yielding, for example, a value of $k_{\text{obs},1} = 38 \text{ s}^{-1}$ for the $62.5 \mu\text{M}$ lipid concentration at ambient pressure, which decreases slightly with increasing pressure, only. The inset of Figure 3.11 exhibits the overlap of normalized fluorescence curves for the different pressures studied, demonstrating the pressure-insensitivity of $k_{\text{obs},1}$. The amplitude of the FRET signal of the binding process decreases markedly with pressure, however, implying a decrease in the equilibrium association constant, which may be due to a continuous increase in lipid chain packing upon pressurization. In fact, ^2H -NMR-experiments on fluid lipid bilayers revealed a decrease of the chain-cross sectional area of about $10 \text{ \AA}^2/\text{kbar}$.¹⁶⁴ However, the intrinsic pressure dependence of the fluorescence intensity of the β -DPH-HPC molecule suggests that a part of the observed

effect may be due to the reduction of the emission intensity of the β -DPH-HPC fluorophore with increasing pressure (Figure 3.12).

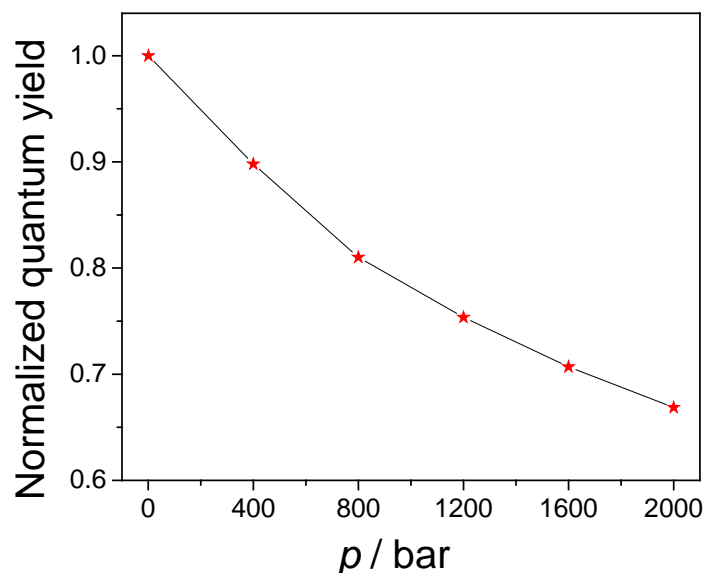


Figure 3.12: Pressure dependence of the fluorescence intensity of the β -DPH-HPC fluorophore. Pressure induced changes on the fluorescence of pure β -DPH-HPC labelled anionic raft-like lipid vesicles ($c_{\text{lipids}} = 0.125$ mM, $c_{\beta\text{-DPH-HPC}} = 5$ μ M, ex: 340 nm, em: 435nm) at 37 $^{\circ}$ C. The steady-state fluorescence intensity data are normalized to the 1 bar fluorescent intensity value.

Considering that charges and the hydration of the membrane surface and also the packing of the lipid head groups are not expected to change markedly in the 1-2000 bar pressure range,¹²⁸ a high packing efficiency of the protein with the membrane interface seems to be mainly responsible for the pressure independence of the association rate and the high stability of the membrane-bound protein, which forms a tight complex. Other studies revealed that membrane-associated mellitin and phospholipase C β are unaffected by pressure, concluding that previously observed displacement of integral membrane proteins with hydrostatic pressure are not a primary effect of increased lipid packing.^{132,165}

3.3.3 Pressure Dependence of the Hydrolysis Reaction of BvPLA2

The kinetics of the hydrolysis reaction of phospholipid vesicles by PLA2s can be described by the Michaelis-Menten formalism.^{35,40} The interfacial binding surface of the sPLA2 is distinct from the active site. Typically, the membrane attached enzyme can be found in three states: without bound substrate in its active site, with a substrate phospholipid molecule forming a classical Michaelis complex, or with bound product.¹⁵⁹ Generally, PLA2 specificity to substrate is regulated by a combination of two factors. First, PLA2's ability of membrane surface binding ($E \leftrightarrow E^*$), which is related to an equilibrium dissociation constant. Second, after attachment to the membrane surface, the rate of hydrolysis of different substrates species by E^* is governed by the relative interfacial specificity constant (k_{cat}^*/K_M^*), where K_M^* is related to the strength of PLA2 binding to a substrate molecule in its active site upon E^*S complex formation ($E^*+S \leftrightarrow E^*S$), while k_{cat}^* displays the rate constant for the breakdown of the E^*S complex ($E^*S \rightarrow E+P$).²³ Hence, binding and activity should be studied separately for allowing a detailed interpretation of PLA2 action.

Figures 3.13 (A-B) display the reaction progress curves, i.e., the increase of Bodipy fluorescence of the reaction product with time, for the action of the bvPLA2 on lipid vesicles containing the heterogeneous raft-mixture and the homogeneous fluid-like DOPC/DOPG mixture, respectively. The rate of hydrolysis is enhanced as the substrate concentration increases and exhibits a curved dependence on lipid vesicle concentration. The initial rates of the corresponding data were fitted to the Lineweaver-Burk equation to determine the steady-state kinetic parameters K_M and k_{cat} of the enzyme (Figure 3.13 C). While the Michaelis constant K_M is inversely proportional to the affinity or strength of a substrate binding to the active site of the enzyme, the turnover number, k_{cat} , provides information on the maximum number of molecules of substrate that an enzyme can convert to product. Precise quantification of the hydrolysis rate is difficult to assess as the available lipid substrate concentration is not easy to determine accurately. The PLA2 kinetics has been extensively studied based on the hydrolysis of only the phospholipids on the outer monolayer of the bilayer under the assumption that the enzyme is operating in a scooting mode (remains in the interface during thousands of catalytic cycles).^{40,159} In contrast to these findings, a later study demonstrated that the reaction kinetics of bvPLA2 is also controlled by flip-flop process and both leaflets of the membrane are apparently hydrolyzed simultaneously.¹⁶⁶

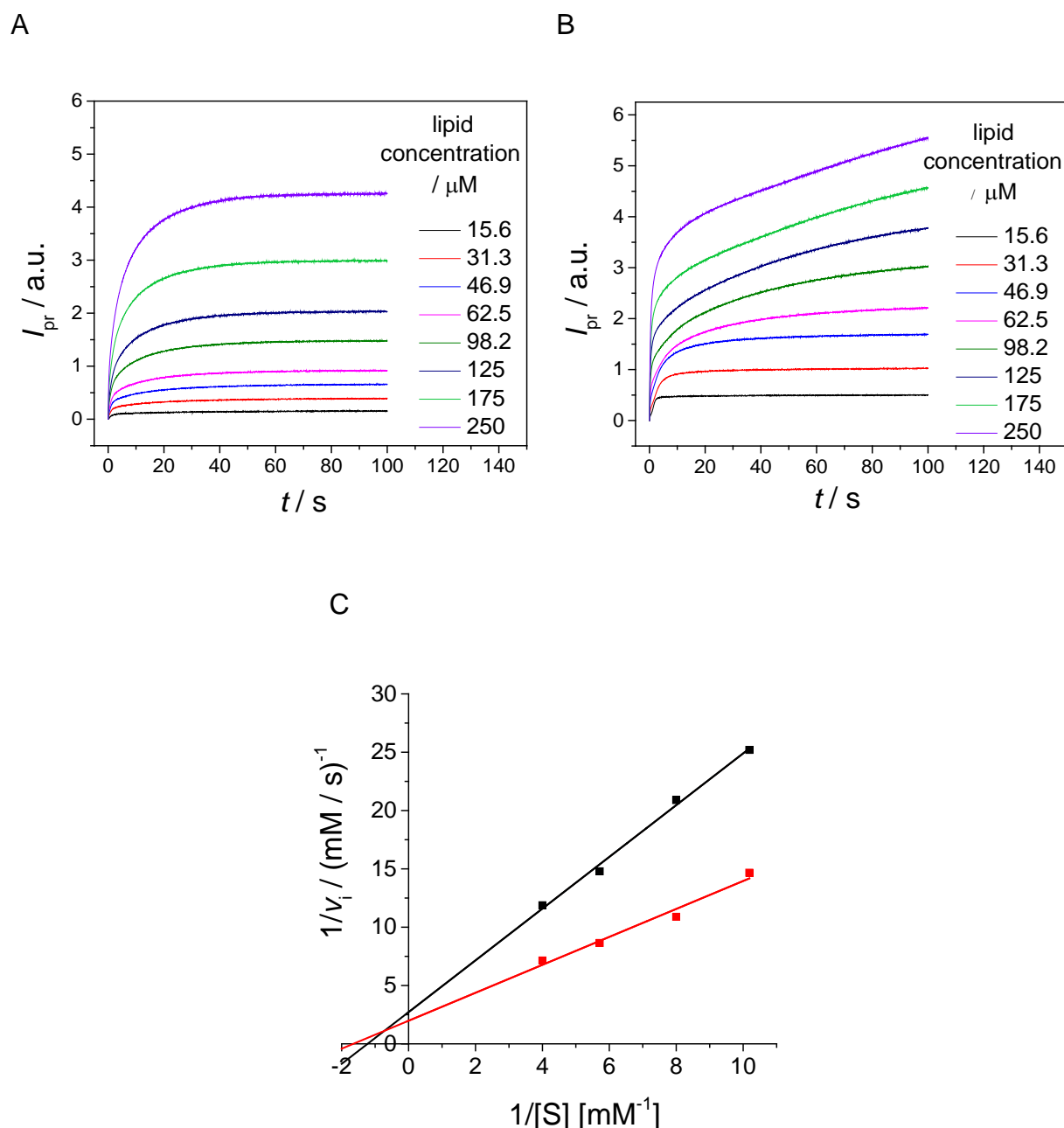


Figure 3.13: PLA2 activity in the presence of lipid membranes monitored by the fluorescence increase of the product (DBPC), I_{pr} , as determined by stopped-flow kinetic experiments using 0.35 μ M bvPLA₂ and increasing concentrations of liposomes: (A) anionic raft membrane DOPC/DOPG/DPPC/DPPG/Chol/DBPC 19.5/5/44/5/24.5/1 mol%, and (B) homogeneous anionic bilayer DOPC/DOPG/DBPC 89/10/1 mol%. (C) Double reciprocal plot of the initial rate of hydrolysis as a function of substrate concentration, [S], for the anionic raft mixture (black) and the DOPC/DOPG membrane (red). Calibration was performed on the same samples after 24 h of the reaction, assuming full hydrolysis of the substrate.

Arbitrary units of the Bodipy containing product fluorescence signal were converted to μ M s $^{-1}$ by using calibration measurements on the same samples assuming full hydrolysis of

the corresponding vesicles after 24 h of the reaction. The Lineweaver-Burk double-reciprocal plot of the kinetic data yield the following values for the anionic raft-like membrane: $K_M = 0.8$ mM, $k_{cat} = 1048$ s⁻¹ and $k_{cat}/K_M = 1.3 \times 10^6$ M s⁻¹, while for DOPC/DOPG vesicles values of $K_M = 0.6$ mM, $k_{cat} = 1442$ s⁻¹, and $k_{cat}/K_M = 2.4 \times 10^6$ M s⁻¹ are obtained, respectively. The k_{cat} values are 10-15 times larger in comparison to those of bvPLA2 on vesicles composed of 1,2-dimyristoylglycero-*sn*-3-phosphomethanol (DMPM) with blocked flip-flop.¹⁵⁹ The catalytic efficiency of the enzyme, k_{cat}/K_M , is comparable to that of human secretory PLA2.¹⁶⁷ PLA2 activation and the recognition of membrane lipids are believed to be largely determined by lipid protrusion.²⁴ The enzyme operating on the DOPC/DOPG model membrane substrate displayed a higher catalytic efficiency compared to that of the phase separated anionic raft-like mixture. This effect is probably due to a lower concentration of hydrolysis-competent disordered fluid lipid phase lipids in the heterogeneous membrane, which contains also 25% cholesterol, which is known to partially block the activation of PLA2.¹⁶⁸

The overall characteristics of the membrane, including lipid packing, curvature, cholesterol level as well as phase separation into domains of different lipid order and fluidity have been shown to have a marked influence on PLA2 activation and hydrolysis.^{29,160} As pressure has a marked effect on all these parameters,^{50,51} pressurization is expected to largely control the hydrolysis rate of PLA2s. In particular, lipid bilayer thickness, dynamic properties and the membrane's lateral organization are significantly altered upon compression.^{133,169} For example, membranes may contain lipid domains, i.e., aggregates of lipids in liquid-ordered (l_o) phases dispersed in liquid-disordered (l_d) phase lipids. The l_o phase is characterized by tight chain packing, reduced fluidity, high cholesterol level and extended lipid chains, although the lipid mobility is still high. Since high pressure promotes chain order, the application of pressure diminishes the disordered domains and the physical properties of the phases will become increasingly similar with pressure. Such scenario is expected to occur in our model raft mixture,¹⁶⁹ but domain coexistence is still persisting up to the 2 kbar region as applied here.⁷⁷ Conversely, DOPC vesicles remain in the liquid-disordered state under all studied pressure conditions, owing to its very low gel-to-fluid transition temperature ($T_m \approx -20$ °C).¹⁷⁰ The lipid bilayer thickness increases by about 1 Å kbar⁻¹ in the liquid-like phase, only.³⁸

The effect of pressure on the activity of bvPLA2 was determined by measuring the steady-state enzyme kinetics at high pressure using rapid-mixing high-pressure stopped-flow (HPSF) methodology, which allows measurements up to 2 kbar with 2 ms time resolution and rapid fluorescence detection. Representative reaction traces for the two membrane systems are displayed in Figures 3.14 (A-B). The slope of the time-dependent fluorescence change of the Bodipy-labelled reporter group in the reaction product decreases drastically with increasing pressure, indicating reduced hydrolysis rates upon pressurization. With respect to ambient pressure, the rate of the hydrolysis reaction decreases by a factor of 1.14 (~12% at 400 bar) at low and of 2.6 (~60% at 1600 bar) at high pressures in the model raft mixture, and by corresponding factors of 1.3 (~22%) and 3.3 (~70%), in the DOPC/DOPG membrane, respectively. As demonstrated by the FTIR data discussed at the beginning, these effects are not due to a pressure-induced denaturation of bvPLA2, which does not change its structure up to 4 kbar (Figure 3.6 D). Analysis of Michaelis–Menten parameters for the pressure dependent study on the anionic raft-like membrane yields K_M values, which are within the experimental error bar of about 20% essentially independent of pressure, whereas k_{cat} decreases by a factor of 4–5 in the pressure range from 1 bar to 2 kbar.

The activation volume, i.e. the volume difference between the transition state and the reactants, ΔV^\ddagger , can be deduced from the slope ($-\Delta V^\ddagger/RT$) of the $\ln(S/S_0)$ vs. p plot (Figure 3.14 C), where S is the slope of the fluorescence signal, $(dI_{pr}/dt)_p$, at pressure p relative to that at 1 bar, S_0 .¹⁷¹ As can be clearly seen, the effect of pressure on the rate of the reaction is non-linear, rendering ΔV^\ddagger pressure dependent. ΔV^\ddagger for the enzyme activity in the anionic raft mixture increases from about $13 \pm 3 \text{ mL mol}^{-1}$ at low pressures to $23 \pm 6 \text{ mL mol}^{-1}$ approaching 2 kbar. Corresponding values for the DOPC/DOPG lipid mixture amount to $26 \pm 10 \text{ mL mol}^{-1}$ and $10 \pm 3 \text{ mL mol}^{-1}$, respectively. The positive ΔV^\ddagger values obtained reveal that the volume increases upon formation of the transition state. Alternatively, the pressure dependence of $\ln(S/S_0)$ can be analyzed using $\ln(k_{cat}/k_0) = -\Delta V^\ddagger p/(RT) + \Delta\kappa^\ddagger p^2/(2RT)$, i.e., by adding a compressibility term, where $\Delta\kappa^\ddagger$ is the activation compressibility, i.e., the partial molar compressibility difference between the transition and the reactant state. In this case, we yield a pressure independent activation volume for the anionic raft-like membrane of $\Delta V^\ddagger = 9 \text{ mL mol}^{-1}$ and a negative $\Delta\kappa^\ddagger$ value of $-8.7 \times 10^{-3} \text{ mL mol}^{-1} \text{ bar}^{-1}$, which reflects a larger compressibility of the enzyme–substrate complex compared to the transition state.

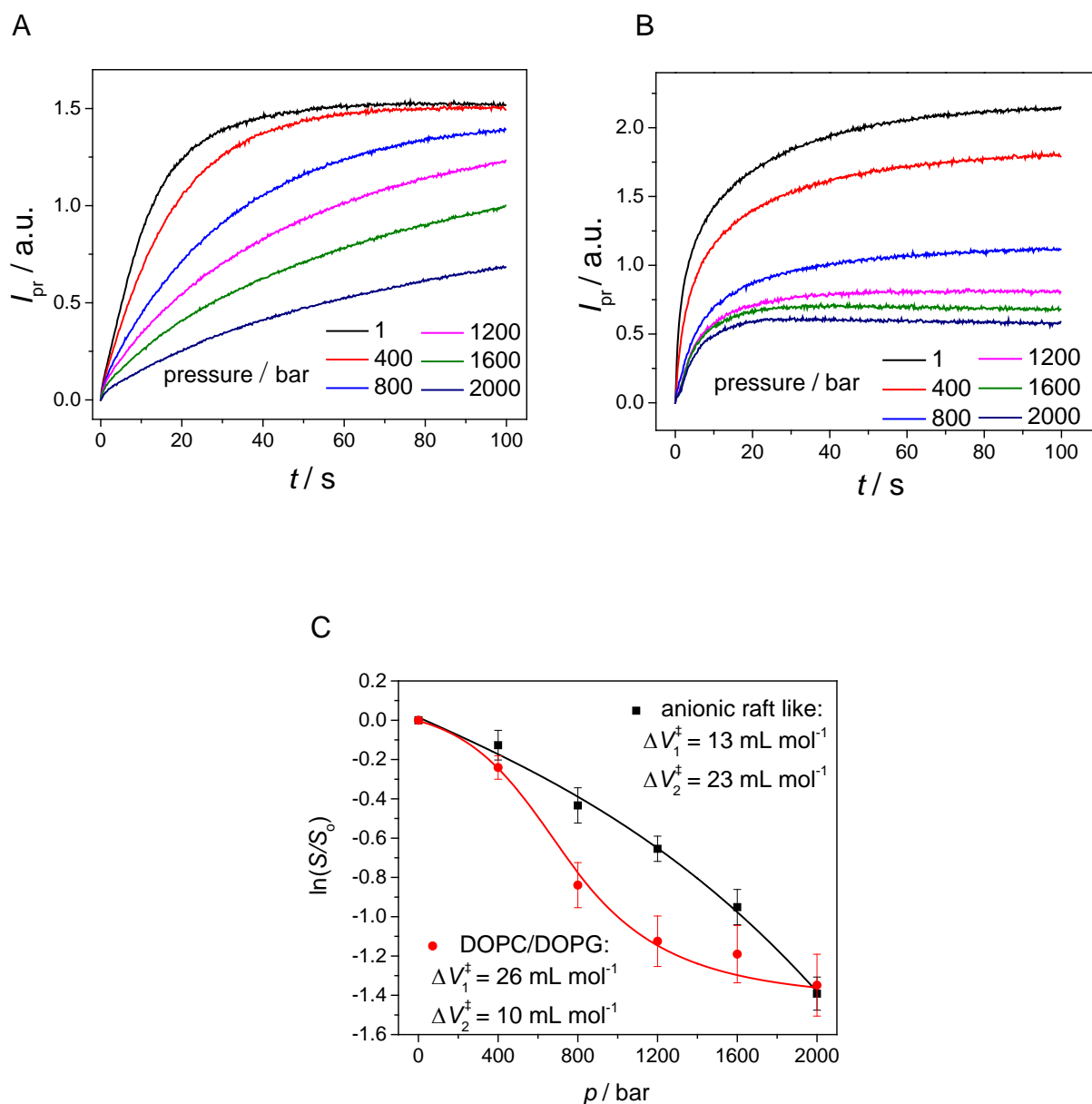


Figure 3.14: Effect of hydrostatic pressure on the rate of DBPC hydrolysis by bvPLA2 for (A) raft-like and (B) DOPC/DOPG lipid vesicles. (C) Pressure dependence of the enzymatic activity in the presence of anionic raft-like (black rectangles) and DOPC/DOPG (red circles) membrane. S and S_0 are the slopes of the fluorescence intensity as a function of time at pressure p and ambient pressure (1 bar), respectively. The slopes of the plots were determined by averaging first derivative of corresponding curves for initial 2 s.

Since the structure of bvPLA2 remains unperturbed up to 2 kbar, changes in activity upon pressure application should mainly result from the activation of the bvPLA2-phospholipid complex. If the transition state has a molecular volume different from that of the total volume of the reactants, i.e. $V(E+S) \neq V(ES^\ddagger)$, a volume change in forming the activated complex can be directly measured from the pressure dependence of the rate constant k_{cat} (Figure 3.14). Clearly, a positive activation volume, ΔV^\ddagger , of 13-26 mL mol⁻¹ indicates that pressure creates an elastic barrier to transformation by favoring the smaller-volume reactant state. Further interpretation of the sign and magnitude of the activation volume is not a straightforward task because the experimentally obtained value can be represented by the sum of various contributions, including (i) intrinsic structural changes that result from disruption or formation of new bonds, (ii) solvation changes, which is often the dominating contribution that arises from the rearrangement of water molecules around interacting groups in the course of the reaction,¹³⁷ which is especially prominent when charge and dipole changes occur in the reacting molecules, and (iii) a substrate-induced volume change of the enzyme's conformation associated with chemical steps of the reaction, which includes possible changes in size of cavities and voids.^{137,146} The proposed mechanism of PLA2 catalysis by Scott et al. suggests that the transition state is stabilized by displacement of two water molecules to the bulk solvent, while no significant deformation of the enzyme structure is required to achieve substrate transfer to the productive binding mode.³¹ Clearly, release of two tightly bound water molecules from the active site of the enzyme to the bulk can increase the net volume of the transition state. On the other hand, it has been shown that the interfacial activation of the enzyme involves allosteric coupling between the membrane-binding site and the catalytic center of PLA2.^{27,172} The latter mechanism could involve creation of cavities, i.e. void volume, to the observed overall volume increase upon formation of the transition state.

3.3.4 AFM Imaging of BvPLA2 Activity

Heterogeneous model membrane systems such as DOPC/DOPG/DPPC/DPPG/Chol have been widely used in studies to gain detailed information about membrane protein interactions.^{83,59} The five component membrane anionic raft-like system leads to segregation into liquid-ordered and liquid-disordered phases and mimics the heterogeneity of biological membranes. To reveal the behavior of PLA2 upon membrane interaction on a nanometer length scale with an imaging technique, time-lapse tapping mode atomic force microscopy (AFM) experiments were carried out (Figure 3.15). The interaction between the enzyme and membrane was followed by imaging the same membrane region at different time points. Lipid spreading forms coexistence of liquid-ordered (l_o phase) and liquid-disordered (l_d phase) phases with a height difference of approximately 1 nm between l_o and l_d domains, which is in good agreement with previous studies (Figure 3.15 A),^{59,77} showing that the thickness of the lipid bilayer is approximately 5.2 nm for the l_o -phase and 4.0 nm for the l_d -phase.⁷⁷ Time-lapse tapping-mode AFM experiments were then carried out first after injection of the enzyme solution under noncatalytic conditions (250 μ L of 0.35 μ M PLA2 in the presence 0.5 mM EGTA in buffer solution) to observe possible rearrangements of lipid phases upon PLA2 insertion into the lipid bilayer. As can be seen from Figure 3.15 (B), no significant changes of the membrane's lateral organization are visible upon bvPLA2 binding. Membrane hydrolysis of the catalytically active enzyme was then monitored in the presence of 2 mM CaCl_2 , revealing hydrolysis of a major part of the membrane already within 10 min after injection (Figure 3.15 C). Moreover, the typical height difference of 1 nm between the l_d - and l_o -phase is no more detectable, implying destruction of the lipid phase co-existence. After 24 hours, the effect of the PLA2 activity on the membrane structure is even more dramatic. Height differences of about 3.7 nm indicate appearance of a remaining thinner disordered phase which is not homogeneously spreading the mica surface anymore, i.e., hole formation is invoked as well. Simonsen et al. pointed out that in case of phase coexistence, PLA2 preferentially hydrolyses the l_d -phase, but a high amount of cholesterol protects lipid bilayers against complete destruction.¹⁶⁸

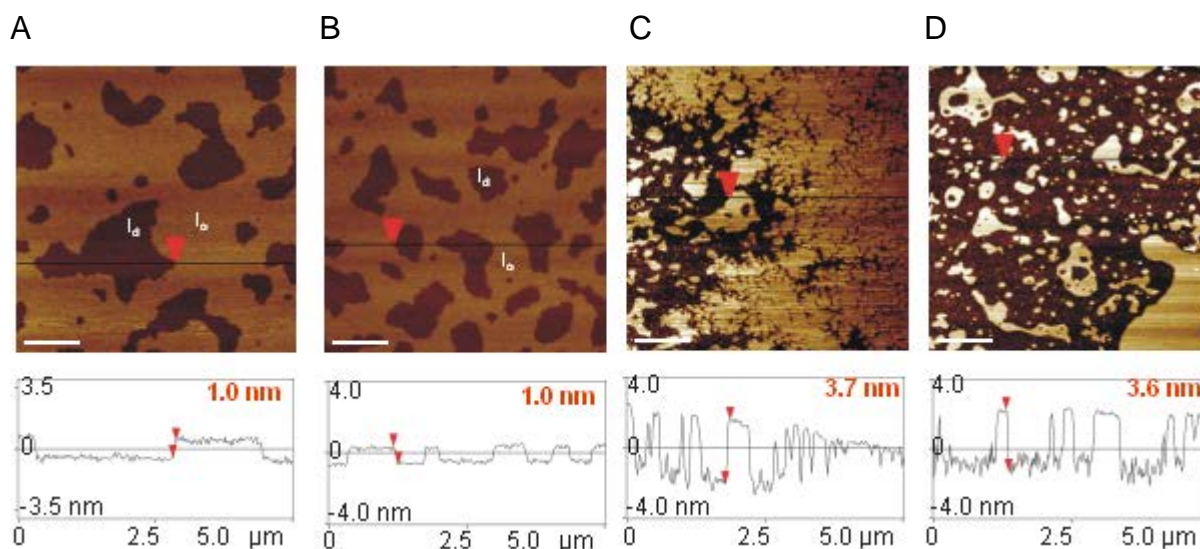


Figure 3.15: AFM visualization of lipid bilayers with coexisting l_o and l_d domains of a heterogeneous DOPC/DOPG/DPPC/DPPG/Chol (20:5:45:5:25 mol%) lipid bilayer membrane on mica at 25 °C of (A) the membrane only, (B) after 10 min of bvPLA2 injection in the presence of EGTA, (C) after 10 min of hydrolysis, and (d) after 24 h of hydrolysis. Corresponding section profile of the AFM images are given below each image. Arrows display height differences between l_o/l_d phases (A-B) or thicknesses of holes in bilayers as a consequence of the hydrolysis reaction (C-D).

3.4 Summary and Outlook

To conclude, in this work we have investigated the structure, membrane binding and catalytic activity of bvPLA2 using pressure modulation and changes in membrane's physical–chemical properties. As demonstrated by our FTIR spectroscopic data, bvPLA2 is a very pressure-stable protein, displaying minor reversible conformational changes between about 1 bar and 10 kbar, only. A small decrease of α -helices is observed with a concomitant small increase of β -structures upon compression. Upon membrane binding, small conformational changes are observed by exposure of α -helical regions to the lipid interface. Membrane binding leads to an enhanced conformational stability of the protein, rendering the protein insensitive to conformational changes upon compression up to 4 kbar (Figure 3.6), which makes the system very suitable for studying pressure effects on its enzymatic activity.

We could show that the PLA2 binding kinetics to DPH-labelled model membranes is not markedly affected by pressure even up to 2 kbar and occurs in at least two kinetically distinct

steps. Followed by fast initial membrane association, structural reorganization of α -helical segments of PLA2 takes place at the lipid water interface. For the interaction of 0.35 μM bvPLA2 with 62.5 μM lipids in raft-like liposomes, the fast association process displayed a rate (k_{obs1}) approximately 10 fold higher than that of the slower process with a rate (k_{obs2}) of about 3.0 s^{-1} . Obtained rate constants displayed an about 2-fold increase of the slower component for the all-fluid DOPC/DOPG mixture compared to that of the heterogeneous raft-like lipid bilayer, which offers more fluid-like hydrolysis-competent phospholipid molecules. In the case of the heterogeneous raft-like lipid mixture, it is very likely that the slower process involves also lipid sorting and lateral diffusion to ensure a suitable lipid environment for optimal function of the bvPLA2. For instance, in heterogeneous phase-separated model membranes, phase boundaries are believed to be a preferential site of phospholipase action.^{160, 29}

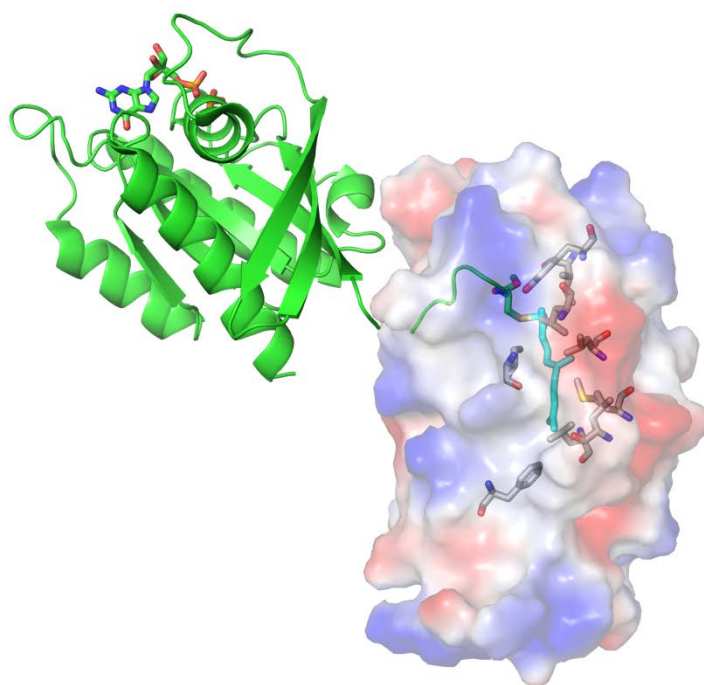
We determined the effect of pressure on the activity of bvPLA2 using an efficient fluorescence dequenching assay with the DBPC fluorophore incorporated into the anionic raft-like and DOPC/DOPG bilayers. To directly proof the heterogeneity of the raft-membrane and to visualize the action upon addition of PLA2, we carried out atomic force microscopy (AFM) measurements. In fact, the hydrolysis reaction has a dramatic effect on the lateral organization of the raft domain, finally leading to a complete loss of the lipid phase separation and to formation of holes in the lipid bilayer due to desorption of product molecules. Our activity measurements reveal that pressure has a drastic inhibitory effect on the lipid hydrolysis rate, rendering it a potentially effective pressure sensing system. The enzymatic activity of bvPLA2 decreases by $\sim 75\%$ in the pressure range from 1 to 2000 bar. The reduced activity is largely due to an expansion of the enzyme–substrate structure upon transition state formation, with an activation volume, ΔV^\ddagger , of about 13-26 mL mol^{-1} , which is in the order of 1-2 water molecules, only. Additionally, a decrease in membrane fluidity upon compression may impede conformational changes accompanying various reaction steps, thereby reducing the rate of the overall reaction bvPLA2.

The study of membrane-bound proteins such as PLA2 using HHP modulation clearly has the potential to provide novel information regarding molecular interactions that cause a protein to bind to membranes and their associates with other proteins on the membrane surface, also for extreme environmental conditions. Hence, these results also deepen our understanding of

membrane-associated pressure effects on phospholipase-controlled processes in deep-sea organisms, where pressures up to the kbar-level are encountered. Next to being a primary osmosensor, PLA2 is prone to sense high hydrostatic pressure as well, leading, by its changes in activity, to changes in signaling transduction cascades involved in accumulation and activation of ion channels and of compatible osmolytes and, thus, also to changes in cell volume.

IV

Dynamic, Thermodynamic and Solvational Properties of PDE δ Binding to Farnesylated Cystein



* The work herein described has been published and subsequently reprinted in parts with permission from Suladze, S., Ismail, S. and Winter, R. (2014). Thermodynamic, dynamic and solvational properties of PDE δ binding to farnesylated cystein: a model study for uncovering the molecular mechanism of PDE δ interaction with prenylated proteins. *J. Phys. Chem. B*, 118, 966–975.

4.1 Background and Overview

4.1.1 Thermodynamics of Ligand-Protein Interactions

The organization and recognition events of cellular molecules are essential for biological processes. A fundamental task faced by the cell is to ensure the correct level of specificity between two molecules. For instance, the specificity for most protein-ligand interactions is derived by the virtue of proteins having a deep cleft with geometrical properties complementary to the ligand.^{64,173} Expectedly, the contributions from both ligand and protein are responsible of the noncovalent, reversible binding that results in the molecular recognition under equilibrium conditions. The binding energy of The protein-ligand interaction depends on several factors, including hydrogen bonding, hydrophobic interactions, van der Waals forces, dynamic properties of both ligand and protein, and solvent effect, such as the reorganization of water molecules and solute-solvent interactions. Hence, the quantitative description of the forces driving protein-ligand recognition requires the determination of the binding energetics acquired through the correlation of thermodynamic parameters with structural knowledge about the geometry of protein-ligand complexes.¹⁷⁴ Such a detailed study into the recognition process provides the fundamental basics for structure-based drug design strategies.¹⁷⁵

The binding affinity of a small molecule ligand to a given protein is characterized by the standard Gibbs free energy difference (ΔG°) between bound and unbound states, and can be expressed in terms of the equilibrium constant for the formation of the complex ($\Delta G^\circ = -RT \ln K$). For any molecular association reaction to be spontaneous, the Gibbs free energy ($\Delta G^\circ = \Delta H^\circ - T\Delta S^\circ$) must be negative, which dictates that both enthalpy and entropy could have a tremendous effect on protein-ligand interaction. Thus, the protein-protein or protein-ligand binding events are accompanied by both structural and dynamic changes of each interacting molecule. A quantitative description of ΔH° , ΔS° , and heat capacity change, ΔC_p , would allow a better understanding of the overall balance between the different molecular forces governing protein-ligand binding interactions.

In solution, a ligand binding represents the process in which a solvated ligand and a protein that are initially separated combine to produce the solvated ligand-protein complex (Figure 4.1). Typically, the Gibbs free energy of binding obtained experimentally is the sum of the

intrinsic (structural) and the solvational contributions. The intrinsic and solvational contributions to the overall energetics of binding often have a compensating effect.¹⁷⁶ Protein–water interactions are central for the biological function of proteins. In the absence of a sufficient amount of water, proteins lose their ability to move and their activity is drastically reduced. There is direct evidence from dehydration studies that at least a monolayer of water molecules is required for a protein to maintain fully functionality.¹⁷⁸ Since the biological processes involving proteins takes place in aqueous cellular environment, the composite physical nature of protein-ligand recognition requires a better understanding of the exact role of water molecules.

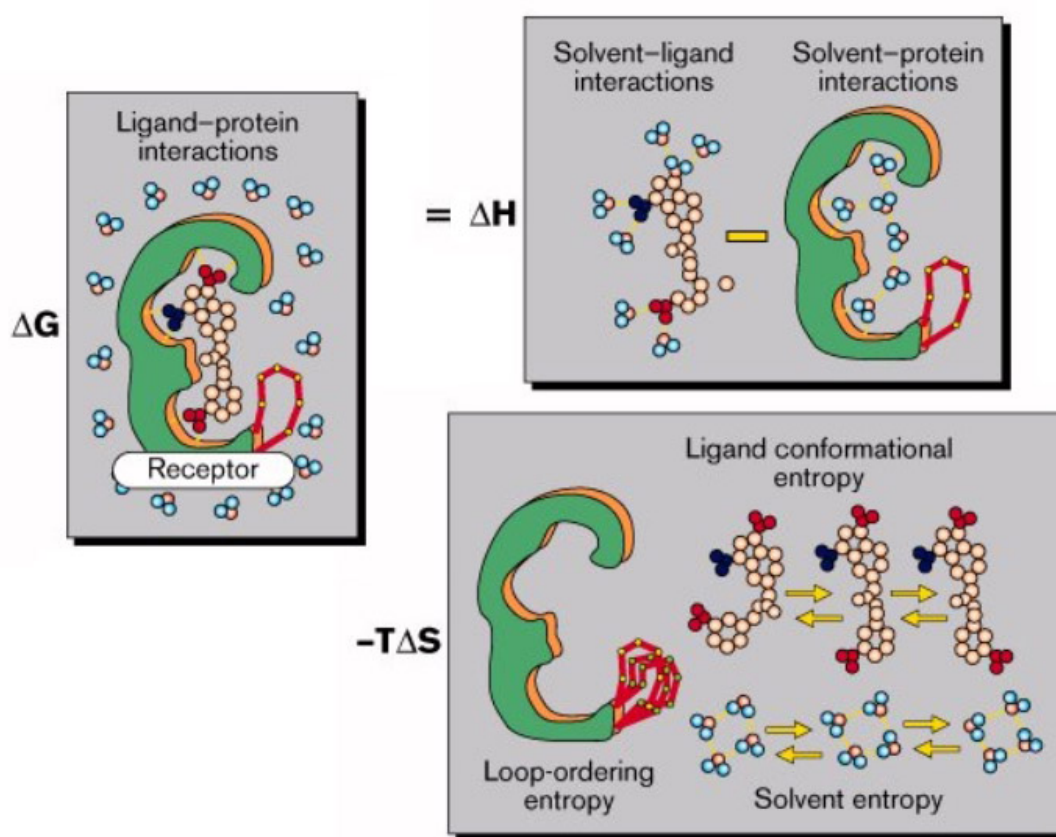


Figure 4.1: A schematic illustration of the free-energy components associated with ligand binding to a macromolecule (receptor) in solvent.¹⁷⁷

The water molecules influence the structural and dynamic properties of proteins through interactions, such as, hydrogen bonding with the protein hydrophilic surface, and the electrostriction of charged residues. Moreover, the unfavourable interaction between the

aqueous environment and protein hydrophobic surfaces results in the self-burial of nonpolar residues into the solvent inaccessible protein core, which is usually considered as a major driving factor to protein folding in solution.¹⁷⁹ It has been recognized that water molecules adjacent to the protein surfaces may also influence the van der Waals interactions and salt bridges responsible for the stability of the protein conformation.¹⁸⁰ Consequently, the reorganization of surrounding water molecules during biological processes modulate the stability of a protein conformation by redistribution of molecular forces. In this way, water has a significant impact on the overall energetics of protein-ligand interactions and the conformational preferences adopted by proteins.

Binding interaction usually induces a release of water molecules from the hydration shells of both interacting molecules into the bulk solvent,¹⁸¹ causing both disruption and formation of hydrogen bonds. Importantly, a ligand is only able to form favourable interactions with the protein after replacing the majority of solvent molecules from the interacting interface. In fact, when the ligand binds to the protein, ligand-water and protein-water contacts are substituted by ligand-protein and water-water contacts. Thus, the ligand-protein binding could be generally dissected into following steps: (1) desolvation of the ligand and the binding site, (2) altering the conformation of both the ligand and the protein and (3) forming new interaction sites between them.

Water molecules frequently are in the complex interface, resulting in a better H-bonding network and the complementarity of the interacting surfaces.¹⁸³ There appears to be a large controversy regarding the contributions from tightly bound water molecules. Their impact on recognition processes can be supportive or unfavorable, enthalpy-driven, or entropy-driven. Water molecules attached to the protein active site prior to binding can be replaced or not.¹⁷⁴ Evaluation of the overall solvation contributions is very challenging. However, what is clear is that the impact of the solvent on the energetics of recognition is very significant. A comprehensive knowledge of water properties, hydrophobicity and hydration is also important for the rationalization of the binding thermodynamics in biological systems.

4.1.2 Binding Enthalpy, Entropy and Heat Capacity Changes

The conformational and dynamic properties of a protein in its free and bound forms vary significantly.¹⁷⁶ Binding is generally accompanied by a conformational rearrangement of both the ligand and the protein, which in most cases imposes an enthalpic penalty. The enthalpic component of the free energy signifies the strength and specificity of the binding between partners. A formation of the ligand-protein complex is normally linked to forming new non-covalent interactions between ligand and its binding site that are enthalpically favorable.¹⁸² These may include electrostatic (Coulomb) and van der Waals interactions, as well as disruption of protein-solvent hydrogen bonds and formation of such bonds between protein and the ligand.^{175,184} The recognition of the ligand limits its rotational and translational freedom, subsequently, ligand and protein flexibility and therefore imposes an entropic penalty. In contrast, the desolvation upon binding i.e restructuring water molecules around the ligand and ligand-binding site on protein results in a significant entropic reward. Hence, the total change in binding entropy comprises a subtle balance between a favorable desolvation (ΔS_{sol} – the entropy change due to solvent reorganization upon binding) and an unfavorable motion reduction of interacting molecules.¹⁸⁵

A complete thermodynamic description of the mechanism of ligand association requires also the estimation of the heat capacity change upon molecular binding. ΔC_p is measured accurately from the difference in enthalpy change with respect to temperatures and is proportional to the size of surface area involved in the binding process. The change in accessible surface area could be of either polar or nonpolar in nature, with latter being believed to be dominant and is related to the hydrophobic effect. Upon binding, a negative heat capacity change implies the formation of hydrophobic contacts, while positive change indicates the disruption of hydrophobic interactions upon binding. These happens because of distinctive ice-like organization of the solvent around hydrophobic surfaces i.e clustered water organization by solvent-exposed hydrophobic groups requires a larger amount of heat to cause an increase in temperature (Figure 4.2).¹⁸⁶ Hence, when large negative ΔC_p is coupled with positive (favorable) entropy change, binding is driven predominantly by the hydrophobic interactions. Thus, the strong relationship between ΔC_p and the surface area buried upon forming a complex (resulting in dehydration) makes this parameter exceptionally helpful for connecting thermodynamic data to structural information of interacting macromolecules.

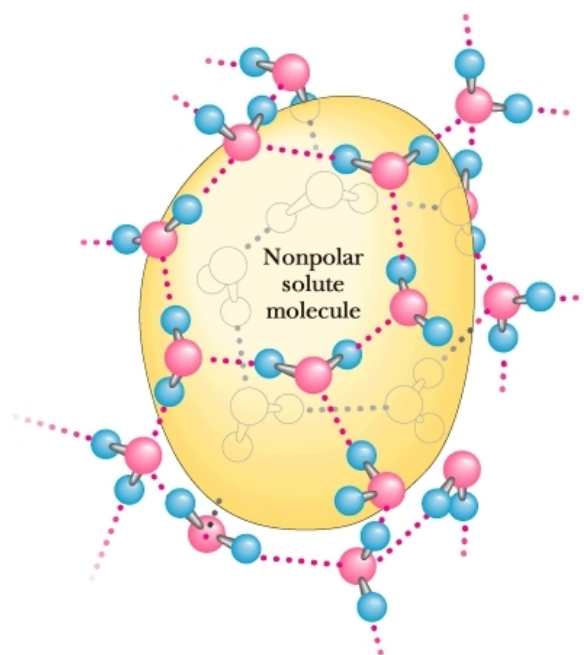


Figure 4.2: A nonpolar molecule residing within an ice-like cage, which exhibits a lower entropy and higher heat capacity as compared to bulk water. Adapted from Garrett & Grisham: Biochemistry 2/e.

Many structural alterations bearing minute ΔG are often of more significant variations in its components ΔH and $-T\Delta S$. In this case, large enthalpy variations commonly compensate an equivalent and opposite contributions of the net entropy. The enthalpy-entropy compensation could be a result of an enthalpically beneficial binding imposing a restriction on the motion of the interacting molecules resulting in a significant unfavourable entropic change.¹⁸⁷ The enthalpy-entropy compensation is a complex phenomenon and largely depends on the nature of interacting molecules. In exceptional cases, some proteins have a tendency to minimize the unfavorable entropic penalty by increasing their flexibility in the regions far from the binding site.¹⁸⁸ Enthalpy-entropy compensation is also contributing to another important phenomenon called 'binding cooperativity'. This phenomenon occurs upon binding processes of enzymes/receptors that have multiple binding sites that in turn act dependently of each other. Thus, cooperativity connects the system's seemingly independent components in order to bring the effect e.g. the regulation of the signaling or reaction pathways.¹⁸⁹ Expectedly, the cooperativity is often coupled to a significant conformational changes in the structure of the protein. It can be caused by additional structural packing induced by the presence of extra interactions characterized by favorable enthalpy changes.¹⁹⁰ On the other hand, cooperativity

does not necessarily involve , a structural alteration but changes in protein dynamics.^{191,192} Because of the thermodynamic nature of cooperativity, it is appropriate to additionally investigate the thermodynamics of this event rather than to study only conformational effects.

4.1.3 Experimental Approaches for Measuring Binding Thermodynamics

The investigation of ligand association to macromolecules of biological interest is crucial for the understanding of biological processes as well as for attempts to control them, for example, by therapeutic molecules. For this reason, a number of biophysical methods are used to provide a detailed mechanistic information on ligand binding. Notably, X-ray crystallography, calorimetry, nuclear magnetic resonance (NMR), plasmon resonance, circular dichroism and thermal shift assays are few among to study protein-ligand interaction. However, every method developed to date provides an incomplete picture, and so the characterization of structural changes and hydration impact on the binding is a challenging task.

Structural effects of binding are often identified by analysis of X-ray structures of the ligand-free protein with that found in the complex. Nevertheless, there is no direct linkage between the observed crystal structures and the free energy change, to accurately predict the binding affinity based on structural information. Hence, although X-ray crystallography is a powerful method for identifying basic structural alterations connected with complex formation, this technique detects prominent structural variations only. On the contrary, energy changes are distributed among a large number of weak non-covalent interactions, each of which could possibly induce considerable changes in the static structure of the respective groups. Additionally, X-ray crystallography provides 'static' structural information of only highly immobilized water molecules that were able to make strong polar interactions with the protein during crystallization. Thereby, this method also does not provide a complete insight into the interaction with solvent, such as water, co-solvents and buffer ions accompanying ligand binding.¹⁸⁰

The hydration shell signifies the entity of water molecules adjacent to the solute accessible surface. This shell has distinctive properties from the remaining bulk and hence has a significant effect on the partial molar volume, entropy, enthalpy, partial molar

compressibility, *etc.*¹⁹³ Various thermodynamic techniques are non-selective to subpopulations of the adjacent solvent molecules and allow the study of the properties of the whole population of solute hydrating water molecules.^{193,194} The effectiveness of exclusively using traditional calorimetric techniques to reveal the details of energetics of proteins significantly increases when combined with volumetric methods. For instance, ultrasound velocimetry and densitometry measure thermodynamic properties, such as, change in volume ΔV and compressibility, ΔK . These parameters are good quantitative indicators of both structural (intrinsic packing of proteins) as well as hydration changes that proteins and ligands undergo upon complex formation.¹⁹⁵ The compressibility is directly coupled with volume fluctuations, providing a description of protein dynamics.¹⁷⁶ One example would be using volumetric methods to gain information about the role of elastic deformations in the mechanism of catalytic activity.¹⁰³ Specifically, the significance of protein compressibility measurements has been highlighted by the works interrelating compressibility and structural properties of globular proteins.^{104,196,197,198} In this study, the authors recognized that the compressibility values of *Escherichia coli* dihydrofolate reductase (DHFR) were sensitively influenced by the ligands along the enzyme reaction coordinate. The measured variation in protein compressibility (and thus, flexibility) was predominantly caused by variation of the cavity volumes with insignificant contributions from hydration.¹⁹⁸ The results imply that the conformational flexibility of the protein kinetic intermediates plays an important role in the enzymatic function of DHFR. Hence, compressibility studies in conjunction with structural X-ray crystallography are able to provide valuable information about global dynamic properties of proteins which are governed by the presence of internal cavities.

4.2 Introduction and Objectives

PDE δ is an important solubilizing factor for several prenylated small G proteins of the Ras-subfamily. Signal transmission from cell surface receptors to intracellular signaling cascades by prenylated Ras proteins critically depends on their subcellular distribution and localization, which in turn requires a farnesylation dependent interaction with PDE δ . The binding occurs mainly through the farnesyl anchor at the C terminus of Ras proteins, which is recognized by a hydrophobic pocket of PDE δ .⁶⁴ Recently, in the attempts of preventing proper cellular localization of Ras proteins and inhibit signaling in cancer cells, there has been growing interest in understanding the interaction of PDE δ to them.^{60,61} It has been demonstrated that suppression of PDE δ levels disrupts Ras association with the plasma membrane and impairs the growth of Ras-mutant cancer cells.^{59,62} The possibility of reducing the presence of Ras at the plasma membrane by targeting the KRas-PDE δ interaction, has generated a great interest in cancer treatment.^{60,199,200} Zimmermann et al. described an approach aimed at disrupting KRas membrane association by a small-molecule inhibitor of PDE δ .⁶⁰ The approach was validated in human KRas-mutant pancreatic-cancer cell lines, where PDE δ no longer sustains the proper KRas localization to the plasma membrane and also in mice xenograft model.⁶⁰ Inhibition of Ras regulation by PDE δ may also have an effect of PDE δ interaction with other farnesylated proteins that act as tumor suppressors or may disrupt signaling by other Ras proteins, leading to toxic effects in normal cells.^{61, 199}

To reveal the multitude of biological functions of prenyl-binding proteins and the search for possible pharmacological inhibitors for oncogenic Ras calls for an in-depth knowledge of the function of PDE δ and its interaction with Ras proteins. In particular, little is known about the structural, energetic, and solvational changes associated with PDE δ while interacting with prenylated proteins. To address this issue, we set out to carry out a detailed study of the thermodynamic and dynamic properties of PDE δ binding to farnesyl-cystein, which serves as a model for PDE δ association to Ras proteins. In order to reveal a complete picture of the binding thermodynamics, isothermal titration calorimetry (ITC), differential scanning calorimetry (DSC), and pressure perturbation calorimetric (PPC) measurements were performed. To explore changes in dynamic properties associated with the binding event, in conjunction with calorimetric data, measurements of the ultrasonic velocity and density were carried out to determine the adiabatic and isothermal compressibilities to yield information

about the volume fluctuations of the system. Lastly, to obtain further insights into solvational properties that accompany the binding, we use the crystallographic structure of PDE δ to calculate binding-induced changes in the protein's solvent accessible surface area and intrinsic volume. These data enable us to calculate the number of water molecules released from the hydration shell of the protein and ligand, respectively. Correlating these numbers with the binding entropy, we estimate the binding-induced changes in hydration entropy and protein conformational entropy. In principle, the results obtained in this study can provide detailed information not just about binding of PDE δ with farnesylated proteins, but also about the interaction of carrier proteins to posttranslationally lipidated G proteins in general. A combination of volumetric and calorimetric methods was employed to specifically address the following questions:

Does a conformational change of the PDE δ structure occur upon binding to the farnesyl group?

What is the balance between the different possible molecular forces that contribute to the binding affinity?

What are the solvation and desolvation effects of interacting molecules upon their association?

How does the binding affect volume fluctuation dynamics of PDE δ ?

What is the detailed dissection of the entropic factor associated with the binding of the farnesyl anchor to the binding pocket of PDE δ ?

4.3 Results and Discussion

4.3.1 Thermodynamic Properties of Binding

Our studies commenced with an ITC experiment that monitors the PDE δ binding to farnesyl-cysteine (Figure 4.3). The titration data are best fitted to a 1:1 binding model. This stoichiometry is consistent with previous studies showing that PDE δ binds farnesyl groups with 1:1 stoichiometry.^{58,201} The dissociation constant, K_d , the reciprocal of the association constant K_a , was determined to be 3.74 μM at 25 °C. Fluorescence assays on similar systems revealed a K_d value of about 0.7 μM .^{58,69} Our thermodynamic parameters obtained by the ITC experiments are summarized in Table 4.1.

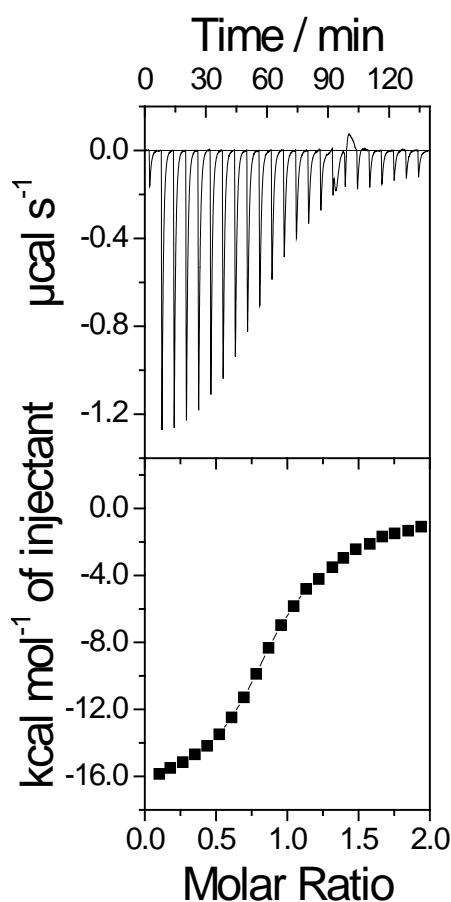


Figure 4.3: The upper panel displays the raw ITC data for titration of farnesylated cysteine into PDE δ at 25 °C, the lower panel exhibits a fit of the integrated calorimetric heats to a 1:1 binding model.

Table 4.1. Thermodynamic parameters obtained from ITC experiments for the association of PDE δ and farnesylated cystein. K_a is the association constant for binding. The values of the standard entropy change upon binding, ΔS° , is obtained using the standard free energy change $\Delta G^\circ = -RT \ln K_a$, and the standard enthalpy change of binding, ΔH° (with $\Delta S^\circ = (\Delta H^\circ - \Delta G^\circ)/T$). (To avoid confusion with other notations, the standard-state sign "°" has been omitted in the following, i. e., $\Delta H^\circ = \Delta H$, $\Delta S^\circ = \Delta S$, $\Delta C_p^\circ = \Delta C_p$).

$T / ^\circ\text{C}$	$K_a / 10^5 \text{ M}^{-1}$	$\Delta H / \text{kJ mol}^{-1}$	$\Delta S / \text{J mol}^{-1} \text{ K}^{-1}$	$\Delta G^\circ / \text{kJ mol}^{-1}$	$\Delta C_p / \text{kJ mol}^{-1}$
5	2.05 ± 0.2	-27.1 ± 0.7	$+4.3 \pm 3.3$	-28.3 ± 0.3	
15	2.24 ± 0.4	-40.2 ± 1.4	-37.1 ± 6.7	-29.5 ± 0.5	-2.35 ± 0.6
25	2.67 ± 0.8	-74.1 ± 4.9	-144.7 ± 20	-30.9 ± 0.9	

The decrease in entropy, ΔS , upon binding at ambient temperature is associated with conformational restrictions of the protein and ligand in the bound state and contributes unfavourably to the binding. The negative sign of the enthalpy change upon binding, ΔH , indicates that the binding enthalpy contributes favourably to the free energy of binding.

The favourable enthalpy change of binding may arise from different types of non-covalent interactions. It has been proposed by Williams and co-workers that favourable enthalpic contributions to binding could also be the consequence of the tightening of the protein around the ligand, thereby strengthening existing non-covalent interactions within the protein rather than being caused by new interactions at the protein–ligand interface.²⁰² More efficient packing may be beneficial for binding but limits dynamical processes at the binding site.²⁰² By contrast, studies on the thermodynamic signatures of binding hydrophobic ligands to a hydrophobic pocket of a protein proposed that for proteins with poorly solvated binding pockets, enthalpy driven binding is dominated by van der Waals interactions between the protein interface and the ligand.⁸⁷

Figure 4.4 displays the temperature dependence of the thermodynamic parameters. The Gibbs free energy change of binding exhibits a negligible dependence on temperature, which is due to the compensation effects of the enthalpic and entropic terms, a phenomenon that is commonly observed for biomolecular association reactions.¹⁸⁷ The heat capacity change upon binding, ΔC_p , as obtained from the slope of $\Delta H(T)$, is determined to be $-2.35 \text{ kJ mol}^{-1}$.

Generally, the sign and magnitude of ΔC_p is found to be correlated to the surface area of protein groups of different nature upon binding.²⁰³ Similar to protein folding, a negative sign of the heat capacity change of binding is believed to be indicative of a decrease in exposure of hydrophobic surface.^{186,204}

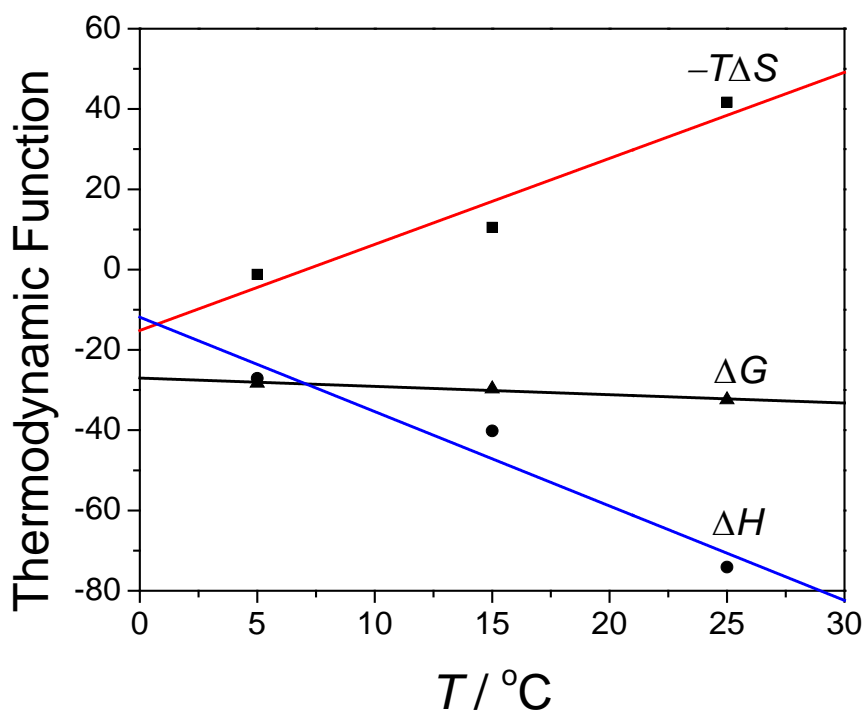


Figure 4.4: Temperature dependence of the thermodynamic parameters for binding of PDE δ and farnesylated cystein. The heat capacity change associated with binding was determined by linear regression analysis as the slope of the plot of ΔH versus temperature.

The negative sign of ΔC_p observed here is consistent with structural data, indicating the presence of significant hydrophobic components in the interaction process. X-ray structural data of PDE δ in complex with a C-terminally modified farnesylated Rheb revealed that binding occurs mainly through the farnesylated C terminus, via main chain interactions, and the prenyl group is deeply buried in the hydrophobic pocket of PDE δ (Figure 4.5).⁶⁴

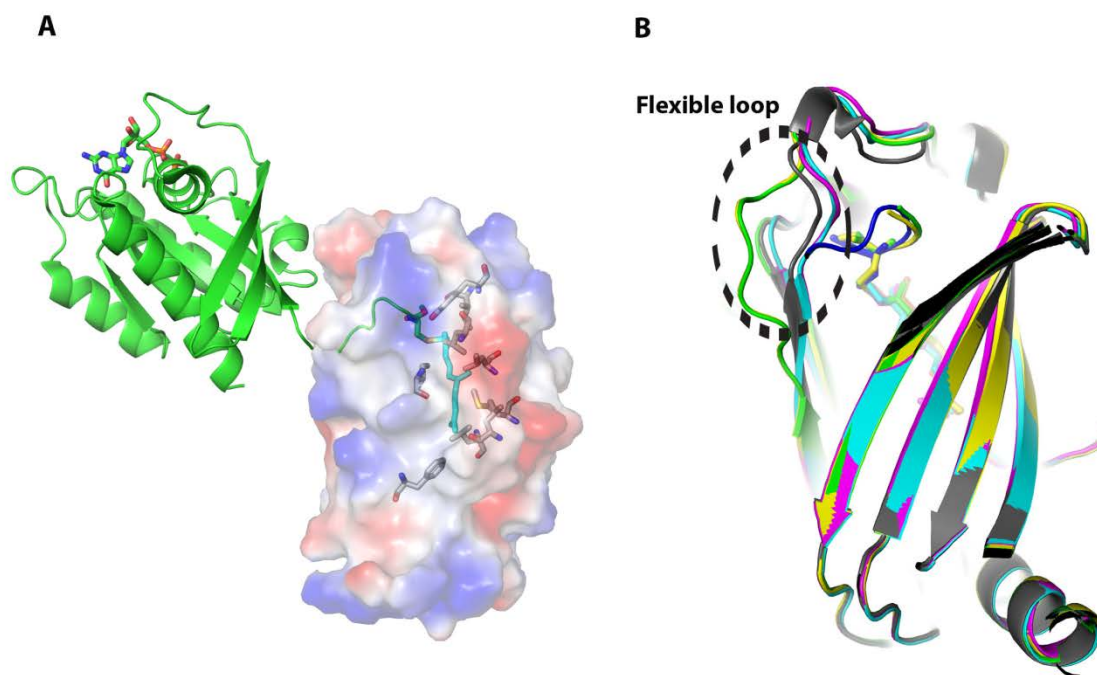


Figure 4.5: (A) Illustration of Rheb (green), a protein member of Ras superfamily, in complex with PDE δ . Residues (Met20, Leu22, Leu38, Ile53, Leu63, Ile129, Phe133, Leu147, Tyr149) forming the hydrophobic pocket are colored in gray around the farnesyl group (cyan) of Rheb. (B) The four molecules of the asymmetric unit superimposed, showing the movement of the flexible PDE δ loop.⁶⁴ Pictures were generated from PDB 3T5G using PyMol.

In addition to the farnesyl group's contact with the hydrophobic pocket, the PDE δ surface close to the C-terminus of Ras proteins is negatively charged, which facilitates binding to positively charged groups of the C-terminus, such as for K-Ras. This effect is believed to be relatively small in comparison with the farnesyl group's contribution, however. As described by Ismail et al., a single mutation of Met20 constituting the farnesyl binding pocket to lysine results in a decrease of the binding affinity of the mutant by a factor of 18 compared to that of the wild type.⁶⁴ Hydrophobic residues constituting the nonpolar binding pocket for farnesylated cysteine are depicted in Figure 4.5. When hydrophobic groups that are accessible to solvent prior to association become buried upon complex formation, subsequent release of water and hence an increase in the number of less structured water molecules can be envisaged. It is generally accepted that water molecules in the hydration shell at hydrophobic surfaces are more ordered than water molecules in bulk water.²⁰⁵ Hence, owing to the disruption of the solvation shell around the interacting largely hydrophobic species, the

entropy driven association of hydrophobic groups in aqueous solution would become favorable. Surprisingly, in contrast, our global analysis of thermodynamics data derived from the ITC experiments indicate that binding is driven by favorable enthalpic contributions rather than being of entropy-driven. As will be revealed from our volumetric analysis, which is discussed later, while a favorable entropic contribution to binding is found from desolvation of the protein's binding pocket and the ligand, this effect is counterbalanced by an unfavorable contribution arising from a reduction of rotational, translational, and internal degrees of freedom of the interacting species.

4.3.2 Changes in Thermal Stability of PDE δ Upon Binding and Links to Hydration, Packing and Fluctuation Properties

The folded structure of a globular protein is the result of many delicately balanced relatively weak forces. Protein stability and the binding of a ligand are governed by the same primary interactions (hydrophobic effect, hydrogen bonding, van der Waals interactions, configurational entropy, protonation and electrostatic contributions). When the environmental conditions change this balance is disrupted and the protein may undergo a conformational transition. Protein unfolding experiments provide fundamental quantitative thermodynamic data describing the stability of a protein. In this regards, calorimetric methods are widely used to monitor the denaturation process with linearly increasing temperature.⁸⁹ Figure 4.6 displays the DSC profiles of thermal denaturation of PDE δ and of PDE δ in complex with the ligand. The midpoint of unfolding of PDE δ appears at the unfolding temperature $T_m = 48.8$ °C. The enthalpy change upon unfolding obtained by integration of the area under the excess heat capacity over the transition temperature range equals 215 ± 7 kJ mol⁻¹. Binding to the ligand increases the thermal stability of the protein: T_m increases to 53.1 °C, and the enthalpy change upon unfolding increases to 282 ± 15 kJ mol⁻¹. Hence, the difference in T_m value caused by the binding is significant and amounts to 4.3 °C. An increase in protein thermostability upon interaction of proteins with small ligands is often observed and is caused by the coupling of binding with the unfolding equilibrium. Generally, mutations that change the packing of the inner core, are able to modify the protein stability significantly.²⁰⁶ Likewise, modifications in protein stability correlate with changes in the packing of the protein induced by ligand binding. Moreover, it has been shown that there is a direct correlation between protein thermostability and flexibility.²⁰⁷ Also, a decrease in protein

flexibility is believed to be a main factor for the increased thermostability in extremophiles living under extreme conditions of temperature, pressure, and pH.²⁰⁸ Changes in flexibility upon binding will be explored below.

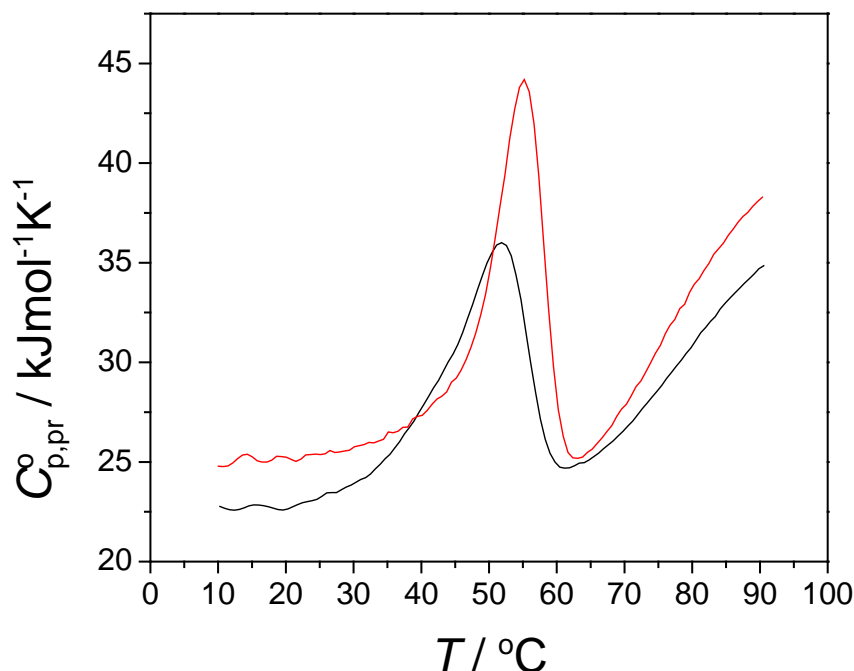


Figure 4.6: Comparison of the partial molar heat capacity (DSC profiles) for PDE δ (black) and the complex with farnesylated cysteine (red).

Pressure perturbation calorimetry (PPC) experiments were also carried out to detect changes in the volume of unfolding upon complex formation and, as the apparent expansion coefficient of the protein, α , and changes in volumetric properties in general are very sensitive to hydration properties, to investigate the effect of binding on the hydration of the protein surface. Generally, relative volume changes of unfolding of proteins are very small ($\Delta V/V \ll 1\%$).^{94,209} Figure 4.7 presents PPC curves of PDE δ and of PDE δ in complex with the lipid anchor. The relative volume changes of unfolding at the transition temperature obtained by integration of $\alpha(T)$ over the transition region revealed a significant difference in the volume change of unfolding for the two samples. Specifically, burial of the farnesyl group inside the protein caused an increase in magnitude of the relative volume change, $\Delta V/V$, of PDE δ from -1.03×10^{-3} to -1.4×10^{-3} . The absolute volume change of unfolding may be estimated using the partial specific volume of the protein as well: ΔV corresponds to $-13.7 \text{ mL mol}^{-1}$ for PDE δ and $-18.6 \text{ mL mol}^{-1}$ for the complex. As the volume change of unfolding

of a protein, $\Delta V(T)$, generally decreases with increasing temperature,²¹⁰ the increase of the absolute value of ΔV for the complexed state (4.9 mL mol^{-1}) may originate from the creation of small solvent inaccessible voids within the PDE δ structure upon complex formation. The unfolding temperatures as revealed from the minima in the $\alpha(T)$ curves are in good agreement with the DSC data.

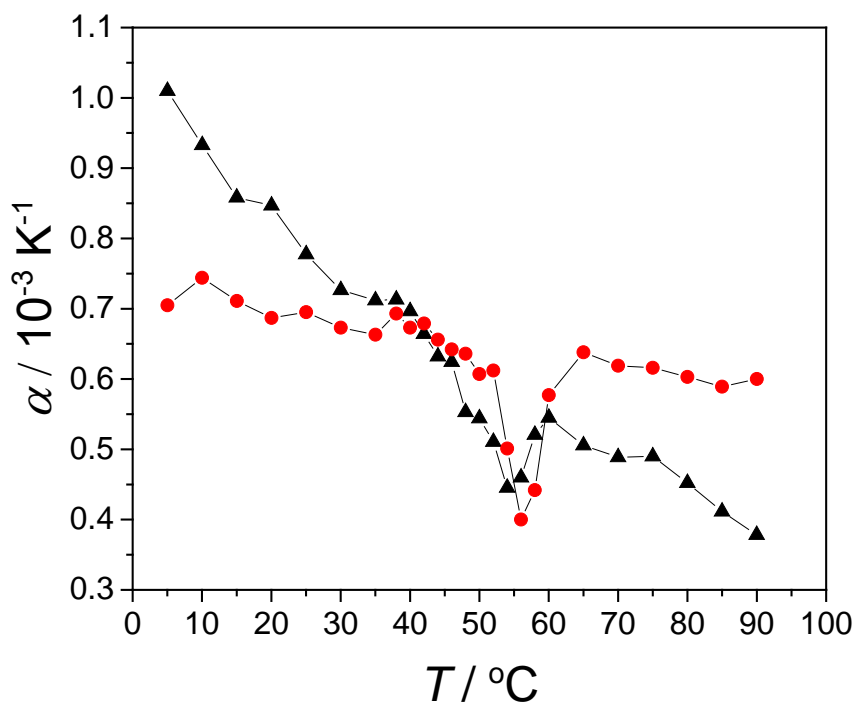


Figure 4.7: The temperature dependence of the thermal expansion coefficient, α , (PPC profiles) for PDE δ (black) and the complex with farnesylated cysteine (red).

For proteins in aqueous solution, the temperature dependent apparent coefficient of thermal expansion, $\alpha(T)$, is markedly influenced by protein–water interactions and the nature of the protein interface, and consequently by the magnitude of the solvent accessible surface area (ASA) of the protein.⁹⁷ At low temperatures, in the folded state of the protein, the values of $\alpha = (1/V)(dV/dT)_p$ are directly proportional to the volume increase caused by dehydration of the protein surface with temperature increase. This effect may even be used to estimate the changes in hydration and ASA upon complex formation. Between 5 and 35 °C, $\alpha(T)$ decreases almost linearly from $1 \times 10^{-3} \text{ K}^{-1}$ to about $0.7 \times 10^{-3} \text{ K}^{-1}$. High α values and their steep decrease up to 35 °C are indicative of the presence of a large number of exposed hydrophilic and charged side chains on the surface of PDE δ . Interestingly, the apparent coefficient of

thermal expansion of PDE δ in complex with farnesylated cystein and its temperature dependence are much less pronounced compared to unbound PDE δ . This clearly indicates a decrease in ASA of the protein and the level of hydration of the PDE δ surface upon binding, and might - at least partially - be attributed to the shielding of charged and polar residues on the surface of the binding pocket of PDE δ .

In order to evaluate also changes in dynamic properties, such as volume fluctuations, of PDE δ associated with binding, in addition to these calorimetric (DSC, PPC) measurements, ultrasonic velocimetry and densitometry measurements were used to obtain the adiabatic and isothermal compressibilities. Compressibility measurements of the structural flexibility in solution are linked to volume fluctuations and hence yield a direct approach to global dynamic properties of proteins. More specifically, compressibility measurements provide insights into protein dynamics from the perspective of atomic packing and cavity or void volume, which cannot be acquired by other methods.

The adiabatic compressibility of a solute is directly accessible by ultrasound velocimetry, and is a macroscopic quantity involving essentially two contributions, i.e. surface hydration and internal cavities due to imperfect atomic packing. The cavities contribute positively and the hydration negatively to the partial molar volume and compressibility of the protein.¹⁹⁶ Hence, the partial molar compressibility of the protein can be positive or negative, depending on the magnitude of both terms. Most globular proteins reveal a positive value, indicating a large contribution of cavities that is outnumbering the hydration effect.¹⁹⁷

Figure 4.8 presents changes in the partial molar adiabatic compressibility, K_s^0 , associated with farnesyl binding to the PDE δ . The results indicate that the burial of the farnesyl anchor dramatically affects the partial molar adiabatic compressibility of the PDE δ molecules, and causes even a change in sign from positive to negative at low temperatures (below 25 °C). Complex formation involves changes in both parameters affecting the compressibility: surface hydration of the protein and changes in internal atomic packing. The partial loss and release of water molecules from the interacting interface, i.e. partial dehydration of the solute molecules, results in an increase in compressibility. On the other hand, an increase in atomic packing upon binding overcompensates the hydration effect, leading to the negative change of the partial molar adiabatic compressibility of PDE δ upon farnesyl binding.

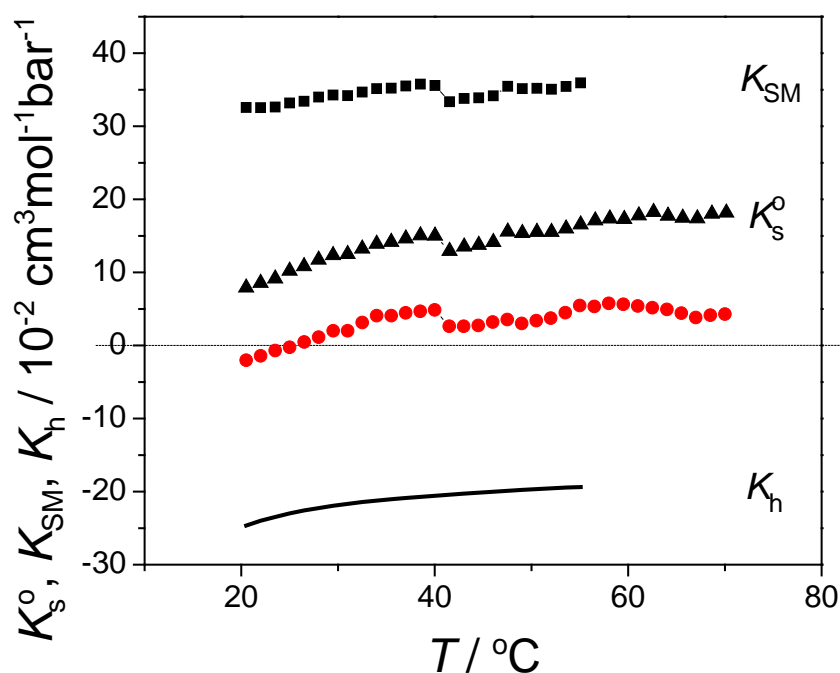


Figure 4.8: Temperature dependence of K_S^0 , the partial molar adiabatic compressibility of PDE δ (black triangles) and of the complex with farnesylated cysteine (red circles), respectively, and the hydration contribution K_h (black line) and intrinsic contribution K_{SM} (black rectangles) to the partial molar adiabatic compressibility of PDE δ .

Still today it is difficult to experimentally dissect the individual contributions of packing and hydration to the adiabatic compressibility of the protein-ligand complexes, although they can be roughly estimated for proteins based on some assumptions using X-ray crystallographic data.¹⁰⁵ Chalikian et al., by cross-correlating structural and volumetric data for a series of native globular proteins as a function of temperature, provided the average hydration contributions to the volume and compressibility of 1 Å² of charged, polar, and nonpolar solvent accessible protein surfaces.¹⁰⁵ Figure 4.8 displays the evaluated hydration and intrinsic contributions to the experimentally determined partial molar adiabatic compressibilities, which were calculated as described above (in materials and methods). It can be clearly seen, that K_S^0 of PDE δ is the result of largely compensating values from the negative K_h and positive K_{SM} . From these data, also the intrinsic coefficient of adiabatic compressibility of PDE δ , $\beta_{SM} = K_{SM}/V_M$, can be calculated, which is $25.03 \times 10^{-6} \text{ bar}^{-1}$ at 25 °C, in excellent agreement with estimates by Chalikian and co-workers for globular proteins.¹⁰⁵ The difference between the intrinsic coefficient of adiabatic compressibility, β_{SM} ,

and the intrinsic coefficient of isothermal compressibility, β_{TM} , has been found to be small.²¹¹ Therefore, β_{TM} , may be substituted in good approximation by β_{SM} to determine the relative volume fluctuations, $\delta V_M/V_M$ (eq. 22). We calculate a $\delta V_M/V_M$ value for the whole unbound PDE δ molecule of about 0.7 %. If concentrated in one area, such magnitude of volume fluctuation is sufficient enough to produce cavities or channels in the protein molecule to allow penetration of solvent or probe molecules.¹⁹⁷

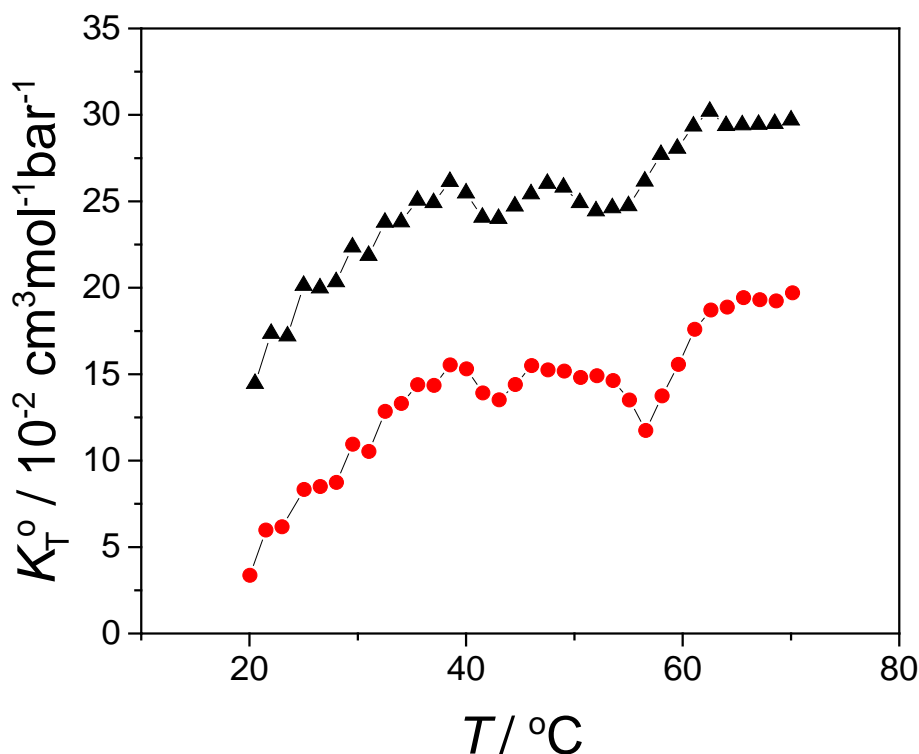


Figure 4.9: Temperature dependence of K_T^0 , the partial molar isothermal compressibility of PDE δ (black triangles) and of the complex with farnesylated cysteine (red circles), respectively.

By ultrasound velocimetry and density measurements, only the adiabatic compressibility, K_S^0 , can be determined. However, the combined results obtained from ultrasonic velocimetry, densimetry, differential scanning and pressure perturbation calorimetry allow calculation of the isothermal compressibility (eq. 23). Figure 4.9 presents the temperature dependence of K_T^0 , the partial isothermal compressibility of the unbound and bound form of PDE δ . K_T^0 decreases drastically (~50 %) upon complexation with the farnesyl anchor, indicating again a drastic reduction of the volume fluctuations of the protein. K_T^0 values increase markedly with increasing temperature, but level off at higher temperatures when the protein is still in its

native state, probably due to size restrictions of the still natively folded protein. Above the unfolding temperature, such restrictions become obsolete, and the isothermal compressibility increases again. For the bound complex, a small minimum seems to appear in this temperature region, which might be due to the dissociation of the complex.

4.3.3 Determination of the Intrinsic Volume and Accessible Surface Area using X-ray Crystallographic Structural Data

The atomic coordinates of PDE δ in complex with farnesylated Rheb protein were derived from the RSCB Protein Data Bank (PDB entry 3T5G). After stripping of water molecules and cleaning using PyMOL,²¹² we calculated the intrinsic volumes V_M and accessible surface areas S_A of the protein-ligand complex, of the free protein and the free ligand (Table 4.2). The values of the intrinsic (solvent-excluded) volumes for each structure were determined by rolling a spherical probe of a water molecule 1.4 Å around the van der Waals surface of the macromolecule, using Voronoi polyhedra approach,²¹³ with a help of the 3V (Cavity, Channel and Cleft Volume) calculator which represents the most recent free version of the original Lee & Richards algorithm.^{214, 215} In order to calculate the solvent-accessible surface, Mark Gerstein's calcs-surface program was used with a 1.4 Å probe radius, which determines the accessible surface area for each structure from the sum of the accessible surface areas of all atoms.²¹⁶

4.3.4 Number of Released Water Molecules upon PDE δ Binding to Farnesylated Cystein

The volumetric analysis of protein recognition events derived from a combination of volumetric and X-ray crystallographic data provides additional insights into the molecular origins associated with the binding process. This approach has been recently established by Chalikian and co-workers and is described in detail in the cited articles.^{176,195} Table 4.2 displays the molecular volumes, V_M , and solvent assessable surface areas, S_A , of free PDE δ , the bound complex, and of free farnesyl-cystein obtained calculated from the known crystallographic structures. In order to quantify changes in hydration, in addition to this structural information, we need the volume change of PDE δ upon binding, ΔV_{pr}^0 , which has been taken from the density measurements (Table 4.3).

Table 4.2. Molecular Volumes, V_M , and Solvent Assessable Surface Areas, S_A , of Free PDE δ , the Complex of PDE δ and Farnesyl-Cystein, and Free Farnesyl-Cystein.

Molecule	$V_M / \text{cm}^3 \text{mol}^{-1}$	$S_A / \text{\AA}^2$
PDEδ	13262	8416
Complex of PDEδ and farnesyl-cystein	13589	8103
Farnesyl-cystein	305	662

The volume change upon protein binding events or conformational transitions in aqueous solution can generally be presented as a sum of intrinsic, thermal and hydration volumes:

$$\Delta V_{\text{pr}} = \Delta V_M + \Delta V_T + \Delta V_h, \quad (24)$$

where the intrinsic volume, V_M , of a solute is the volume inaccessible to solvent molecules.^{209,215} It consists of the sum of the van der Waals volumes of all the protein's constitutive atoms plus the volume of the "structural" voids within the solvent-inaccessible core of the protein that result from imperfect atomic packing. Using structural data, the change in the intrinsic volume, ΔV_M , was obtained to be $22 \text{ cm}^3 \text{mol}^{-1}$ by subtracting the sum of the molecular volumes of the free protein ($13262 \text{ cm}^3 \text{mol}^{-1}$) and the ligand ($305 \text{ cm}^3 \text{mol}^{-1}$) from the molecular volume of the complex ($13589 \text{ cm}^3 \text{mol}^{-1}$), the values being obtained from the crystallographic data (Table 4.3).

Table 4.3. Change in Partial Molar Volume, ΔV_{pr}^0 , and Partial Molar Adiabatic Compressibility, ΔK_S^0 , upon Binding Determined by Density and Ultrasound Velocimetry Measurements at 25 °C.

$\Delta V_{\text{pr}}^0 / \text{cm}^3 \text{mol}^{-1}$	-173
$\Delta K_S^0 / 10^{-2} \text{ cm}^3 \text{mol}^{-1} \text{bar}^{-1}$	-10.47

V_T is the thermal volume which corresponds to a layer of empty space around the solute molecule that results from thermally induced molecular vibrations and reorientations of both the solute and solvent molecules. The thermal volume is directly proportional to the solvent

accessible surface area and does not seem to be dependent on the nature of the solvent exposed protein groups.²⁰⁹ The change in thermal volume, ΔV_T , associated with the binding process can be estimated using the following equation:

$$\Delta V_T = \delta_L \Delta S_{AL} + \delta_P \Delta S_{AP}, \quad (25)$$

where δ_L and δ_P are the thicknesses of the thermal volume of the ligand and the protein, respectively, and ΔS_{AL} and ΔS_{AP} are the changes in the solvent accessible surface area of the ligand and the protein upon complex formation. Estimates of δ_L of 0.6 Å for small molecules and δ_P of 1.0 Å for proteins²¹⁷ leads us to the following relationship between the changes in thermal volume and solvent accessible surface area: $\Delta V_T = 0.8 \Delta S_A$.¹⁹⁵ Consequently, the change in the thermal volume contribution, ΔV_T , to overall volume change, ΔV_{pr}^0 , associated with protein-ligand binding process can be well estimated if the change in the solvent-accessible surface area, ΔS_A , is known. The change in solvent accessible surface area upon binding, ΔS_A , as calculated from the parameters listed in Table 3, equals to -974 \AA^2 . Correspondingly, the change in thermal volume, ΔV_T , accompanying the binding of PDE δ to farnesyl-cystein amounts to -779 \AA^3 or $-469 \text{ cm}^3 \text{ mol}^{-1}$, respectively.

The hydration term, ΔV_h , is the overall change in volume associated with the solvent–solute interaction.¹⁷⁹ Thus, by using the estimates for ΔV_M and ΔV_T , and the total volume change in solution obtained from the density measurements, the change in hydration volume, ΔV_h , upon complex formation can be determined to be $274 \text{ cm}^3 \text{ mol}^{-1}$. Presence of polar and charged atomic groups in water due to hydrogen bonding and electrostriction contributes to hydration volume negatively. Likewise, burial of previously solvent-exposed polar or charged groups upon protein-ligand association produces less negative contribution, resulting in an increase in the value of hydration volume.²¹⁸ The positive sign of ΔV_h reflects the release of water molecules from the hydration shells of the interacting species to the bulk. The number of water molecules, Δn_h , released from the protein ligand interface upon binding can be retrieved from the ΔV_h value as well. For uniform hydration shells of the ligand and the protein, one obtains

$$\Delta V_h = \Delta n_h (V_{sh} - V_b), \quad (26)$$

where V_{sh} is the partial molar volume of water in the hydration shell, which is generally about 10 % smaller than the molar volume of bulk water, V_b , for proteins.^{219, 220} Based on this approximation, $(V_{sh} - V_o) = -1.8 \text{ cm}^3 \text{ mol}^{-1}$, and the number of water molecules that become released to the bulk from the hydration shells upon binding of farnesyl-cystein to PDE δ equals to 152 ± 2 . Chalikian and co-workers determined the uncertainty of the current approach based on their previous works on protein–ligand association reactions. The error bar for the number of released water molecules (± 2) reflects the experimental error of the measurements, only. The error bar may increase up to 25–50 %, however, considering the parameters derived from calculations using X-ray crystallographic structures, such as the intrinsic volume, V_M , and the solvent accessible area, S_A .⁴⁶ We estimated water molecules directly contacting the interacting surfaces from a decrease in the solvent-accessible surface area, S_A , upon binding and the effective cross section of a water molecule (9 \AA^2), resulting in about 108 ($-974 \text{ \AA}^2/9 \text{ \AA}^2$). It is interesting that the number of released water molecules is larger than the number of waters within the first hydration shell of the interacting surface. This implies that the hydration shell of globular proteins consists also of water molecules from the second hydration layer, in agreement with ref²⁰⁹.

4.3.5 Dissection of Hydration and Configurational Contributions to the Binding Entropy

As revealed by our ITC experiments, binding of farnesylated cystein to PDE δ is accompanied by an unfavorable change in entropy, $\Delta S = -144.7 \text{ J mol}^{-1} \text{ K}^{-1}$ at 25 °C. Generally, the change in entropy for ligand-protein binding can be subdivided into configurational, hydration, and translational contributions:²²¹

$$\Delta S = \Delta S_{\text{conf}} + \Delta S_{\text{h}} + \Delta S_{\text{rt}}, \quad (27)$$

where ΔS_{conf} is the change in the configurational entropy of the ligand and the protein upon binding, ΔS_{h} is the entropic contribution due to a change in the hydration of the ligand and the protein, and ΔS_{rt} is the change in entropy due to the loss of rotational and translational degrees of freedom upon binding. Knowledge of the number of water molecules released upon complex formation allows us to calculate the favorable entropic contribution of

hydration. Using the estimated difference of the partial molar entropy of the water molecules in the hydration shell of the protein and bulk water of $-5.44 \text{ J mol}^{-1} \text{ K}^{-1}$ at room temperature,^{180,186} the hydration contribution to the binding entropy can be calculated: $\Delta S_h = -5.44 \times \Delta n_h \text{ J mol}^{-1} \text{ K}^{-1} = 826 \text{ J mol}^{-1} \text{ K}^{-1}$. ΔS_{rt} may be approximated to equal $-33.5 \text{ J mol}^{-1} \text{ K}^{-1}$ for a binding stoichiometry of 1:1.²²¹ Combining all these contributions to ΔS , we obtain for the change in configurational entropy, ΔS_{conf} , a value of $-937 \text{ J mol}^{-1} \text{ K}^{-1}$. ΔS_{conf} involves changes due to both interacting molecules, i.e., the configurational entropy of the ligand, $\Delta S_{conf}(L)$, and the protein, $\Delta S_{conf}(P)$. $\Delta S_{conf}(L)$ can be estimated to be $-275 \text{ J mol}^{-1} \text{ K}^{-1}$ from the number of rotatable bonds (N_{rb}) and the total number of atoms (N_{atoms}) of the farnesylated cystein using the following relationship:²²¹

$$\Delta S_{conf}(L) = -7.36N_{rb} + 1.73 N_{atoms}. \quad (28)$$

Consequently, ΔS_{conf} of PDE δ has an unfavorable contribution to the binding free energy of $-662 \text{ J mol}^{-1} \text{ K}^{-1}$. The absolute values of ΔS_{conf} are usually significantly larger than the entropy change of a protein-binding reaction, ΔS , which is the net effect of largely opposing hydration and configurational contributions.²²² A direct experimental determination of ΔS_{conf} is difficult. The first-order approach discussed here allows to estimate the order of magnitudes of ΔS_{conf} and ΔS_h and the degree of their compensation, however.¹⁷⁶

4.3.6 Changes in Protein Dynamics upon Complex Formation

From eq. 19, the experimentally measured change in partial molar adiabatic compressibility associated with binding, $\Delta K_S^0 = -1047 \times 10^{-4} \text{ cm}^3 \text{ mol}^{-1} \text{ bar}^{-1}$, can be represented by the sum of intrinsic and hydration contributions:

$$\Delta K_S^0 = \Delta K_{SM} + \Delta n_h (K_{sh} - K_b), \quad (29)$$

Where K_{SM} K_{sh} is the partial molar adiabatic compressibility of water molecules in the hydration shell, which is about 20 % smaller compared to that of bulk water K_b .²¹¹ For uniform hydration shells of the ligand and the protein, $(K_{sh} - K_b) = -1.3 \times 10^{-4} \text{ cm}^3 \text{ mol}^{-1} \text{ bar}^{-1}$.¹⁷⁶ Consequently, $\Delta K_h = 197.6 \times 10^{-4} \text{ cm}^3 \text{ mol}^{-1} \text{ bar}^{-1}$. By subtracting the

hydration contribution from the overall change in compressibility, the change in the intrinsic compressibility is obtained, $\Delta K_{SM} = -1244 \times 10^{-4} \text{ cm}^3 \text{ mol}^{-1} \text{ bar}^{-1}$. The corresponding change in the intrinsic coefficient of adiabatic compressibility is $\Delta\beta_{SM} = \Delta K_{SM}/V_M = -9.38 \times 10^{-6} \text{ bar}^{-1}$ (for a negligibly small ΔV_M). Using the intrinsic compressibility value, β_{SM} , of PDE δ of $25.03 \times 10^{-6} \text{ bar}^{-1}$, we obtain a 37.5 % ($\Delta\beta_{SM}/\beta_{SM}$) decrease in the intrinsic compressibility of PDE δ upon binding to the farnesyl anchor, which corresponds to 6 % (according to eq. 20) smaller intrinsic volume fluctuations ($\delta V_M/V_M$) of PDE δ in the complex compared to those of the unbound PDE δ . Thus, the binding of the farnesyl anchor to PDE δ causes a markedly more rigid and less dynamic structure of the protein.

4.4 Summary and Outlook

We carried out a detailed study of the thermodynamic and global dynamic properties of PDE δ binding to farnesyl-cystein, which serves as a model for PDE δ association to Ras and other prenylated proteins. The binding affinity, in terms of the equilibrium constant of dissociation, was determined to be $K_d = 3.74 \text{ }\mu\text{M}$ at 25 °C. Surprisingly, the thermodynamics data derived from the ITC experiments indicate that binding of the largely hydrophobic ligand is driven by favorable enthalpic contributions rather than being controlled by an entropy-driven signature. We find a marked decrease in entropy, ΔS , upon binding of $-144.7 \text{ J mol}^{-1}\text{K}^{-1}$, which is associated with conformational restrictions of the protein and ligand in the bound state. By combination with crystallographic data, we were also able to estimate the favorable hydration contribution, $\Delta S_{\text{hydr}} = 826 \text{ J mol}^{-1}\text{K}^{-1}$, and the unfavorable configurational contribution, $\Delta S_{\text{conf}} = -937 \text{ J mol}^{-1}\text{K}^{-1}$, to the overall negative binding entropy, ΔS . Hence, the sign and magnitude of ΔS is largely determined by the balance between the hydrational and conformation terms. The negative sign of the enthalpy change upon binding, $\Delta H = -74 \text{ kJ mol}^{-1}$ at ambient temperature, is hence responsible for the favorable free energy of binding. The negative sign of the heat capacity change upon binding, ΔC_p , is indicative of the decrease in exposure of hydrophobic surface. The apparent coefficient of thermal expansion of PDE δ in complex with farnesylated cystein and its temperature dependence are much less pronounced compared to unbound PDE δ . This indicates a decrease in solvent accessible surface area of the protein and the level of hydration of the PDE δ surface upon binding, which can be attributed to partial shielding of charged and polar residues on the surface of the binding pocket of PDE δ . We have also performed a dissection of the hydration and conformational contributions to the

adiabatic compressibility. Using our estimates of the intrinsic compressibility, the volume fluctuations of unbound PDE δ could be determined to be about 0.7 % of whole protein volume. The number of water molecules that become released to the bulk from the hydration shells upon binding of farnesyl-cystein to PDE δ equals to 152. From the complementary ultrasound velocimetry data we also find that the complex is more rigid and less dynamic compared to uncomplexed PDE δ , as reflected in a 37.5 % decrease in its intrinsic coefficient of adiabatic compressibility and a 6 % decrease in relative volume fluctuations of the system. This result is consistent with the presumption that the broad substrate specificity of PDE δ is related to a high flexibility of this protein.⁶⁴ In conclusion, our data lead to a better understanding of the molecular mechanism of PDE δ interaction with prenylated proteins, which may have substantial implications for evaluating affinity and specificity predictions of interaction partners of the molecule, such as for designing drugs against Ras related cancer.

V

**SUMMARY AND FUTURE
PERSPECTIVES**

Pressure modulation of PLA2 activity

Membrane-associated PLA2 protein is a class of enzymes that catalyzes the hydrolysis of membrane phospholipids at the *sn*-2 ester bond to produce lysophospholipids and free fatty acids. It plays an important role in diverse cellular processes, such as membrane remodeling, cell signaling and inflammation. For the catalytic function, PLA2 directly associates with the polar head groups of phospholipids at the membrane-water interface. This is mediated by the conformational change of PLA2 upon the attachment to the membrane that presumably opens the channel lined with hydrophobic amino acids and tethers the protein to the phospholipid head groups. The phospholipid substrates gain access through the hydrophobic channel towards the active site of the enzyme, which is comprised of catalytic Asp–His dyad and water molecules. As the phospholipid diffuses into the hydrophobic channel, a Ca²⁺ ion that is near the active site binds the phosphate group located in the phospholipid head, thus positioning the ester bond to be cleaved by a catalytic residues. The rates of interfacial activation and hydrolysis are largely determined by physical–chemical properties of the membrane. The region of PLA2 that is responsible for membrane attachment is different from that of the enzyme's active site. Therefore, the membrane binding and the activity after the membrane–association are usually considered as two separate events.

High hydrostatic pressure (HHP) is widely used as a thermodynamic and kinetic tool to study the structural and functional aspects of biological macromolecules in solution. In contrast, the effects of high pressure on the binding and activity of membrane-associated proteins are largely unexplored. In general, the physical properties of biological membranes can act as information pathways, through which the protein can sense a change in a physical property of the membrane. In analogous fashion, mechanisms by which external pressure stress is sensed and this information transmitted in organisms being exposed to high pressure stress is of great interest. In addition to the use of high pressure as a trigger for a structural change of biological assemblies, high pressure studies have direct relevance in understanding of the biology of deep-sea organisms.

As PLA2s play an important role in membrane remodeling processes as well as in cellular signaling cascades, they may potentially act as a pressure sensor. In the present work, the high pressure was employed as a tool to explore membrane-associated processes,

specifically the bee venom PLA2–association with membranes and subsequent enzymatic reaction in order to uncover the underlying structural, kinetic and volumetric changes. Another aim of this study was to elucidate the pressure sensitivity of bvPLA2, by studying its structure, membrane binding and enzymatic activity in response to HHP environmental changes which also affect the biophysical properties of the membranes. Combined with a specifically designed high pressure cell, the FTIR method was used to probe structural changes in the protein and a rapid mixing high-pressure stopped-flow spectroscopy platform to obtain data of lipid binding and the enzymatic activity as a function of pressure.

As indicated by our FTIR spectroscopic data, bvPLA2 maintained its folded structure up to 10 kbar in both free and membrane-bound forms, rendering the bvPLA2-membrane complex as a suitable system for studying pressure effects on its enzymatic activity. Comparison of FTIR spectra of free and membrane-associated enzyme provided a direct evidence for conformational changes. The membrane binding of bvPLA2 lead to an increased α -helical content, suggesting that this structural feature is involved in the membrane binding. Moreover, a relatively minute conformational change appeared for the membrane-associated protein at significantly higher pressures, suggesting that a strong stabilization of the conformation occurred for membrane-bound bvPLA2.

A FRET-based stopped-flow approach was used to monitor the binding of bvPLA2 protein to a heterogenous raft-like membrane. The association curve displayed a rapid concentration-dependent and a slow concentration independent rate. Thus bvPLA2 activation with model lipid membranes proceeds in at least two steps: In the first high-affinity step, protein rapidly associates with the membranes, which is followed by the PLA2's conformational change, as seen in the change in the α -helical content of PLA2, which eventually leads to interfacial activation of the enzyme. In contrast, analysis of bvPLA2 binding to a pure homogeneous fluid DOPC/DOPG membranes resulted in only minor differences in the fast association rate constants (first step), but the second phase exhibited a two-fold slower phase compared to that of heterogeneous raft-like lipid membranes. Thus, a model of PLA2 activation upon binding to the heterogeneous raft membrane binding of PLA2 should include an additional intermediate step. This likely occurs as a result of lipid sorting of coexisting islands in raft membranes that makes it relatively difficult to find the optimal fluid environment required for PLA2 activation.

Interestingly, the high hydrostatic pressure conditions resulted in only minor differences in the association rate constants of bvPLA2 protein to lipid membranes, independent of the lipid composition. This could be explained by a high packing efficiency of the protein with the membrane interface and the high stability of the membrane-bound protein forming a tight complex.

The activity measurements of bvPLA2 was performed using an efficient fluorescence dequenching assay with the DBPC fluorophore incorporated into the bilayer of model membranes. Interestingly, the enzyme operating on the pure homogeneous DOPC/DOPG fluid membrane displayed a higher catalytic efficiency compared to that of the phase separated anionic raft-like mixture. This effect can be attributed to a lower concentration of hydrolysis-competent disordered fluid lipid phase lipids in the raft-like membrane, which contains also 25% cholesterol, known to partially block the activation of PLA2. Applying the pressure drastically inhibited the activity of membrane-attached enzyme as revealed from the slope decrease of the time-dependent fluorescence change of the Bodipy-labelled reporter group. Calculation of the activation volumes for the hydrolysis reaction displayed an expanded transition state with increased overall volume, characterized with a positive activation volume, ΔV^\ddagger , in the range of 13–26 mL mol⁻¹. This implies that the pressure creates an elastic barrier to transformation by favoring a smaller-volume reactant state.

In conclusion, the effect of pressure on the enzymatic activity of bvPLA2 has been characterized in the presence of model membranes. The data showed that the structure of bvPLA2 is not significantly affected by pressures up to 4 kbar. Furthermore, the rate of penetration of bvPLA2 into the membrane is little influenced by pressure and occurs in at least two kinetically distinct steps. On the other hand, pressure caused a drastic inhibition of the enzymatic activity of the membrane-associated enzyme. The calculated activation volume for the catalytic step revealed that the transition state exhibits an overall volume expansion compared to the ground state, which is largely determined by solvation and packing effects. In light of our data it is tempting to speculate that the PLA2 is a potential pressure sensing system *in vivo*, required for the activation of adaptation processes of microorganisms under HHP stress. It is relatively little known as to how mechanical forces in stressed membranes are translated into biological signals at the cell membrane. In this regards, further studies should concentrate on the characterization of pressure effects on various membrane-associated G-protein, receptors, mechanically gated channels and reconstructed complex

biological signaling pathways *in vitro*. These studies may also improve our understanding of mechanotransduction and membrane-mediated protein-protein communication mechanisms.

PDE δ and farnesylated cysteine interaction

Originally identified as a subunit of phosphodiesterase, PDE δ acts as a shuttling factor for several farnesylated proteins like K-Ras in the cell. Signal transmission from cell surface receptors to intracellular signaling cascades by prenylated Ras proteins is strongly linked to the localization of K-Ras in the cell. In particular, K-Ras enrichment at the plasma membrane is required for proper Ras signaling, which in turn requires a farnesylation dependent interaction with PDE δ . The suppression of active PDE δ by small-molecule inhibitors disrupts Ras association with plasma membrane and impairs the growth of Ras-mutant cancer cells. In addition to the biochemical characterization of PDE δ -farnesylated Ras interactions, a detailed quantitative biophysical investigation of this binding is lacking. For instance, the understanding of the thermodynamic forces contributing to the control of protein-ligand recognition events is necessary for the evaluation and further prediction of the affinity and specificity of such events.

To this end, in the second part of this thesis, we described the thermodynamic (ITC, DSC, PPC), and volumetric (densitometry, ultrasonic velocimetry) properties of the association of PDE δ protein to farnesyl-cysteine anchor as a model for the binding of PDE δ binding to Ras proteins. Volumetric studies of protein-ligand binding events yield insights into changes in the hydration of the binding interfaces, perturbations of the dynamics, and structural transitions of the protein. The strength of complementary volumetric and more abundant calorimetric measurements is that their combination can provide further details about the thermodynamic forces that govern protein recognition. Among these forces, the hydration contribution to the net thermodynamic effects occupies a central place due to the sizable impact of hydration on the binding affinity and specificity. One possibility to characterize hydration in protein recognition is the use of volumetric parameters (volume, expansibility and compressibility). Estimated hydration contributions can be further used to discriminate between the role of hydration and intrinsic terms in the energetics of protein-ligand association.

ITC was used to gain information about the energetics (ΔG , ΔH , ΔS and ΔC_p) associated with PDE δ interaction to the farnesyl moiety. This binding is driven by favorable enthalpic contributions, rather than a classical entropy-driven signature that might be expected considering the hydrophobicity of the binding pocket of PDE δ . Enthalpic contributions to binding are likely because of the tightening of the protein around the ligand and the strengthening of existing non-bonded interactions within the protein. Additionally, our DSC and PPC experiments revealed that modifications in the packing of the protein induced by ligand binding is accompanied by an enhancement in protein stability and a subsequent decrease in the level of hydration of the PDE δ surface. High precision densitometric and ultrasonic velocimetric methods were used to obtain binding induced changes in volume, ΔV_{pr}^0 , and adiabatic compressibility, ΔK_s^0 . Measured changes in macroscopic properties (volume and compressibility) of PDE δ upon binding were explained in terms of microscopic events (hydration and internal dynamics). Specifically, we used these volumetric results in conjunction with the available X-ray crystallographic structural data to evaluate the change in hydration related to this binding process quantitatively. Desolvation of the protein's binding pocket and the ligand is characterized by a release of approximately 150 water molecules to the bulk water. Evaluated hydrational and intrinsic contributions to the experimentally determined partial molar adiabatic compressibilities were used to determine the relative volume fluctuations for the entire unbound PDE δ molecule, yielding 0.7 % of the total protein volume. Furthermore, our analysis of the compressibility data uncovers that the protein becomes less dynamic upon the farnesyl anchor binding as reflected in a 6% decrease in the relative volume fluctuations of the protein. Finally, the acquired results enable us to dissect the binding entropy, ΔS , into a the favorable hydration, $\Delta S_{hydr} = 826 \text{ J mol}^{-1}\text{K}^{-1}$, and an unfavorable configurational, $\Delta S_{conf} = -937 \text{ J mol}^{-1}\text{K}^{-1}$, contribution. The results suggest that the sign and magnitude of the net binding entropy is largely controlled by the delicate balance between these two terms.

To sum up, the present study endeavours to gain a deeper understanding of structural, energetic and solvational changes associated with PDE δ interaction with prenylated proteins. The results show that the binding is mainly enthalpy driven, likely caused by the protein compaction upon binding to the farnesylated cysteine and the reduction in volume fluctuations. Approximately 150 water molecules are released upon binding, but this increase in entropy by solvent release is overcompensated by other effects, which also lead to an

increase in thermal stability of the protein-ligand complex. Altogether, farnesyl anchor binding to PDE δ renders it less hydrated, more stable, compact and thus, less dynamic compared to the free unbound state.

Previous studies have demonstrated that the PDE δ – Ras complex dissociates upon contact with the membrane, leading to stable membrane insertion of Ras proteins through the farnesyl moiety. This dissociation of Ras protein from the binding pocket of PDE δ is assisted by an Arl displacement factor. Further studies will aim to determine precisely how the lipid membrane and Arl proteins regulate the biophysics of Ras-PDE δ binding. For instance, the energetic factors driving PDE δ -Ras complex to be associated to the Arl displacement factor and subsequent release of the farnesyl moiety from the binding pocket are yet to be determined. Such a characterization of the association of the biomolecules not only provides insights into the complex recognition events, but may also lead to improvement in the rational design of therapeutic agents for targeting specific protein sites with predicted affinity and specificity.

V

**ZUSAMMENFASSUNG UND
AUSBLICK**

Druckmodulation der PLA2-Aktivität

Das membranassoziierte Protein PLA2 gehört zu einer Klasse von Enzymen, welche die Hydrolyse von Phospholipiden an der *sn*-2 Esterbindung zu Lysophospholipiden und freien Fettsäuren katalysiert. Es spielt eine wichtige Rolle bei diversen zellulären Prozessen wie der Umstrukturierung der Membran, der Signaltransduktion und bei Entzündungsprozessen. Für seine katalytische Funktion assoziiert PLA2 direkt mit den polaren Kopfgruppen der Phospholipide an der Membran-Wasser Phasengrenze. Dies wird durch eine konformationelle Änderung in PLA2 bei der Membranbindung vermittelt, welche vermutlich zur Öffnung eines mit hydrophoben Aminosäuren bestückten Kanals und zu einer stabilen Bindung der Phospholipid-Kopfgruppen führt. Die Phospholipide erhalten durch den hydrophoben Kanal Zugang zum aktiven Zentrum des Enzyms, welches aus einer Asp-His Dyade und Wassermolekülen besteht. Sobald das Phospholipid in den hydrophoben Kanal diffundiert, bindet ein Ca^{2+} -Ion an die Phosphatgruppe und positioniert die Esterbindung für die hydrolytische Spaltung. Die Raten der Aktivierung und Hydrolyse an der Phasengrenze sind größtenteils durch die physiko-chemischen Eigenschaften der Membran bestimmt. Da die Region von PLA2, welche für die Membranbindung verantwortlich ist, nicht mit dem aktiven Zentrum überlappt, werden die Membranbindung und die Katalyse durch PLA2 üblicherweise als zwei separate Vorgänge betrachtet.

Hoher hydrostatischer Druck (engl.: *high hydrostatic pressure*, HHP) ist eine weit verbreitete Methode um sowohl thermodynamische, kinetische, strukturelle und funktionelle Aspekte der Funktion biologischer Makromoleküle in Lösung zu untersuchen. Im Gegensatz hierzu ist der Einfluss hohen Druckes auf die Bindung und die Aktivität membran-assoziiierter Proteine bisher nur unzureichend charakterisiert. Im Allgemeinen können die physikalischen Eigenschaften biologischer Membranen als Informationsquellen dienen, welche durch Proteine ausgelesen werden. Somit sind Mechanismen, die hohen Druck detektieren und diese Information weiterleiten, insbesondere in Organismen, die hohem Druck ausgesetzt sind, von großem Interesse. Neben der Nutzung hohen Druckes als Auslöser für strukturelle Änderungen in biologischen Komplexen, haben Hochdruckstudien aber auch direkte Relevanz für das Verständnis der Biologie von Tiefsee-Organismen.

Da Enzyme der PLA2-Familie eine wichtige Funktion bei der Umstrukturierung von Membranen und Signaltransduktionsprozessen besitzen, könnten sie potentiell auch als

Drucksensoren dienen. In der vorliegenden Arbeit wurden Hochdruckstudien als Werkzeug genutzt, um membranständige Prozesse zu charakterisieren. Als Modell wurde die Membranassoziation, sowie die anschließende enzymatische Katalyse der PLA2 aus Bienengift (engl.: *bee venom* PLA2, bvPLA2) untersucht, um die zugrundeliegenden strukturellen, kinetischen, sowie volumetrischen Änderungen zu bestimmen. Ein weiteres Ziel der vorliegenden Studie war ferner die Untersuchung der Drucksensitivität von bvPLA2 und der Einfluss auf die Struktur, die Membranbindung sowie die enzymatische Aktivität durch HHP-Änderungen, welche ebenso die biophysikalischen Eigenschaften der Membran beeinflussen. In einer dafür angefertigten Hochdruckzelle wurden FTIR-spektroskopische Messungen genutzt, um strukturelle Änderungen des Proteins zu charakterisieren. Eine Hochdruck *Stopped-flow* Apparatur wurde genutzt, um den Einfluss hohen Druckes auf die Lipidbindung und die enzymatische Aktivität zu bestimmen.

Anhand der FTIR spektroskopischen Daten konnte gezeigt werden, dass die Struktur von bvPLA2 sowohl in der freien, als auch der membrangebundenen Form bis zu einem Druck von 10 kbar stabil war. Dieser Protein-Membran-Komplex ist somit ein geeignetes Modell zur Untersuchung des Einflusses von Druck auf die enzymatische Aktivität von bvPLA2. Der Vergleich der FTIR-Spektren von freier und membrangebundener bvPLA2 ergab weiterhin den direkten Beweis für eine konformationelle Änderung. Die Membranbindung führte zu einem erhöhten α -helikalen Anteil und legte außerdem eine Beteiligung der α -Helices an der Membranbindung nahe. Zudem ergab die Anwendung sehr hoher Drücke Hinweise auf eine sehr starke Stabilisierung der Konformation des membrangebundenen bvPLA2, bei einer kleinen Konformationsänderung des membrangebundenen Proteins im Vergleich zum freien Protein.

Ein FRET basierter *stopped-flow* Ansatz wurde genutzt, um die Bindung von bvPLA2 an heterogene raft-ähnliche Membranen zu untersuchen. Die Assoziationskinetiken zeigten eine schnelle konzentrationsabhängige und eine langsame konzentrationsunabhängige Phase, die Aktivierung von bvPLA2 muss also mindestens nach einem Zwei-Schritt-Mechanismus geschehen. Im ersten Schritt bindet das Protein sehr schnell an die Membran, gefolgt von einem zweiten langsamen konformationellen Übergang der bvPLA2, der durch die Änderung des α -helikalen Anteils beobachtet werden konnte und so schließlich zur Aktivierung der bvPLA2 an der Membran führt. Im Gegensatz hierzu zeigte die Bindung der bvPLA2 an homogene fluide DOPC/DOPG Membranen nur kleine Unterschiede in der schnellen

Assoziationsrate (erster Schritt), jedoch war der zweite Schritt 2-fach langsamer im Vergleich zu den heterogenen raft-ähnlicher Lipimembranen. Daher muss ein Modell der Bindung und Aktivierung der PLA2 an heterogene raft-ähnliche Membranen einen weiteren intermediären Schritt enthalten. Vermutlich ist dieser Schritt ein Resultat der notwendigen Sortierung der Lipide in nebeneinander vorkommenden Domänen der raft-ähnlichen Membranen, welche eine Bindung und Aktivierung der bvPLA2 an die fluide Phase der Membran erschwert. Interessanterweise resultierten HHP-Bedingungen nur in geringen Änderungen der Assoziationsratenkonstanten der bvPLA2 an Lipidmembranen, unabhängig von der Zusammensetzung der Membran. Dies könnte durch die hohe Packungseffizienz des Proteins an die Membran und die hohe Stabilität des membrangebundenen Proteins erklärt werden.

Die Aktivitätsmessungen der bvPLA2 wurden mit einem Fluoreszenz Dequenching-Ansatz mit DBPC Fluorophor in der Doppelschicht der Modellmembranen durchgeführt. Interessanterweise zeigte das Enzym auf der homogenen DOPC/DOPG fluiden Membran eine höhere katalytische Effizienz im Vergleich zu der anionischen raft-ähnlichen Membran. Dieser Effekt kann einer geringeren Konzentration der Hydrolyse-kompetenten Lipide in der raft-ähnlichen Membran zugeschrieben werden, welche zudem 25% Cholesterin enthält, das bekannterweise die Aktivierung der PLA2 partiell blockiert. Hoher Druck inhibiert ebenfalls die Aktivität von Membran-gebundenem Enzym, was aus einer geringeren Steigung der zeitabhängigen Änderung der Fluoreszenz der Bodipy-markierten Reporter-Gruppe ersichtlich ist. Die Berechnung der Aktivierungsvolumina für die Hydrolysereaktion impliziert einen expandierten Übergangszustand mit einem erhöhten Gesamtvolumen, was sich in einem positiven Aktivierungsvolumen ΔV^\ddagger im Bereich von 13-26 mL mol⁻¹ widerspiegelt. Dies impliziert, dass der Druck eine elastische Barriere für den Übergang erzeugt, indem das kleinere Volumen der Reaktanden favorisiert wird.

Zusammenfassend wurde der Effekt hohen Druckes auf die enzymatische Aktivität der bvPLA2 in Gegenwart von Modellmembranen untersucht. Die Daten zeigen, dass die Struktur der bvPLA2 bis zu Drücken von etwa 4 kbar nicht signifikant beeinflusst wird. Weiterhin ist die Rate der Bindung der bvPLA2 an die Membran nur in geringem Maße druckabhängig und findet in mindestens zwei kinetisch unterscheidbaren Schritten statt. Die Aktivität der membrangebundenen bvPLA2 hingegen ist durch hohe Drücke stark inhibiert. Das berechnete Aktivierungsvolumen des katalytischen Schrittes zeigt, dass der Übergangszustand im Vergleich zum Grundzustand stattfindet expandiert ist, was weitgehend

durch Solvations- und Packungseffekte begründet ist. Angesichts dieser Daten kann spekuliert werden, dass die bvPLA2 *in vivo* als Drucksensor fungiert und für Anpassungsprozesse gegenüber HHP-Stress genutzt wird. Bisher ist wenig darüber bekannt wie mechanische Kräfte an belasteten Membranen in ein biologisches Signal umgewandelt werden. In dieser Hinsicht sollten weitere Studien zur Charakterisierung von Druckeffekten auf membranassoziierte G-Proteine, Rezeptoren, mechanisch regulierte Ionenkanäle sowie komplexe rekonstituierte biologische Systeme *in vitro* durchgeführt werden. Derlei Studien könnten auch unser Verständnis mechanischer Signaltransduktion und membran-vermittelter Kommunikation zwischen Proteinen erweitern.

Die Interaktion von PDE δ mit farnesylierten Cysteinen

Ursprünglich als Untereinheit der Phosphodiesterase identifiziert ist heute bekannt, dass PDE δ als Transportfaktor verschiedener farnesylierter Proteine in der Zelle, wie beispielsweise K-Ras, dient. Für die Signaltransmission von Rezeptoren an der Zellmembran zu intrazellulären Signalkaskaden durch prenylierte Ras Proteine ist die Lokalisierung von K-Ras entscheidend. Hierzu ist insbesondere eine Anreicherung von K-Ras an der Zellmembran erforderlich, was wiederum eine farnesylierungs-abhängige Interaktion mit PDE δ benötigt. Als Konsequenz bewirkt eine Inhibition von aktivem PDE δ durch niedermolekulare Inhibitoren die Assoziation des Ras-Proteins mit der Zellmembran und stört so das Wachstum von Ras-abhängigen Krebszelllinien. Während die Wechselwirkung von farnesyliertem Ras-Protein mit PDE δ bereits biochemisch charakterisiert wurde, sind die genauen quantitativen und biophysikalischen Details unbekannt. So ist beispielsweise die Kenntnis der thermodynamischen Kräfte, die zur Kontrolle der Protein-Liganden Erkennung und Bindung beitragen eine notwendige Voraussetzung, um die Affinität und Spezifität derlei Bindungen evaluieren und voraussagen zu können.

Zu diesem Zweck sind im zweiten Teil dieser Arbeit die thermodynamischen (ITC, DCS, PPC) und volumetrischen (Densitometrie, Ultraschall-Geschwindigkeitsmessung) Eigenschaften der Assoziation zwischen PDE δ und farnesylierten Cysteinen als Modell für die Bindung von PDE δ an Ras-Proteine untersucht worden. Volumetrische Studien von Protein-Liganden-Bindungen ergeben Einblicke in Veränderungen in der Hydratation der Bindungsgrenzflächen sowie Störungen der Dynamik und Strukturübergänge des Proteins. Die Vorteile der komplementären Anwendung volumetrischer und thermodynamischer

Messungen liegen darin, dass zusätzliche Details der thermodynamischen Kräfte der Proteinerkennung erhalten werden können. Unter diesen Kräften hat die Hydratation aufgrund ihrer beträchtlichen Auswirkungen auf die Affinität und Spezifität der Bindung einen zentralen Einfluss auf die Thermodynamik einer Reaktion. Eine Möglichkeit zur Charakterisierung des Hydratationseinflusses auf die Bindungsaffinität ist die Bestimmung volumetrischer Parameter (Volumen, Ausdehnungskoeffizient und Kompressibilität). Weiterhin kann dies genutzt werden, um zwischen dem Einfluss der Hydratation auf die Protein-Liganden Wechselwirkung und intrinsische Faktoren zu unterscheiden.

ITC wurde verwendet, um Informationen über die Energetik (ΔG , ΔH , ΔS und ΔC_p) der Bindung von PDE δ und Farnesylresten zu erhalten. Die Ergebnisse zeigen, dass die Bindung durch enthalpische Beiträge angetrieben wird, im Gegensatz zu einer entropiegetriebenen Reaktion, wie sie bei der Betrachtung der hydrophoben Bindungstasche von PDE δ erwartet werden könnte. Dies ist vermutlich auf eine verringerte Flexibilität des Proteins im Bereich der Bindungstasche und eine Verstärkung nicht-kovalenter Interaktionen im Protein zurückzuführen. Zusätzlich zeigten die DSC und PPC Experimente, dass eine durch die Bindung des Liganden induzierte veränderte Packung des Proteins mit einer erhöhten Proteinstabilität und einer verringerten Hydratation der Oberfläche von PDE δ einher geht. Hochpräzisionsdichtemessungen und Ultraschall-Geschwindigkeitsmessungen wurden genutzt, um die bindungsinduzierten Änderungen des Volumens, ΔV_{pr}^o , und der adiabatischen Kompressibilität, ΔK_s^o , zu bestimmen. Die veränderten makroskopischen Eigenschaften (Volumen und Kompressibilität) von PDE δ nach Bindung wurden durch Veränderungen der Hydratation und Dynamik des Proteins erklärt. Insbesondere wurden die gemessenen volumetrischen Veränderungen zusammen mit bekannten Röntgenkristallstrukturdaten genutzt, um die Veränderung der Hydratation durch die Bindung zu erklären. Die Desolvatation der Bindungstasche des Proteins und des Liganden setzt etwa 150 Wassermoleküle in die Umgebung frei. Erhaltene Hydratations- und intrinsische Beiträge zu der experimentell bestimmten partiellen molaren adiabatischen Kompressibilität wurden genutzt, um die relativen Volumenfluktuationen für das gesamte ligandenfreie PDE δ mit 0.7% des totalen Proteinvolumens zu bestimmen. Zudem zeigen unsere Analysen, dass das Protein durch Bindung des Farnesyl-Restes weniger flexibel wird, was sich in einer 6%igen Verringerung der Volumenfluktuation widerspiegelt. Die erhaltenen Ergebnisse erlauben uns schließlich die Bindungsenthalpie, ΔS , in die begünstigende Hydratation ($\Delta S_{hydr} = 826 \text{ J}$

$\text{mol}^{-1} \text{K}^{-1}$) und ungünstige strukturelle ($\Delta S_{\text{conf}} = -937 \text{ J mol}^{-1} \text{K}^{-1}$) Beiträge zu unterteilen. Die Ergebnisse legen nahe, dass das Vorzeichen und die Größe der Entropieänderung weitgehend durch die feine Balance dieser beider Beiträge gesteuert wird.

Zusammenfassend soll die vorliegende Arbeit ein tieferes Verständnis der strukturellen, energetischen und Solvatationsänderungen ermöglichen, die durch die Bindung von PDE δ an prenylierte Proteine hervorgerufen wird. Die Ergebnisse zeigen, dass die Bindung hauptsächlich Enthalpie-getrieben ist, vermutlich aufgrund einer kompakteren Struktur durch die Bindung des Farnesyl-Cysteins, sowie verringert Volumenfluktuationen. Etwa 150 Wassermoleküle werden durch Bindung in die Umgebung freigesetzt, dies wird jedoch durch andere Effekte überkompensiert und führt dadurch zu einer erhöhten thermischen Stabilität des Protein-Liganden Komplexes. Insgesamt führt die Bindung des Farnesyl-Restes somit zu einer weniger hydratisierten, stabileren, kompakteren und insgesamt weniger dynamischen Struktur von PDE δ im Vergleich zum Liganden-freien Protein.

Frühere Studien haben gezeigt, dass der PDE δ -Ras Komplex bei Kontakt mit der Membran dissoziiert, was zu einer stabilen Membraninsertion des Farnesyl-Restes von Ras führt. Unterstützt wird die Dissoziation von PDE δ und Ras dabei von einem Arl *displacement factor*. Weitere Studien werden darauf ausgerichtet sein, die genaue biophysikalische Funktion der Arl Proteine bei der Regulation der Ras-PDE δ Bindung zu charakterisieren. So sind bisher die energetischen Faktoren der Dissoziation von Ras und PDE δ durch den Arl *displacement factor* und die damit einhergehende Freisetzung des Farnesyl-Restes aus der Bindungstasche nicht bestimmt. Derlei Untersuchungen werden zukünftig zur Erweiterung des Verständnisses komplexer Erkennungsvorgänge in Biomolekülen beitragen, sowie auch das zielgerichtete Design therapeutischer Reagenzien zur Bindung an bestimmte Proteinbindestellen mit vorhersagbarer Affinität und Spezifität vereinfachen.

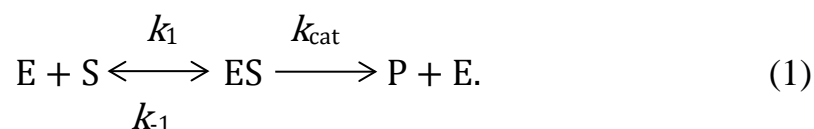
VI

An Example of Using the HPSF Method to Characterize Enzymatic Reactions

6.1 Basics of Ambient and High Pressure Enzymology

Enzymes are responsible for many crucial processes in living cells since they accelerate chemical reactions which would occur too slowly, or would lead to different products without their contribution. Enzymes are biocatalysts that usually show high affinity to a specific substrate under particular environmental conditions. The binding of the substrate and the subsequent catalysis takes place at a specific small region, around 10 amino acids, within the enzyme known as active site. The active site usually represents a hydrophobic cleft where substrate molecules attach in an optimal orientation, exploiting the full range of possible intermolecular forces. Some enzymes also contain sites that bind cofactors, for example an inorganic metal ion, which directly participates in the catalytic event, and hence are required for enzyme activity. Generally, enzymes are globular proteins that can bind one or more substrate molecules. As the activity of an enzyme is mainly determined by its three-dimensional structure that even small structural changes in the active site might result in a complete loss of enzymatic activity. After an enzyme binds to its substrate, it stabilizes the transition state by reducing the activation energy and hence increases the rate of a reaction by providing an alternative chemical pathway for the reaction. Enzymes have rather flexible structures and the active site of an enzyme can be modified by the fact that the substrate interacts with the enzyme. The initial interaction between enzyme and substrate is relatively weak, but this weak interaction can rapidly induce structural rearrangements in the enzyme that subsequently strengthen the binding. Therefore, the older theory about "the lock and key" model where a particular domain on the surface of the enzyme is structured to have a precise complementary fit to the substrate is not always a requirement for binding. Enzyme activity can be affected by various environmental parameters such as pH, temperature, pressure, by the addition of organic solvents or various kosmotropes and chaotropic ions which may stabilize or destabilize enzymes in solutions.

Traditionally, the simplest case when a single substrate is converted into a product is often written as:



Where E=free enzyme, ES=enzyme-substrate complex, k_1 , k_{-1} , and k_{cat} are reaction rate constants required for the description of this equation, for the formation of ES, reversible dissociation of this complex into the reactants, and for the catalytic step of product formation, respectively.

In 1913, Michaelis and Menten proposed a quantitative theory of enzyme kinetics, in which they show that the rate of an enzyme-catalyzed reaction is proportional to the concentration of enzyme-substrate complex [ES] described by the Michaelis-Menten equation.²²³ Briggs and Haldane on the assumption that the enzyme substrate complex quickly reaches steady state ($d[ES]/dt \approx 0$) introduced a more general formulation in 1925. The time-dependent variation of the individual reactants can be expressed using the following differential equations:

$$\frac{d[E]}{dt} = (k_{-1} + k_{cat})[ES] - k_1[E][S], \quad (2)$$

$$\frac{d[ES]}{dt} = k_1[E][S] - (k_{-1} + k_{cat}) [ES], \quad (3)$$

$$\frac{d[S]}{dt} = k_{-1}[ES] - k_1[E][S], \quad (4)$$

$$\frac{d[P]}{dt} = k_{cat}[ES] = v \quad (5)$$

The reaction rate, v , is defined as the increase in product concentration, which is directly proportional to the concentration of the enzyme-substrate complex ES, according to eq. 5. Considering the following assumptions: the concentration of substrate is higher than that of the enzyme, the catalytic rate constant k_{cat} is the limiting rate for the reaction as a whole and [E] and [ES] are essentially in equilibrium, then, the concentration of enzyme substrate complex is expressed by:

$$[\text{ES}] = \frac{k_1[\text{E}_0][\text{S}]}{k_{-1} + k_{\text{cat}} + k_1[\text{S}]} \quad (6)$$

Combination of this equation with eq. 5 yields the Michaelis-Menten equation:

$$v = \frac{v_{\text{max}}[\text{S}]}{K_{\text{M}} + [\text{S}]} \quad (7)$$

where the Michaelis-Menten constant is $K_{\text{M}} = \frac{k_{-1} + k_{\text{cat}}}{k_1}$ and the maximum possible rate of reaction $v_{\text{max}} = k_{\text{cat}}[\text{E}_0]$. At the maximum rate, v_{max} , of the enzyme, all enzyme active sites are saturated with substrate, and the concentration of enzyme-substrate complex, $[\text{ES}]$, equals the concentration of enzyme.

Inverting the conventional Michaelis-Menten equation leads to the Lineweaver-Burk equation

$$\frac{1}{v} = \frac{K_{\text{M}}}{v_{\text{max}}} \frac{1}{[\text{S}]} + \frac{1}{v_{\text{max}}} \quad (8)$$

A plot of $1/v$ against $1/[\text{S}]$ gives a straight line with the intercepts on the y-axis amounting to $1/v_{\text{max}}$, the intercept on the x-axis equals to $-1/K_{\text{M}}$ and the slope equals to $v_{\text{max}}/K_{\text{M}}$. Thus, such type of plot allows for easy determination of both v_{max} and K_{M} . K_{M} usually describes the substrate concentration that is required for an enzyme to reach one-half of the maximum reaction rate. Each enzyme has a characteristic K_{M} for a given substrate, which reveals how tight the binding of the substrate is to the enzyme. In practical terms, a low K_{M} value indicates that the ES-complex is held together very tightly and hence that the enzyme works efficiently even at low substrate levels and vice versa at high substrate levels. The efficiency of an enzyme can be expressed in terms of $k_{\text{cat}}/K_{\text{M}}$. This is also called the specificity constant and incorporates the rate constants for all steps in the reaction.¹⁴⁶

The transition state theory predicts that pressure effects on the rate constant k_{cat} of an elementary process are described by the equation:¹³⁸

$$\Delta V^\ddagger = \left(\frac{d\Delta G^\ddagger}{dp} \right)_T = -RT \left(\frac{d \ln k_{\text{cat}}}{dp} \right)_T \quad (9)$$

Where ΔG^\ddagger and ΔV^\ddagger are the activation free energy and the activation volume, which represents the difference in volumes of the activated and ground state of an enzyme-substrate complex (Figure 6.1). Based on this equation if the volume of a system in the activated state is smaller than that in the ground state ($\Delta V^\ddagger < 0$), reactions can be accelerated by pressure.

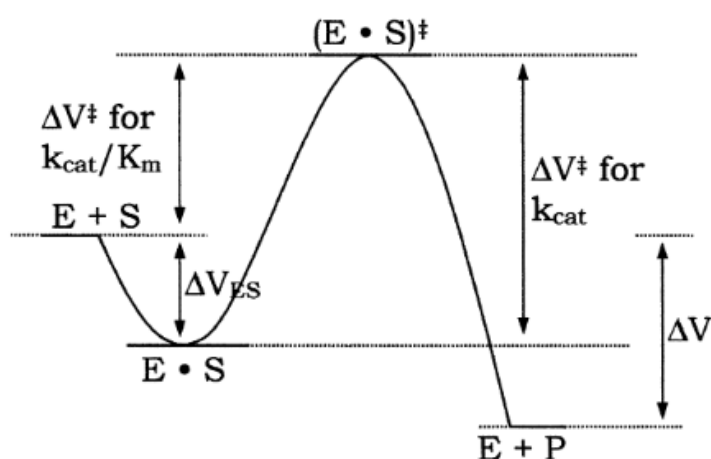


Figure 6.1: Activation volumes, ΔV^\ddagger , and the binding volume, ΔV_{ES} , for an enzymatic reaction. ΔV_{ES} reflects the volume change associated with the formation of the ES complex, which is typically a small positive or negative value at atmospheric pressure.²²⁴

Activation volume changes can involve contributions from the volume changes of the reacting molecules in addition to solvent effects. In general, dissection of the activation volume into separate contributions is a difficult task. However, the effect of pressure on an enzyme reaction is known to be particularly strong for reactions that are accompanied by a significant change in hydration between the ground and the transition state.²²⁴

Motivation

This chapter elucidates the application of high hydrostatic pressure for modulating the catalytic activity of enzymes. Moderate pressure application or addition of co-solvents does not often change the protein structure on the whole, however may induce local changes. These local changes often lead to another active state of a protein which may possess an altered activity, specificity, and stability. To evaluate the potential of pressure application to enzymatic processes using a relatively new HPSF method, we investigated the combined action of high hydrostatic pressure and the kosmotropic cosolvent TMAO (trimethylamine-*N*-oxide) on the enzymatic activity of α -chymotrypsin in the pressure range from ambient pressure up to 2000 bar. This work has been conducted together with a master student (Kathrin Estel) and has been part of her master thesis.

6.2 The Influence of High Pressure on the Kinetics of α -chymotrypsin

The main reason for choosing α -chymotrypsin as a model protein for this study was that the catalytic mechanism as well as pressure stability of this enzyme is relatively well established. The α -chymotrypsin-catalyzed hydrolysis proceeds according to the Michaelis–Menten mechanism. The initial process involves creation of a stable enzyme substrate complex ES, which is related to K_M , afterwards activation of the ES^\ddagger takes place and finally the subsequent reaction steps are governed by the catalytic rate constant, k_{cat} . As a model peptide an anilide substrate for hydrolysis SAAPPpNA (*N*-succinyl-L-alanyl-L-alanyl-L-prolyl-L-phenyl-alanine-*p*-nitroanilide) was selected. The reaction was observed as a function of time by monitoring increments of absorbance at 410 nm as a result of the *p*-nitroaniline product formation. The initial reaction rate, v_0 , was determined by converting the raw absorption data units to moles per second using the molar extinction coefficient of the substrate. Reaction rates were plotted as a function of substrate concentration to obtain a Michaelis-Menten plot. The Lineweaver - Burk plot was used to obtain the kinetic parameters K_M and k_{cat} . The activation volume, ΔV^\ddagger was derived from the slope of $\ln v_{max}$ vs. pressure p . The raw data, Michaelis-Menten plot, the double reciprocal plot, i.e., the Lineweaver - Burk plot and logarithmic plot of v_{max} (in relation to the rate at ambient pressure) as a function of pressure

for the hydrolysis of the substrate by α -chymotrypsin are displayed in Figure 6.2, respectively.

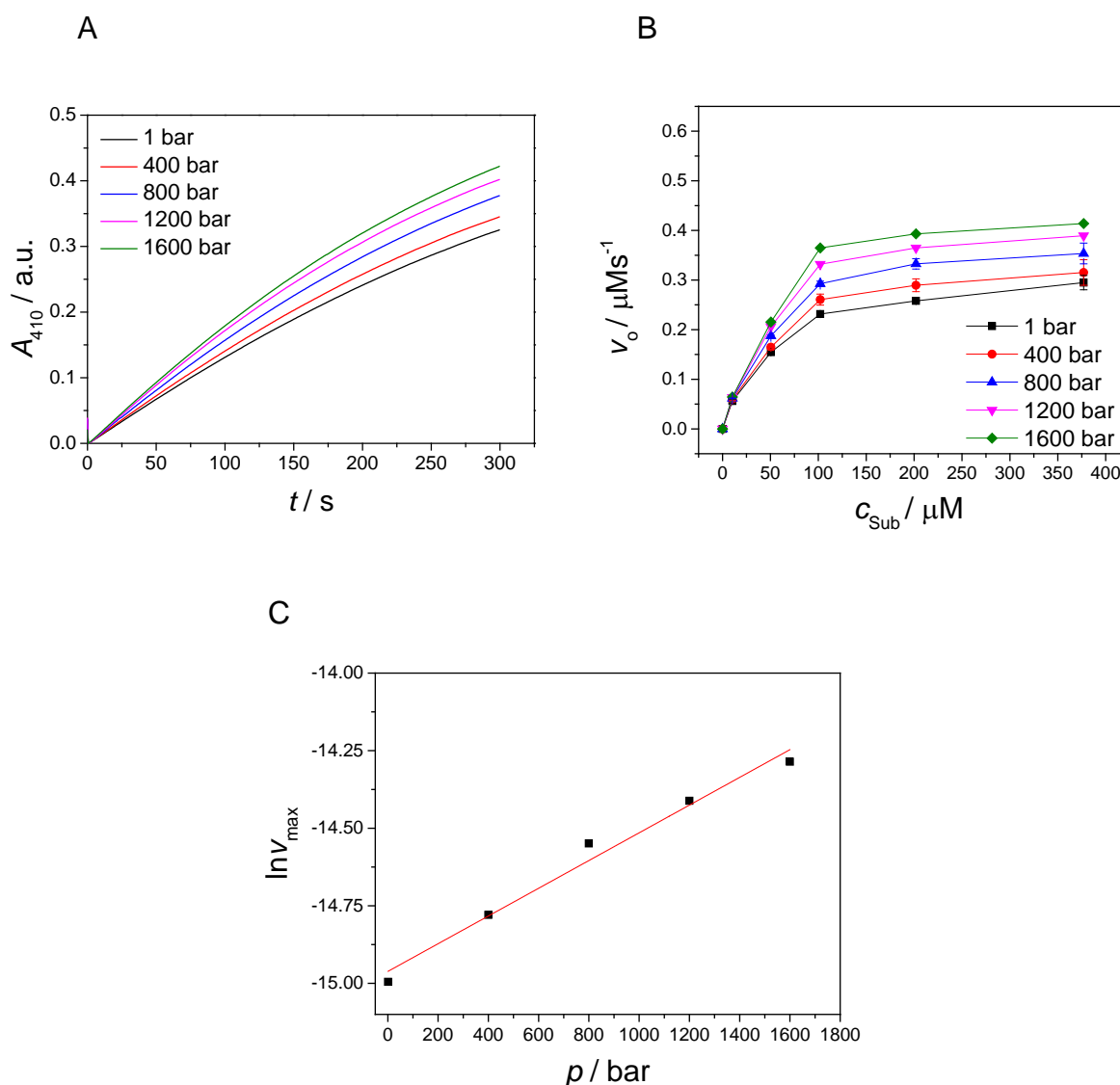


Figure 6.2: Pressure induced acceleration of α -chymotrypsin-catalyzed hydrolysis. (A) raw data of 8 nM α -chymotrypsin and 50 μM substrate at various pressures (B) Michaelis-Menten kinetic plot and (C) pressure dependence of the maximal rate of hydrolysis v_{max} in logarithmic scale for 8 nM α -chymotrypsin with varying concentrations of substrate in Tris-HCl buffer (pH 8.0) at 25 $^{\circ}\text{C}$.

Based on these plots several conclusions can be drawn: a) the slope of absorbance increases (implying a faster reaction rate) with increasing substrate concentration; b) changes in absorbance data are linear with time over the initial 50 seconds, indicating that the reaction rate is constant over that period of time; c) the maximum rate of the enzymatic reaction, v_{max} ,

increases with increasing pressure, meaning that the reaction rate is accelerated with increasing pressure; d) the pressure-induced increase in the activity is larger at higher substrate concentrations; e) the linear dependence of $\ln v_{\max}$ vs p suggests that the catalytic mechanism and the active conformation of α -chymotrypsin is preserved up to 1600 bar, which was found to be in agreement with Raman spectroscopic investigations.²²⁵

The value of the Michaelis-Menten constant, K_M , equals to 46 μM at 1 bar. With increasing pressure, K_M is nearly unchanged, indicating that the binding volume is negligibly small ($\Delta V_{\text{ES}} \approx 0$) in buffer solution, while k_{cat} increases linearly, resulting in a negative value of activation. The activation volume calculated from the slope of the curve in Fig. 6.2c (eq. 9) yielded an activation volume of $-11 \pm 1 \text{ mL mol}^{-1}$, which corresponds to a 2-fold reaction rate increase at a pressure of 1600 bar, in excellent agreement with previously published data, but for a different HHP equipment.¹³⁸

A negative value of activation volume may have different origins. One possibility might be that small conformational changes in the enzyme forming the transition state may be linked to the filling of void volume inside the enzyme's active pocket, which decreases the overall volume. Another reason might be the exposure of charged and polar amino acid residues to water during the formation of the transition state that would cause a higher hydration density due to electrostriction effect. It is proposed that a key point in understanding the action of pressure on activity of α -chymotrypsin may be a well-known ability of high pressure to increase protein hydration.²²⁶ Therefore, the observed negative activation volume in the present case might be mainly due to an increased hydration of the polar transition state of peptide-bond hydrolysis. This effect of high pressure is quite opposite to a tendency of loosening the contacts of water molecules with functional groups of proteins usually seen at high temperatures.¹³⁸

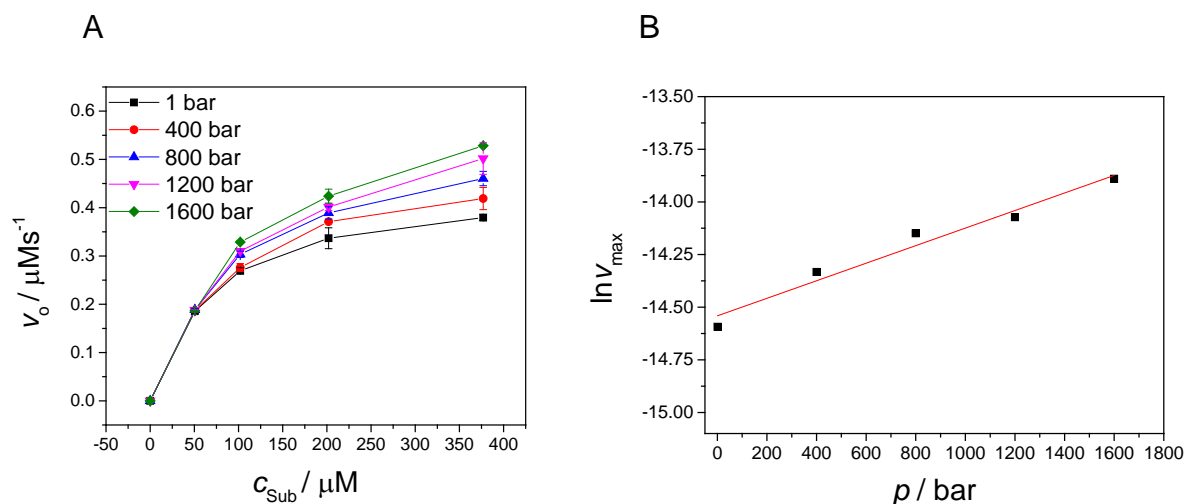


Figure 6.3: Combined effect of high hydrostatic pressure and the kosmotropic cosolvent TMAO. (A) Michaelis-Menten plot for the hydrolysis of the substrate SAAPPpNA by α -chymotrypsin in the presence of 1 M TMAO. (B) v_{max} as a function of pressure (in logarithmic scale).

Protein stabilization can also be achieved by the addition of low-molecular-mass compounds. Among these additives, TMAO is known as one of the most effective protecting osmolytes found in deep-sea organisms.^{227,228} TMAO tends to be excluded from the enzyme surface, forcing the polypeptide to adopt a compactly folded structure with a minimum of exposed surface area to water molecules. As a result, the protein becomes less susceptible to destabilizing forces such as high temperature or pressure.²²⁹ It has been suggested that the protein-stabilizing ability of TMAO is a consequence of both enthalpic and entropic factors. Whereas the enthalpic contribution arises from a reduced H-bonding ability of water, the entropic contribution results from the crowding effect of TMAO.²³⁰

The influence of high pressure on the kinetics of the reaction in the presence of 1 M TMAO is displayed in Figure 6.3. In the presence of 1 M TMAO, the catalytic reaction of α -chymotrypsin displays relatively higher rates in comparison to that in pure buffer. However, the effect of 1 M TMAO on K_{M} and k_{cat} is found to be marginal, implying that the protein is already in a compact functional state in buffer. These results also confirm the assumption that the TMAO does not affect the catalytic mechanism, but only reinforces the hydration shell around the protein.²²⁹ In this case, the activation volume of the reaction equals to $-4 \pm 0.5 \text{ mL mol}^{-1}$, implying that pressure has a much smaller effect on the acceleration of the reaction

compared to that in pure buffer. Thus, high pressure and TMAO display competitive effects on the enzymatic activity of α -chymotrypsin. This is in agreement with the hypothesis that TMAO may serve as a counteractant of pressure in marine organisms.²²⁷ A mechanism has been suggested in which TMAO might be able to counteract pressure effects by opposing the tendency of pressure to favor exposure of hydrated protein surfaces.²²⁸

To summarize, effects of pressure on the α -chymotrypsin-catalyzed reaction is characterized by a negative activation volume in buffer, $\Delta V^\ddagger = -11 \pm 1 \text{ mL mol}^{-1}$, which corresponds well to a previously reported value.¹³⁸ The acceleration in the hydrolysis rate by pressure is explained by the increase of the preferential hydration in the transition state. We found a competitive effect on the enzymatic activity of high pressure and the osmolyte TMAO, most likely due to their opposite impacts on the structure of the enzyme. These high pressure activity measurements of enzymatic activity approved of the HPSF as an effective method to unravel molecular aspects of enzymatic reactions. The activation volume obtained, also yields a better understanding of adaptation mechanisms in enzymes at high pressure and additionally, have numerous biotechnological applications by optimization of the reaction conditions.

VII

Bibliography

- (1) Six, D. A.; Dennis, E. A. (2000). The expanding superfamily of phospholipase A(2) enzymes: classification and characterization. *Biochim. Biophys. Acta* 1488, 1–19.
- (2) Dennis, E. A. (1994). Diversity of group types, regulation, and function of phospholipase A2. *J. Biol. Chem.* 269, 13057–13060.
- (3) Triggiani, M.; Granata, F.; Frattini, A.; Marone, G. (2006). Activation of human inflammatory cells by secreted phospholipases A2. *Biochim. Biophys. Acta* 1761, 1289–1300.
- (4) Funk, C. D. (2001). Prostaglandins and leukotrienes: advances in eicosanoid biology. *Science* 294, 1871–1875.
- (5) Anliker, B.; Chun, J. (2004). Lysophospholipid G Protein-coupled Receptors. *J. Biol. Chem.* 279, 20555–20558.
- (6) Rivera, R.; Chun, J. (2008). Biological effects of lysophospholipids. *Rev. Physiol. Biochem. Pharmacol.* 160, 25–46.
- (7) Lodish, H.; Berk, A.; Matsudaira, P.; Kaiser, C. A.; Krieger, M.; Scott, M. P.; Zipursky, L. Darnell, J. (2003). *Molecular Cell Biology* - 5th ed.; W. H. Freeman & Co Ltd, New York, USA
- (8) Atsumi, G.I.; Murakami, M.; Tajima, M.; Shimbara, S.; Hara, N.; Kudo, I. (1997). The perturbed membrane of cells undergoing apoptosis is susceptible to type II secretory phospholipase A2 to liberate arachidonic acid. *Biochim. Biophys. Acta* 1349, 43–54.
- (9) Nielson, K. H.; Olsen, C. A.; Allred, D. V.; O'Neill, K. L.; Burton, G. F.; Bell, J. D. (2000). Susceptibility of S49 lymphoma cell membranes to hydrolysis by secretory phospholipase A(2) during early phase of apoptosis. *Biochim. Biophys. Acta* 1484, 163–174.
- (10) Bailey, R. W.; Olson, E. D.; Vu, M. P.; Brueseke, T. J.; Robertson, L.; Christensen, R. E.; Parker, K. H., et al. Bell, J. D. (2007). Relationship between membrane physical properties and secretory phospholipase A2 hydrolysis kinetics in S49 cells during ionophore-induced apoptosis. *Biophys. J.* 93, 2350–2362.
- (11) Bailey, R. W.; Nguyen, T.; Robertson, L.; Gibbons, E.; Nelson, J.; Christensen, R. E.; Bell, J. P., et al. Bell, J. D. (2009). Sequence of physical changes to the cell membrane during glucocorticoid-induced apoptosis in S49 lymphoma cells. *Biophys. J.* 96, 2709–2718.
- (12) Belinsky, G. S.; Rajan, T. V.; Saria, E. A.; Giardina, C.; Rosenberg, D. W. (2007). Expression of secretory phospholipase A2 in colon tumor cells potentiates tumor growth. *Mol. Carcinog.* 46, 106–116.
- (13) Dong, Z.; Liu, Y.; Scott, K. F.; Levin, L.; Gaitonde, K.; Bracken, R. Bruce; Burke, B., et al. Lu, S. (2010). Secretory phospholipase A2-IIa is involved in prostate cancer progression and may potentially serve as a biomarker for prostate cancer. *Carcinogenesis* 31, 1948–1955.
- (14) Kupert, E.; Anderson, M.; Liu, Y.; Succop, P.; Levin, L.; Wang, J.; Wikenheiser-brokamp, K., et al. Lu, S. (2011). Plasma secretory phospholipase A2-IIa as a potential biomarker for lung cancer in patients with solitary pulmonary nodules. *BMC Cancer* 11, 513.

- (15) Andresen, T. L.; Davidsen, J.; Begtrup, M.; Mouritsen, O. G.; Jorgensen, K. (2004). Enzymatic release of antitumor ether lipids by specific phospholipase A2 activation of liposome-forming prodrugs. *J. Med. Chem.* 47, 1694–1703.
- (16) Mock, J. N.; Costyn, L. J.; Wilding, S. L.; Arnold, R. D.; Cummings, B. S. (2013). Evidence for distinct mechanisms of uptake and antitumor activity of secretory phospholipase A2 responsive liposome in prostate cancer. *Integr. Biol.* 5, 172–182.
- (17) Burke, J. E.; Dennis, E. A. (2009). Phospholipase A2 structure/function, mechanism, and signaling. *J. Lipid Res.* 50, S237-42.
- (18) Burke, J. E.; Dennis, E. A. (2009). Phospholipase A2 Biochemistry. *Cardiovasc. Drugs Ther.* 23, 49.
- (19) Gelb, M. H.; Jain, M. K.; Hanel, A. M.; Berg, O. G. (1995). Interfacial enzymology of glycerolipid hydrolases: lessons from secreted phospholipases A2. *Annual Rev. Biochem.* 64, 653–688.
- (20) Nicolas, J.P.; Lin, Y.; Lambeau, G.; Ghomashchi, F.; Lazdunski, M.; Gelb, M. H. (1997). Localization of Structural Elements of Bee Venom Phospholipase A2 Involved in N-type Receptor Binding and Neurotoxicity. *J. Biol. Chem.* 272, 7173–7181.
- (21) Lambeau, G.; Lazdunski, M. (1999). Receptors for a growing family of secreted phospholipases A2. *Trends Pharmacol. Sci.* 20, 162–170.
- (22) Scott, D. L.; Otwinowski, Z.; Gelb, M. H.; Sigler, P. B. (1990). Crystal structure of bee-venom phospholipase A2 in a complex with a transition-state analogue. *Science* 250, 1563–1566.
- (23) Lambeau, G.; Gelb, M. H. (2008). Biochemistry and physiology of mammalian secreted phospholipases A2. *Annual Rev. Biochem.* 77, 495–520.
- (24) Mouritsen, O. G.; Andresen, T. L.; Halperin, A.; Hansen, P. Lyngs; Jakobsen, A. F.; Jensen, U. Bernchou; Jensen, M. O., et al. Weiss, M. (2006). Activation of interfacial enzymes at membrane surfaces. *J. Phys. Condens. Matter* 18, 1293-1304.
- (25) Zhou, F.; Schulten, K. (1996). Molecular dynamics study of phospholipase A2 on a membrane surface. *Proteins* 25, 12–27.
- (26) Gelb, M. H.; Cho, W.; Wilton, D. C. (1999). Interfacial binding of secreted phospholipases A(2): more than electrostatics and a major role for tryptophan. *Curr. Opin. Struc. Biol.* 9, 428–432.
- (27) Tatulian, S. A. (2001). Toward understanding interfacial activation of secretory phospholipase A2 (PLA2): membrane surface properties and membrane-induced structural changes in the enzyme contribute synergistically to PLA2 activation. *Biophys. J.* 80, 789–800.
- (28) Tatulian, S. A.; Biltonen, R. L.; Tamm, L. K. (1997). Structural changes in a secretory phospholipase A2 induced by membrane binding: a clue to interfacial activation? *J. Mol. Biol.* 268, 809–815.
- (29) Burack, W. R.; Biltonen, R. L. (1994). Lipid bilayer heterogeneities and modulation of phospholipase A2 activity. *Chem. Phys. Lipids* 73, 209–222.
- (30) Lehtonen, J. Y.; Kinnunen, P. K. (1995). Phospholipase A2 as a mechanosensor. *Biophys. J.* 68, 1888–1894.

- (31) Scott, D. L.; White, S. P.; Browning, J. L.; Rosa, J. J.; Gelb, M. H.; Sigler, P. B. (1991). Structures of free and inhibited human secretory phospholipase A2 from inflammatory exudate. *Science* 254, 1007–1010.
- (32) den Berg, Bert van; Tessari, M.; Boelens, R.; Dijkman, R.; de Hass, Gerard H.; Kaptein, R.; Verheij, H. M. (1995). NMR structures of phospholipase A2 reveal conformational changes during interfacial activation. *Nat. Struct. Mol. Biol.* 2, 402–406.
- (33) Arni, R. K.; Ward, R. J. (1996). Phospholipase A2-a structural review. *Toxicon* 34, 827–841.
- (34) Bollinger, J. G.; Diraviyam, K.; Ghomashchi, F.; Murray, D.; Gelb, M. H. (2004). Interfacial binding of bee venom secreted phospholipase A2 to membranes occurs predominantly by a nonelectrostatic mechanism. *Biochemistry* 43, 13293–13304.
- (35) Berg, O. G.; Gelb, M. H.; Tsai, M. D.; Jain, M. K. (2001). Interfacial enzymology: the secreted phospholipase A(2)-paradigm. *Chem. Rev.* 101, 2613–2654.
- (36) Singer, A. G.; Ghomashchi, F.; Le Calvez, C.; Bollinger, J.; Bezzine, S.; Rouault, M.; Sadilek, M., et al. Gelb, M. H. (2002). Interfacial kinetic and binding properties of the complete set of human and mouse groups I, II, V, X, and XII secreted phospholipases A2. *J. Biol. Chem.* 277, 48535–48549.
- (37) Lin, Y.; Nielsen, R.; Murray, D.; Hubbell, W. L.; Mailer, C.; Robinson, B. H.; Gelb, M. H. (1998). Docking phospholipase A2 on membranes using electrostatic potential-modulated spin relaxation magnetic resonance. *Science* 279, 1925–1929.
- (38) Ghomashchi, F.; Lin, Y.; Hixon, M. S.; Yu, B. Z.; Annand, R.; Jain, M. K.; Gelb, M. H. (1998). Interfacial recognition by bee venom phospholipase A2: insights into nonelectrostatic molecular determinants by charge reversal mutagenesis. *Biochemistry* 37, 6697–6710.
- (39) Pande, A. H.; Qin, S.; Nemecek, K. N.; He, X.; Tatulian, S. A. (2006). Isoform-specific membrane insertion of secretory phospholipase A2 and functional implications. *Biochemistry* 45, 12436–12447.
- (40) Berg, O. G.; Yu, B. Zhu; Rogers, J.; Jain, M. Kumar (1991). Interfacial catalysis by phospholipase A2: determination of the interfacial kinetic rate constants. *Biochemistry* 30, 7283–7297.
- (41) Jain, M. Kumar; Rogers, J.; Jahagirdar, D. V.; Marecek, J. F.; Ramirez, F. (1986). Kinetics of interfacial catalysis by phospholipase A2 in intravesicle scooting mode, and heterofusion of anionic and zwitterionic vesicles. *Biochim. Biophys. Acta* 860, 435–447.
- (42) Ghomashchi, F.; Yu, B. Zhu; Berg, O.; Jain, M. Kumar; Gelb, M. H. (1991). Interfacial catalysis by phospholipase A2: substrate specificity in vesicles. *Biochemistry* 30, 7318–7329.
- (43) Scott, D. L.; White, S. P.; Otwinowski, Z.; Yuan, W.; Gelb, M. H.; Sigler, P. B. (1990). Interfacial catalysis: the mechanism of phospholipase A2. *Science* 250, 1541–1546.
- (44) Rogers, J.; Yu, B. Z.; Serves, S. V.; Tsvigoulis, G. M.; Sotiropoulos, D. N.; Ioannou, P. V.; Jain, M. K. (1996). Kinetic basis for the substrate specificity during hydrolysis of phospholipids by secreted phospholipase A2. *Biochemistry* 35, 9375–9384.

- (45) Edwards, S. H.; Thompson, D.; Baker, S. F.; Wood, S. P.; Wilton, D. C. (2002). The crystal structure of the H48Q active site mutant of human group IIA secreted phospholipase A2 at 1.5 Å resolution provides an insight into the catalytic mechanism. *Biochemistry* 41, 15468–15476.
- (46) Gysin, S.; Salt, M.; Young, A.; McCormick, F. (2011). Therapeutic strategies for targeting ras proteins. *Genes Cancer* 2, 359–372.
- (47) Brooker, R. J. (2014). *Biology*, 3rd ed.; McGraw-Hill: New York, USA
- (48) Cherfils, J.; Zeghouf, M. (2013). Regulation of small GTPases by GEFs, GAPs, and GDIs. *Physiol. Rev.* 93, 269–309.
- (49) Goodsell, D. S. (1999). The Molecular Perspective: The ras Oncogene. *The Oncologist* 4, 263–264.
- (50) Ahearn, I. M.; Haigis, K.; Bar-Sagi, D.; Philips, M. R. (2012). Regulating the regulator: post-translational modification of RAS. *Nat. Rev. Mol. Cell Biol.* 13, 39–51.
- (51) Zhang, F. L.; Casey, P. J. (1996). Protein prenylation: molecular mechanisms and functional consequences. *Annu. Rev. Biochem.* 65, 241–269.
- (52) Nguyen, U. T. T.; Wu, Y.; Goodall, A.; Alexandrov, K. (2010). Analysis of protein prenylation in vitro and in vivo using functionalized phosphoisoprenoids. *Curr. Protoc. Protein Sci.* 62, 14.3.1–14.3.15.
- (53) DerMardirossian, C.; Bokoch, G. M. (2005). GDIs: central regulatory molecules in Rho GTPase activation. *Trends Cell Biol.* 15, 356–363.
- (54) Polans, A.; Baehr, W.; Palczewski, K. (1996). Turned on by Ca²⁺! The physiology and pathology of Ca²⁺-binding proteins in the retina. *Trends Neurosci.* 19, 547–554.
- (55) Nancy, V.; Callebaut, I.; El Marjou, A.; Gunzburg, J. de (2002). The delta subunit of retinal rod cGMP phosphodiesterase regulates the membrane association of Ras and Rap GTPases. *J. Biol. Chem.* 277, 15076–15084.
- (56) Baehr, W. (2014). Membrane protein transport in photoreceptors: the function of PDEdelta: the Proctor lecture. *Invest. Ophthalmol. Vis. Sci.* 55, 8653–8666.
- (57) Zhang, H.; Constantine, R.; Frederick, J. M.; Baehr, W. (2012). The prenyl-binding protein PrBP/δ: a chaperone participating in intracellular trafficking. *Vision Res* 75, 19–25.
- (58) Zhang, H.; Liu, X. H.; Zhang, K.; Chen, C. K.; Frederick, J. M.; Prestwich, G. D.; Baehr, W. (2004). Photoreceptor cGMP phosphodiesterase delta subunit (PDEdelta) functions as a prenyl-binding protein. *J. Biol. Chem.* 279, 407–413.
- (59) Weise, K.; Kapoor, S.; Werkmuller, A.; Mobitz, S.; Zimmermann, G.; Triola, G.; Waldmann, H.; Winter, R. (2012). Dissociation of the K-Ras4B/PDEdelta complex upon contact with lipid membranes: membrane delivery instead of extraction. *J. Am. Chem. Soc.* 134, 11503–11510.
- (60) Zimmermann, G.; Papke, B.; Ismail, S.; Vartak, N.; Chandra, A.; Hoffmann, M.; Hahn, S. A., et al. Waldmann, H. (2013). Small molecule inhibition of the KRAS–PDEδ interaction impairs oncogenic KRAS signalling. *Nature* 497, 638–642.
- (61) Baker, N. M.; Der, C. J. (2013). Cancer: Drug for an 'undruggable' protein. *Nature* 497, 577–578.

- (62) Chandra, A.; Grecco, H. E.; Pisupati, V.; Perera, D.; Cassidy, L.; Skoulidis, F.; Ismail, S. A., et al. Bastiaens, P. (2011). The GDI-like solubilizing factor PDE δ sustains the spatial organization and signalling of Ras family proteins. *Nat. Cell Biol.* 14, 148–158.
- (63) Schmick, M.; Vartak, N.; Papke, B.; Kovacevic, M.; Truxius, D. C.; Rossmannek, L.; Bastiaens, P. (2014). KRas localizes to the plasma membrane by spatial cycles of solubilization, trapping and vesicular transport. *Cell* 157, 459–471.
- (64) Ismail, S. A.; Chen, Y. X.; Rusinova, A.; Chandra, A.; Bierbaum, M.; Gremer, L.; Triola, G., et al. Wittinghofer, A. (2011). Arl2-GTP and Arl3-GTP regulate a GDI-like transport system for farnesylated cargo. *Nat. Chem. Biol.* 7, 942–949.
- (65) Hanzal-Bayer, M.; Renault, L.; Roversi, P.; Wittinghofer, A.; Hillig, R. C. (2002). The complex of Arl2-GTP and PDE delta: from structure to function. *EMBO J.* 21, 2095–2106.
- (66) Hoffman, G. R.; Nassar, N.; Cerione, R. A. (2000). Structure of the Rho family GTP-binding protein Cdc42 in complex with the multifunctional regulator RhoGDI. *Cell* 100, 345–356.
- (67) Constantine, R.; Zhang, H.; Gerstner, C. D.; Frederick, J. M.; Baehr, W. (2012). Uncoordinated (UNC)119: coordinating the trafficking of myristoylated proteins. *Vision Res.* 75, 26–32.
- (68) Ismail, S. A.; Chen, Y. X.; Miertschke, M.; Vetter, I. R.; Koerner, C.; Wittinghofer, A. (2012). Structural basis for Arl3-specific release of myristoylated ciliary cargo from UNC119. *EMBO J.* 31, 4085–4094.
- (69) Chen, Y. X.; Koch, S.; Uhlenbrock, K.; Weise, K.; Das, D.; Gremer, L.; Brunsveld, L., et al. Waldmann, H. (2010). Synthesis of the Rheb and K-Ras4B GTPases. *Angew. Chem., Int. Ed.* 49, 6090–6095.
- (70) Kong, J.; Yu, S. (2007). Fourier transform infrared spectroscopic analysis of protein secondary structures. *Acta Biochim. Biophys. Sinica* 39, 549–559.
- (71) Dong, A.; Malecki, J. M.; Lee, L.; Carpenter, J. F.; Lee, J. Ching (2002). Ligand-induced conformational and structural dynamics changes in Escherichia coli cyclic AMP receptor protein. *Biochemistry* 41, 6660–6667.
- (72) Barth, A. (2007). Infrared spectroscopy of proteins. *Biochim. Biophys. Acta* 1767, 1073–1101.
- (73) Panick, G.; Malessa, R.; Winter, R.; Rapp, G.; Frye, K. J.; Royer, C. A. (1998). Structural characterization of the pressure-denatured state and unfolding/refolding kinetics of staphylococcal nuclease by synchrotron small-angle X-ray scattering and Fourier-transform infrared spectroscopy. *J. Mol. Biol.* 275, 389–402.
- (74) Garidel P.; Schott H. (2006). Fourier-Transform Midinfrared Spectroscopy for Analysis and Screening of Liquid Protein Formulations: Part 2: Detailed Analysis and Applications. *Bioprocess Int.* 4, 48–55
- (75) Matsunami, M., Okamura, H., Ochiai, A. Nanba, T. (2009). Pressure tuning of an ionic insulator into a heavy electron metal: An infrared study of YbS. *Phys. Rev. Lett.* 103, 1–4.
- (76) Wong, P. T. T.; Moffat, D. J. (1989). A new internal pressure calibrant for high-pressure infrared spectroscopy of aqueous systems. *Appl. Spectrosc.* 43, 1279–1281.

- (77) Kapoor, S.; Werkmuller, A.; Denter, C.; Zhai, Y.; Markgraf, J.; Weise, K.; Opitz, N.; Winter, R. (2011). Temperature-pressure phase diagram of a heterogeneous anionic model biomembrane system: results from a combined calorimetry, spectroscopy and microscopy study. *Biochim. Biophys. Acta* 1808, 1187–1195.
- (78) Goormaghtigh, E.; Cabiaux, V.; Ruyschaert, J. M. (1994). Determination of soluble and membrane protein structure by Fourier transform infrared spectroscopy. III. Secondary structures. *Subcell. Biochem.* 23, 405–450.
- (79) Bugnon, P.; Laurency, G.; Ducommun, Y.; Sauvageat, P. Y.; Merbach, A. E.; Ith, R.; Tschanz, R., et al. Grell, E. (1996). High-pressure stopped-flow spectrometer for kinetic studies of fast reactions by absorbance and fluorescence detection. *Anal. Chem.* 68, 3045–3049.
- (80) Rosin, C.; Estel, K.; Hälker, J.; Winter, R. (2015). Combined effects of temperature, pressure, and co-solvents on the polymerization kinetics of actin. *ChemPhysChem* 16, 1379–1385.
- (81) Lakowicz, J. R. (2006). *Principles of Fluorescence Spectroscopy*, Third Edition; Springer ebook collection / Chemistry and Materials Science 2005-2008; Springer Science&Business Media, LLC: Boston, MA.
- (82) Feng, L.; Manabe, K.; Shope, J. C.; Widmer, S.; DeWald, D. B.; Prestwich, G. D. (2002). A real-time fluorogenic Phospholipase A2 assay for biochemical and cellular activity measurements. *Chem. Biol.* 9, 795–803.
- (83) Weise, K.; Triola, G.; Brunsveld, L.; Waldmann, H.; Winter, R. (2009). Influence of the lipidation motif on the partitioning and association of N-Ras in model membrane subdomains. *J. Am. Chem. Soc.* 131, 1557–1564.
- (84) Weise, K.; Kapoor, S.; Denter, C.; Nikolaus, J.; Opitz, N.; Koch, S.; Triola, G., et al. Winter, R. (2011). Membrane-mediated induction and sorting of K-Ras microdomain signaling platforms. *J. Am. Chem. Soc.* 133, 880–887.
- (85) Lopez, M. M.; Makhatadze, G. I. (2002). Isothermal titration calorimetry. *Methods Mol. Biol.* 173, 121–126.
- (86) Wiseman, T.; Williston, S.; Brandts, J. F.; Lin, L. N. (1989). Rapid measurement of binding constants and heats of binding using a new titration calorimeter. *Anal. Biochem.* 179, 131–137.
- (87) Barratt, E.; Bingham, R. J.; Warner, D. J.; Laughton, C. A.; Phillips, Simon E V; Homans, S. W. (2005). Van der Waals interactions dominate ligand-protein association in a protein binding site occluded from solvent water. *J. Am. Chem. Soc.* 127, 11827–11834.
- (88) Chaires, J. B. (2008). Calorimetry and thermodynamics in drug design. *Annu. Rev. Biophys.* 37, 135–151.
- (89) Makhatadze, G.I. (1998). Measuring protein thermostability by differential scanning calorimetry, *Current Protocols in Protein Science*, 7.9.1-7.9.14. John Wiley & Sons, Inc., New York, USA.
- (90) Privalov G, Kavina V, Freire E, Privalov PL. (1995). Precise scanning calorimeter for studying thermal properties of biological macromolecules in dilute solution. *Anal. Biochem.* 20, 79–85.

- (91) Layton, C. J.; Hellinga, H. W. (2011). Quantitation of protein-protein interactions by thermal stability shift analysis. *Protein Sci.* 20, 1439–1450.
- (92) Waldron, T. T.; Murphy, K. P. (2003). Stabilization of Proteins by Ligand Binding: Application to Drug Screening and Determination of Unfolding Energetics. *Biochemistry* 42, 5058–5064.
- (93) Lin, L.N.; Brandts, J. F.; Brandts, J. Michael; Plotnikov, V. (2002). Determination of the volumetric properties of proteins and other solutes using pressure perturbation calorimetry. *Anal. Biochem.* 302, 144–160.
- (94) Ravindra, R.; Winter, R. (2004). Pressure perturbation calorimetry: a new technique provides surprising results on the effects of co-solvents on protein solvation and unfolding behaviour. *ChemPhysChem* 5, 566–571.
- (95) Ravindra, R.; Royer, C.; Winter, R. (2004). Pressure perturbation calorimetric studies of the solvation properties and the thermal unfolding of staphylococcal nuclease. *Phys. Chem. Chem. Phys.* 6, 1952.
- (96) Zhai, Y.; Okoro, L.; Cooper, A.; Winter, R. (2011). Applications of pressure perturbation calorimetry in biophysical studies. *Biophys. Chem.* 156, 13–23.
- (97) Mitra, L.; Smolin, N.; Ravindra, R.; Royer, C.; Winter, R. (2006). Pressure perturbation calorimetric studies of the solvation properties and the thermal unfolding of proteins in solution--experiments and theoretical interpretation. *Phys. Chem. Chem. Phys.* 8, 1249–1265.
- (98) Suladze, S.; Kahse, M.; Erwin, N.; Tomazic, D.; Winter, R. (2015). Probing volumetric properties of biomolecular systems by pressure perturbation calorimetry (PPC) - the effects of hydration, cosolvents and crowding. *Methods* 76, 67–77.
- (99) Makhatadze, G. I.; Privalov, P. L. (1990). Heat capacity of proteins. I. Partial molar heat capacity of individual amino acid residues in aqueous solution: hydration effect. *J. Mol. Biol.* 213, 375–384.
- (100) Buckin, V.; O’Driscoll, B.; Smyth, C.; Alting, AC.; Visschers, R.W. (2003). Ultrasonic spectroscopy for material analysis: recent advances. *Spectrosc. Eur.* 15, 20–25.
- (101) Krivanek, R.; Okoro, L.; Winter, R. (2008). Effect of Cholesterol and Ergosterol on the Compressibility and Volume Fluctuations of Phospholipid-Sterol Bilayers in the Critical Point Region: A Molecular Acoustic and Calorimetric Study. *Biophys. J.* 94, 3538–3548.
- (102) Kratky, O.; Leopold, H.; Stabinger, H. (1973). The determination of the partial specific volume of proteins by the mechanical oscillator technique. *Methods Enzymol.* 27, 98–110.
- (103) Taulier, N.; Chalikian, T. V. (2002). Compressibility of protein transitions. *Biochim. Biophys. Acta* 1595, 48–70.
- (104) Sarvazyan, A. P. (1991). Ultrasonic velocimetry of biological compounds. *Annu. Rev. Biophys. Biophys. Chem.* 20, 321–342.
- (105) Chalikian, T. V.; Totrov, M.; Abagyan, R.; Breslauer, K. J. (1996). The hydration of globular proteins as derived from volume and compressibility measurements: cross correlating thermodynamic and structural data. *J. Mol. Biol.* 260, 588–603.
- (106) Blandamer, M. J.; Davis, M. I.; Douhéret, G.; Reis, João Carlos R. (2001). Apparent molar isentropic compressions and expansions of solutions. *Chem. Soc. Rev.* 30, 8–15.

- (107) Alberts, B. (2002). *Molecular biology of the cell*, 4th ed.; Garland Science: New York, USA
- (108) Vereb, G.; Szöllösi, J.; Matkó, J.; Nagy, P.; Farkas, T.; Vígh, L.; Mátyus, L., et al. Damjanovich, S. (2003). Dynamic, yet structured: The cell membrane three decades after the Singer–Nicolson model. *Proc. Natl. Acad. Sci. U. S. A.* 100, 8053–8058.
- (109) Shaikh, S. R.; Dumaul, A. C.; Jenki, L. J.; Stillwell, W. (2001). Lipid phase separation in phospholipid bilayers and monolayers modeling the plasma membrane. *Biochim. Biophys. Acta* 1512, 317–328.
- (110) Escribá, P. V.; González-Ros, J. M.; Goñi, F. M.; Kinnunen, Paavo K J; Vigh, L.; Sánchez-Magraner, L.; Fernández, A. M., et al. Barceló-Coblijn, G. (2008). Membranes: a meeting point for lipids, proteins and therapies. *J. Cell Mol. Med.* 12, 829–875.
- (111) Vogler, O.; Casas, J.; Capó, D.; Nagy, T.; Borchert, G.; Martorell, G.; Escriba, P. V. (2004). The Gbetagamma dimer drives the interaction of heterotrimeric Gi proteins with nonlamellar membrane structures. *J. Biol. Chem.* 279, 36540–36545.
- (112) Larsen, J. Bruun; Jensen, M. Borch; Bhatia, V. K.; Pedersen, S. L.; Bjørnholm, T.; Iversen, L.; Uline, M., et al. Stamou, D. (2015). Membrane curvature enables N-Ras lipid anchor sorting to liquid-ordered membrane phases. *Nat. Chem. Biol.* 11, 192–194.
- (113) Funari, S. S.; Prades, J.; Escriba, P. V.; Barcelo, F. (2005). Farnesol and geranylgeraniol modulate the structural properties of phosphatidylethanolamine model membranes. *Molec. Membrane Biol.* 22, 303–311.
- (114) Harris, F. M.; Smith, S. K.; Bell, J. D. (2001). Physical properties of erythrocyte ghosts that determine susceptibility to secretory phospholipase A2. *J. Biol. Chem.* 276, 22722–22731.
- (115) Simons, K.; Ikonen, E. (1997). Functional rafts in cell membranes. *Nature* 387, 569.
- (116) Vequi-Suplicy, C. C.; Riske, K. A.; Knorr, R. L.; Dimova, R. (2010). Vesicles with charged domains. *Biochim. Biophys. Acta* 1798, 1338–1347.
- (117) Jeworrek, C.; Puhse, M.; Winter, R. (2008). X-ray kinematography of phase transformations of three-component lipid mixtures: a time-resolved synchrotron X-ray scattering study using the pressure-jump relaxation technique. *Langmuir* 24, 11851–11859.
- (118) Silvius, J. R.; del Giudice, D.; Lafleur, M. (1996). Cholesterol at different bilayer concentrations can promote or antagonize lateral segregation of phospholipids of differing acyl chain length. *Biochemistry* 35, 15198–15208.
- (119) Schroeder, R.; London, E.; Brown, D. (1994). Interactions between saturated acyl chains confer detergent resistance on lipids and glycosylphosphatidylinositol (GPI)-anchored proteins: GPI-anchored proteins in liposomes and cells show similar behavior. *Proc. Natl. Acad. Sci. U. S. A.* 91, 12130–12134.
- (120) Van Meer, G.; Voelker, D. R.; Feigenson, G. W. (2008). Membrane lipids: where they are and how they behave. *Nat. Rev. Mol. Cell Biol.* 9, 112–124.
- (121) Picard, A.; Daniel, I. (2013). Pressure as an environmental parameter for microbial life--a review. *Biophys. Chem.* 183, 30–41.
- (122) Brooks, N. J. (2014). Pressure effects on lipids and bio-membrane assemblies. *IUCrJ*, 470–477.

- (123) Silva, J. L.; Foguel, D.; Royer, C. A. (2001). Pressure provides new insights into protein folding, dynamics and structure. *Trends. Biochem. Sci.* 26, 612–618.
- (124) Casadei, M. A.; Manas, P.; Niven, G.; Needs, E.; Mackey, B. M. (2002). Role of membrane fluidity in pressure resistance of *Escherichia coli* NCTC 8164. *Appl. Environ. Microbiol.* 68, 5965–5972.
- (125) Royer, C. A. (1995). Application of pressure to biochemical equilibria: the other thermodynamic variable. *Methods Enzymol.* 259, 357–377.
- (126) Skanes, I. D.; Stewart, J.; Keough, K. M. W.; Morrow, M. R. (2006). Effect of chain unsaturation on bilayer response to pressure. *Phys. Rev. E* 74, 51913.
- (127) Brooks, N. J.; Ces, O.; Templer, R. H.; Seddon, J. M. (2011). Pressure effects on lipid membrane structure and dynamics. *Chem. Phys. Lipids* 164, 89–98.
- (128) Scarlata, S. (2005). The effect of hydrostatic pressure on membrane-bound proteins. *Braz. J. Med. Biol. Res.* 38, 1203–1208.
- (129) McMahon, H. T.; Gallop, J. L. (2005). Membrane curvature and mechanisms of dynamic cell membrane remodelling. *Nature* 438, 590–596.
- (130) Winter, R.; Köhling, R. (2004). Static and time-resolved synchrotron small-angle x-ray scattering studies of lyotropic lipid mesophases, model biomembranes and proteins in solution. *J. Phys. Condens. Matter* 16, S327-S352.
- (131) Scarlata, S. F.; Rosenberg, M. (1990). Effect of increased lipid packing on the surface charge of micelles and membranes. *Biochemistry* 29, 10233–10240.
- (132) Rebecchi, M.; Bon Homme, M.; Scarlata, S. (1999). Role of lipid packing in the activity of phospholipase C-delta1 as determined by hydrostatic pressure measurements. *Biochem. J.* 341, 571–576.
- (133) Winter, R.; Jeworrek, C. (2009). Effect of pressure on membranes. *Soft Matter* 5, 3157–3173.
- (134) Winter, R. (2002). Synchrotron X-ray and neutron small-angle scattering of lyotropic lipid mesophases, model biomembranes and proteins in solution at high pressure. *Biochim. Biophys. Acta* 1595, 160–184.
- (135) Roche, J.; Caro, J. A.; Norberto, D. R.; Barthe, P.; Roumestand, C.; Schlessman, J. L.; Garcia, A. E., et al. Royer, C. A. (2012). Cavities determine the pressure unfolding of proteins. *Proc. Natl. Acad. Sci. U.S.A.* 109, 6945–6950.
- (136) Kapoor, S.; Triola, G.; Vetter, I. R.; Erkkamp, M.; Waldmann, H.; Winter, R. (2012). Revealing conformational substates of lipidated N-Ras protein by pressure modulation. *Proc. Natl. Acad. Sci. U. S. A.* 109, 460–465.
- (137) Masson, P.; Balny, C. (2005). Linear and non-linear pressure dependence of enzyme catalytic parameters. *Biochim. biophys. acta* 1724, 440–450.
- (138) Mozhaev, V. V.; Lange, R.; Kudryashova, E. V.; Balny, C. (1996). Application of high hydrostatic pressure for increasing activity and stability of enzymes. *Biotechnol. Bioeng.* 52, 320–331.
- (139) Siebenaller, J. F.; Garrett, D. J. (2002). The effects of the deep-sea environment on transmembrane signaling. *Comp. Biochem. Physiol., Part B Biochem. Mol. Biol.* 131, 675–694.

- (140) Chong, P. L.; Fortes, P. A.; Jameson, D. M. (1985). Mechanisms of inhibition of (Na,K)-ATPase by hydrostatic pressure studied with fluorescent probes. *J. Biol. Chem.* 260, 14484–14490.
- (141) Staubach, S.; Hanisch, F.-G. (2011). Lipid rafts: signaling and sorting platforms of cells and their roles in cancer. *Expert Rev. Proteomics* 8, 263–277.
- (142) Bethani, I.; Skanland, S. S.; Dikic, I.; Acker-Palmer, A. (2010). Spatial organization of transmembrane receptor signalling. *EMBO J.* 29, 2677–2688.
- (143) Van den Brink-van der Laan, Els; Killian, J. Antoinette; Kruijff, B. de (2004). Nonbilayer lipids affect peripheral and integral membrane proteins via changes in the lateral pressure profile. *Biochim. Biophys. Acta* 1666, 275–288.
- (144) Dennis, E. A.; Cao, J.; Hsu, Y.-H.; Magrioti, V.; Kokotos, G. (2011). Phospholipase A2 enzymes: physical structure, biological function, disease implication, chemical inhibition, and therapeutic intervention. *Chem. Rev.* 111, 6130–6185.
- (145) Jackman, J. A.; Cho, N.-J.; Duran, R. S.; Frank, C. W. (2010). Interfacial binding dynamics of bee venom phospholipase A2 investigated by dynamic light scattering and quartz crystal microbalance. *Langmuir* 26, 4103–4112.
- (146) Krajewska, B.; van Eldik, R.; Brindell, M. (2012). Temperature- and pressure-dependent stopped-flow kinetic studies of jack bean urease. Implications for the catalytic mechanism. *J. Biol. Inorg. Chem.* 17, 1123–1134.
- (147) Lendermann, J.; Winter, R. (2003). Interaction of cytochrome c with cubic monoolein mesophases at limited hydration conditions: The effects of concentration, temperature and pressure. *Phys. Chem. Chem. Phys.* 5, 1440–1450.
- (148) Kraineva, J.; Narayanan, R. Aravinda; Kondrashkina, E.; Thiyagarajan, P.; Winter, R. (2005). Kinetics of lamellar-to-cubic and inter-cubic phase transitions of pure and cytochrome c containing monoolein dispersions monitored by time-resolved small-angle X-ray diffraction. *Langmuir* 21, 3559–3571.
- (149) Mishra, R.; Winter, R. (2008). Cold and pressure-induced dissociation of protein aggregates and amyloid fibrils. *Angew. Chem. Int. ed.* 47, 6518–6521.
- (150) Hochachka, P. W.; Somero, G. N. (2002). Biochemical adaptation: Mechanism and process in physiological evolution; Oxford University Press: New York.
- (151) Tzima, E. (2006). Role of small GTPases in endothelial cytoskeletal dynamics and the shear stress response. *Circ. Res.* 98, 176–185.
- (152) Myers, K. A.; Rattner, J. B.; Shrive, N. G.; Hart, D. A. (2007). Hydrostatic pressure sensation in cells: integration into the tensegrity model. *Biochem. Cell Biol.* 85, 543–551.
- (153) Abe, F.; Kato, C.; Horikoshi, K. (1999). Pressure-regulated metabolism in microorganisms. *Trends Microbiol.* 7, 447–453.
- (154) Dennis, E. A.; Rhee, S. G.; Billah, M. M.; Hannun, Y. A. (1991). Role of phospholipase in generating lipid second messengers in signal transduction. *FASEB J.* 5, 2068–2077.
- (155) Zhang, Y.; Lemasters, J.; Herman, B. (1999). Secretory group IIA phospholipase A(2) generates anti-apoptotic survival signals in kidney fibroblasts. *J. Biol. Chem.* 274, 27726–27733.

- (156) Qu, X. D.; Lehrer, R. I. (1998). Secretory phospholipase A2 is the principal bactericide for staphylococci and other gram-positive bacteria in human tears. *Infect. Immun.* 66, 2791–2797.
- (157) Dzwolak, W.; Kato, M.; Taniguchi, Y. (2002). Fourier transform infrared spectroscopy in high-pressure studies on proteins. *Biochim. Biophys. Acta.* 1595, 131–144.
- (158) Shan, S. O.; Loh, S.; Herschlag, D. (1996). The energetics of hydrogen bonds in model systems: implications for enzymatic catalysis. *Science* 272, 97–101.
- (159) Yu, B. Z.; Ghomashchi, F.; Cajal, Y.; Annand, R. R.; Berg, O. G.; Gelb, M. H.; Jain, M. K. (1997). Use of an imperfect neutral diluent and outer vesicle layer scooting mode hydrolysis to analyze the interfacial kinetics, inhibition, and substrate preferences of bee venom phospholipase A2. *Biochemistry* 36, 3870–3881.
- (160) Leidy, C.; Mouritsen, O. G.; Jorgensen, K.; Peters, G. H. (2004). Evolution of a rippled membrane during phospholipase A2 hydrolysis studied by time-resolved AFM. *Biophys. J.* 87, 408–418.
- (161) Kinkaid, A.; Wilton, D. C. (1991). Comparison of the catalytic properties of phospholipase A2 from pancreas and venom using a continuous fluorescence displacement assay. *Biochem. J.* 278, 843–848.
- (162) Tatulian, S. A.; Qin, S.; Pande, A. H.; He, X. (2005). Positioning membrane proteins by novel protein engineering and biophysical approaches. *J. Mol. Biol.* 351, 939–947.
- (163) Gerlach, H.; Laumann, V.; Martens, S.; Becker, Christian F W; Goody, R. S.; Geyer, M. (2010). HIV-1 Nef membrane association depends on charge, curvature, composition and sequence. *Nat. Chem. Biol.* 6, 46–53.
- (164) Eisenblätter, J.; Winter, R. (2006). Pressure effects on the structure and phase behavior of DMPC-gramicidin lipid bilayers: a synchrotron SAXS and 2H-NMR spectroscopy study. *Biophysical. J.* 90, 956–966.
- (165) Teng, Q.; Scarlata, S. (1993). Effect of high pressure on the association of melittin to membranes. *J. Biol. Chem.* 268, 12434–12442.
- (166) Tong, Y.; Li, N.; Liu, H.; Ge, A.; Osawa, M.; Ye, S. (2010). Mechanistic studies by sum-frequency generation spectroscopy: hydrolysis of a supported phospholipid bilayer by phospholipase A2. *Angew. Chem., Int. Ed.* 49, 2319–2323.
- (167) Snitko, Y.; Koduri, R. S.; Han, S. K.; Othman, R.; Baker, S. F.; Molini, B. J.; Wilton, D. C., et al. Cho, W. (1997). Mapping the interfacial binding surface of human secretory group IIa phospholipase A2. *Biochemistry* 36, 14325–14333.
- (168) Simonsen, A. Cohen (2008). Activation of phospholipase A2 by ternary model membranes. *Biophys. J.* 94, 3966–3975.
- (169) Winter, R.; Dzwolak, W. (2005). Exploring the temperature-pressure configurational landscape of biomolecules: from lipid membranes to proteins. *Philos. Trans. A Math. Phys. Eng. Sci.* 363, 537-562
- (170) Ulrich, A. S.; Sami, M.; Watts, A. (1994). Hydration of DOPC bilayers by differential scanning calorimetry. *Biochim. biophys. acta* 1191, 225–230.
- (171) Schuabb, V.; Czeslik, C. (2014). Activation volumes of enzymes adsorbed on silica particles. *Langmuir* 30, 15496–15503.

- (172) Tatulian, S. A. (2003). Structural Effects of Covalent Inhibition of Phospholipase A2 Suggest Allosteric Coupling between Membrane Binding and Catalytic Sites. *Biophys. J.* 84, 1773–1783.
- (173) Krumm, B. E.; Grisshammer, R. (2015). Peptide ligand recognition by G protein-coupled receptors. *Front. Pharmacol.* 6, 48
- (174) Agnieszka A.K. (2011). Chapter 1: Thermodynamics of Ligand-Protein Interactions: Implications for Molecular Design. *Thermodynamics - Interaction Studies - Solids, Liquids and Gases* (ed. Moreno-Piraján J. C.), Publisher: InTech, 1–48
- (175) Perozzo, R.; Folkers, G.; Scapozza, L. (2004). Thermodynamics of protein-ligand interactions: history, presence, and future aspects. *J. Recept. Signal Transduct. Res.* 24, 1–52.
- (176) Son, I.; Selvaratnam, R.; Dubins, D.N.; Melacini, G.; Chalikian T.V. (2013). Ultrasonic and densimetric characterization of the association of cyclic AMP with the cAMP-binding domain of the exchange protein EPAC1. *J. Phys. Chem. B.* 117, 10779-10784
- (177) Salemme, F. R.; Spurlino, J.; Bone, R. (1997). Serendipity meets precision: the integration of structure-based drug design and combinatorial chemistry for efficient drug discovery. *Structure* 5, 319–324.
- (178) Mattos, C. (2002). Protein–water interactions in a dynamic world. *Trends in Biochem. Sci.* 27, 203–208.
- (179) Kauzmann, W. (1959). Some factors in the interpretation of protein denaturation. *Adv. Protein. Chem.* 14, 1–63.
- (180) Dubins, D. N.; Filfil, R.; Macgregor, R. B.; Chalikian, T. V. (2000). Role of Water in Protein–Ligand Interactions: Volumetric Characterization of the Binding of 2'-CMP and 3'-CMP to Ribonuclease A. *J. Phys. Chem. B* 104, 390–401.
- (181) Suladze, S.; Ismail, S.; Winter, R. (2014). Thermodynamic, dynamic and solvational properties of PDEδ binding to farnesylated cystein: a model study for uncovering the molecular mechanism of PDEδ interaction with prenylated proteins. *J. Phys. Chem. B* 118, 966–975.
- (182) Ferenczy, G. G.; Keserű, G. M. (2010). Thermodynamics guided lead discovery and optimization. *Drug Discov. Today* 15, 919–932.
- (183) Böhm, H.-J.; Klebe, G. (1996). What Can We Learn from Molecular Recognition in Protein–Ligand Complexes for the Design of New Drugs? *Angew. Chem. Int. Ed.* 35, 2588–2614.
- (184) Fisher, H. F.; Singh, N. (1995). Calorimetric methods for interpreting protein-ligand interactions. *Methods Enzymol.* 259, 194–221.
- (185) Marlow, M. S.; Dogan, J.; Frederick, K. K.; Valentine, K. G.; Wand, A. Joshua (2010). The role of conformational entropy in molecular recognition by calmodulin. *Nat. Chem. Biol.* 6, 352–358.
- (186) Makhatadze, G. I. (1998). Heat capacities of amino acids, peptides and proteins. *Biophys. Chem.* 71, 133–156.
- (187) Dunitz, J. D. (1995). Win some, lose some: enthalpy-entropy compensation in weak intermolecular interactions. *Chem. Biol.* 2, 709–712.

- (188) MacRaild, C. A.; Daranas, A. Hernandez; Bronowska, A.; Homans, S. W. (2007). Global changes in local protein dynamics reduce the entropic cost of carbohydrate binding in the arabinose-binding protein. *J. Mol. Biol.* 368, 822–832.
- (189) Ferrell, J. E. (2009). Q&A: Cooperativity. *J. Biol.* 8, 53.
- (190) Williams, M. A. and Ladbury, J. E. (2003). Chapter 6: Hydrogen Bonds in Protein-Ligand Complexes, *From Molecular Recognition to Drug Design* (eds. Böhm, H.J.; Schneider G.) Wiley-VCH Verlag GmbH & Co. KGaA, Weinheim
- (191) Homans, S. W. (2005). Probing the binding entropy of ligand-protein interactions by NMR. *ChemBioChem* 6, 1585–1591.
- (192) Popovych, N.; Sun, S.; Ebright, R. H.; Kalodimos, C. G. (2006). Dynamically driven protein allostery. *Nat. Struct. Mol. Biol.* 13, 831–838.
- (193) Chalikian, T. V.; Sarvazyan, A. P.; Breslauer, K. J. (1994). Hydration and partial compressibility of biological compounds. *Biophys. Chem.* 51, 89–109
- (194) Showalter, S. A.; Brüschweiler, R. (2007). Validation of Molecular Dynamics Simulations of Biomolecules Using NMR Spin Relaxation as Benchmarks: Application to the AMBER99SB Force Field. *J. Chem. Theory Comput.* 3, 961–975.
- (195) Son, I.; Shek, Y. Lai; Dubins, D. N.; Chalikian, T. V. (2012). Volumetric characterization of tri-N-acetylglucosamine binding to lysozyme. *Biochemistry* 51, 5784–5790.
- (196) Gekko, K.; Noguchi, H. (1979). Compressibility of globular proteins in water at 25.degree.C. *J. Phys. Chem.* 83, 2706–2714.
- (197) Gekko, K. (2002). Compressibility gives new insight into protein dynamics and enzyme function. *Biochim. biophys. acta* 1595, 382–386.
- (198) Kamiyama, T.; Gekko, K. (2000). Effect of ligand binding on the flexibility of dihydrofolate reductase as revealed by compressibility. *Biochim. Biophys. Acta* 1478, 257–266.
- (199) Iwig, J. S.; Kuriyan, J. (2013). Fixing a Hole Where the Ras Gets In. *Cell* 153, 1191–1193.
- (200) Frett, B.; Wang, Y.; Li, H. Y. (2013). Targeting the K-Ras/PDE δ Protein-Protein Interaction: The solution for Ras-driven cancers or just another therapeutic mirage? *ChemMedChem* 8, 1620-1622
- (201) Alexander, M.; Gerauer, M.; Pechlivanis, M.; Popkirova, B.; Dvorsky, R.; Brunsveld, L.; Waldmann, H.; Kuhlmann, J. (2009). Mapping the isoprenoid binding pocket of PDEdelta by a semisynthetic, photoactivatable N-Ras lipoprotein. *ChemBioChem* 10, 98–108.
- (202) Williams, D. H.; Stephens, E.; O'Brien, D. P.; Zhou, M. (2004). Understanding noncovalent interactions: ligand binding energy and catalytic efficiency from ligand-induced reductions in motion within receptors and enzymes. *Angew. Chem., Int. Ed. Engl.* 43, 6596–6616.
- (203) Brokx, R. D.; Lopez, M. M.; Vogel, H. J.; Makhatadze, G. I. (2001). Energetics of target peptide binding by calmodulin reveals different modes of binding. *J. Biol. Chem.* 276, 14083–14091.
- (204) Pierce, M. M.; Raman, C. S.; Nall, B. T. (1999). Isothermal titration calorimetry of protein-protein interactions. *Methods* 19, 213–221.

- (205) Head-Gordon, T. (1995). Is water structure around hydrophobic groups clathrate-like? *Proc. Natl. Acad. Sci. U. S. A.* 92, 8308–8312.
- (206) Munson, M.; Balasubramanian, S.; Fleming, K. G.; Nagi, A. D.; O'Brien, R.; Sturtevant, J. M.; Regan, L. (1996). What makes a protein a protein? Hydrophobic core designs that specify stability and structural properties. *Protein Sci.* 5, 1584–1593.
- (207) Celej, M. Soledad; Montich, G. G.; Fidelio, G. D. (2003). Protein stability induced by ligand binding correlates with changes in protein flexibility. *Protein Sci.* 12, 1496–1506.
- (208) Jaenicke, R. (2000). Stability and stabilization of globular proteins in solution. *J. Biotechnol.* 79, 193–203.
- (209) Chalikian, T. V.; Bresiauer, K. J. (1996). On volume changes accompanying conformational transitions of biopolymers. *Biopolymers* 39, 619–626.
- (210) Schweiker, K. L.; Fitz, V. W.; Makhatadze, G. I. (2009). Universal Convergence of the Specific Volume Changes of Globular Proteins upon Unfolding. *Biochemistry* 48, 10846–10851.
- (211) Kharakoz, D. P.; Sarvazyan, A. P. (1993). Hydrational and intrinsic compressibilities of globular proteins. *Biopolymers* 33, 11–26.
- (212) Delano, W. (2002). The PyMOL Molecular Graphics System. The PyMOL Molecular Graphics System. version 1.5.0.4; Schrödinger, LLC: Portland, OR.
- (213) Richards, F. M. (1977). Areas, volumes, packing and protein structure. *Annu. Rev. Biophys. Bioeng.* 6, 151–176.
- (214) Voss, N. R.; Gerstein, M. (2010). 3V: cavity, channel and cleft volume calculator and extractor. *Nucleic Acids. Res.* 38, W555–62.
- (215) Lee, B.; Richards, F. M. (1971). The interpretation of protein structures: estimation of static accessibility. *J. Mol. Biol.* 55, 379–400.
- (216) Gerstein, M.; Tsai, J.; Levitt, M. (1995). The Volume of Atoms on the Protein Surface: Calculated from Simulation, using Voronoi Polyhedra. *J. Mol. Biol.* 249, 955–966.
- (217) Patel, N.; Dubins, D. N.; Pomes, R.; Chalikian, T. V. (2012). Size dependence of cavity volume: a molecular dynamics study. *Biophys. Chem.* 161, 46–49.
- (218) Lee, S.; Chalikian, T. V. (2009). Volumetric properties of solvation in binary solvents. *J. Phys. Chem. B* 113, 2443–2450.
- (219) Gerstein, M.; Chothia, C. (1996). Packing at the protein-water interface. *Proc. Natl. Acad. Sci. U. S. A.* 93, 10167–10172.
- (220) Chalikian, T. V. (2001). Structural Thermodynamics of Hydration. *J. Phys. Chem. B* 105, 12566–12578.
- (221) Luque, I.; Freire, E. (1998). Structure-based prediction of binding affinities and molecular design of peptide ligands. *Methods Enzymol.* 295, 100–127.
- (222) Sapienza, P. J.; Lee, A. L. (2010). Using NMR to study fast dynamics in proteins: methods and applications. *Curr. Opin. Pharmacol.* 10, 723–730.
- (223) Michaelis, L.; Menten, M. Leonora; Johnson, K. A.; Goody, R. S. (2011). The original Michaelis constant: translation of the 1913 Michaelis-Menten paper. *Biochemistry* 50, 8264–8269.

- (224) Boonyaratanakornkit, B. B.; Park, C. Beum; Clark, D. S. (2002). Pressure effects on intra- and intermolecular interactions within proteins. *Biochim. biophys. acta* 1595, 235–249.
- (225) Heremans, L.; Heremans, K. (1989). Raman spectroscopic study of the changes in secondary structure of chymotrypsin: effect of pH and pressure on the salt bridge. *Biochim. biophys. acta* 999, 192–197.
- (226) Eisenmenger, M. J.; Reyes-De-Corcuera, J. I. (2009). High pressure enhancement of enzymes: A review. *Enzyme Microb. Tech.* 45, 331–347.
- (227) Yancey, P. H. (2005). Organic osmolytes as compatible, metabolic and counteracting cytoprotectants in high osmolarity and other stresses. *J. Exp. Biol.* 208, 2819–2830.
- (228) Yancey, P. H.; Blake, W. R.; Conley, J. (2002). Unusual organic osmolytes in deep-sea animals: adaptations to hydrostatic pressure and other perturbants. *Comp. Biochem. Physiol. A* 133, 667–676.
- (229) Kumar, A.; Venkatesu, P. (2012). Overview of the stability of α -chymotrypsin in different solvent media. *Chem. Rev.* 112, 4283–4307.
- (230) Ma, J.; Pazos, I. M.; Gai, F. (2014). Microscopic insights into the protein-stabilizing effect of trimethylamine N-oxide (TMAO). *Proc. Natl. Acad. Sci. U. S. A.* 111, 8476–8481.

VIII

PUBLICATIONS AND PRESENTATIONS

Results presented in this thesis have contributed to the following peer-reviewed publications

1. Suladze, S., Cinar, S., Sperlich, B. and Winter, R. (2015). Pressure modulation of the enzymatic activity of phospholipase A2, a putative membrane-associated pressure sensor. *J. Am. Chem. Soc.* 137(39), 12588-12596
2. Suladze, S., Ismail, S. and Winter, R. (2014). Thermodynamic, dynamic and solvational properties of PDE δ binding to farnesylated cystein: a model study for uncovering the molecular mechanism of PDE δ interaction with prenylated proteins. *J. Phys. Chem. B*, 118, 966–975.

Work undertaken in collaborations has contributed to the following peer-reviewed publications

3. Suladze, S., Kahse, M., Erwin, N., Tomazic, D. and Winter, R. (2015). Probing volumetric properties of biomolecular systems by pressure perturbation calorimetry (PPC) - the effects of hydration, cosolvents and crowding. *Methods*, 76, 67–77.
4. Decaneto, E., Suladze, S., Rosin, C., Havenith, M., Lubitz, W., and Winter, R. (2015). Pressure and temperature effects on the activity and structure of the catalytic domain of human MT1-MMP. *Biophys. J.*, 109, 2371–2381.
5. Kapoor, S., Berghaus, M., Suladze, S., Prumbaum, D., Grobelny, S., Degen, P., Raunser, S. and Winter, R. (2014). Prebiotic cell membranes that survive extreme environmental pressure conditions. *Angew. Chem. Int. Ed. Engl.*, 53, 8397–8401.

Conferences Proceeding and Talks

1. Annual Scientific Retreat of the IMPRS-CB, SportSchloss Velen, October 2015. **Presentation**
2. Joint AIRAPT-25 & EHPRG-53 International Conference on High Pressure Science and Technology, Madrid, Spain. September 2015. **Presentation**
3. 114th General Assembly of the German Bunsen Society for Physical Chemistry, Ruhr-Universität, Bochum, Germany. May 2015. **Presentation**

Chapter 8: Publications and Presentations

4. Tag Der Chemie, Technische Universität Dortmund, Germany. February 2015. **Presentation**
5. IMPRS Student Symposium: “From molecules to cells and back again”, Max Planck Institute of Molecular Physiology, Dortmund, Germany. November 2014. **Poster**
6. 113th General Assembly of the German Bunsen Society for Physical Chemistry, University of Hamburg in Hamburg, Germany. May 2014. **Poster**
7. Tag Der Chemie, Technische Universität Dortmund, Germany. February 2014. **Poster**
8. Annual Scientific Retreat of the IMPRS-CB, Schloss Ringberg, April 2013. **Presentation**

IX

CURRICULUM VITAE

Personal Details

Name: Saba Suladze

Address: Otto-Hahn-Straße 4a, 44227 Dortmund, Germany

Telephone: (+49)17687637705; (+49)2317558705

Email: suladzesaba@gmail.com; saba.suladze@tu-dortmund.de

Date of Birth: 6th July 1987

Nationality: Georgian

University Matriculation Number: 163671 (TU Dortmund)

Education and Scientific Research Experiences

- *Doctoral Thesis*
Institution: Technische Universität Dortmund & International Max Planck Research School in Chemical Biology, Germany
Duration: September 2012 - Present
Title: Impact of Volumetric Properties on Protein Structure and Function
Supervisor: Prof. Dr. Roland Winter
- *Master of Science in Biophysics*
Institution: Tbilisi State University & Institute of Molecular Biology and Biological Physics, Georgia
Duration: 2008-2010
Title: Poly (ADP-ribose) Polymerase-1 Mediated Post-translational Modification of Nuclear Proteins.
Supervisor: Prof. Tengiz Zaalishvili
- *Bachelor of Science in Physics*
Institution: Tbilisi State University, Georgia
Duration: 2004-2008
- *Visiting Research Scholar*
Institution: Rensselaer Polytechnic Institute & Center for Biotechnology and Interdisciplinary Studies, Troy, New York, USA
Duration: September 2010 – August 2012
Title: The Use of Pressure Perturbation Calorimetry to Characterize the Volume of Cavities and Voids in Globular Proteins.
Supervisor: Prof. George Makhatadze